Involvement of brain pericytes in age-related impairment of the blood–brain barrier

加齢性血液脳関門機能障害における脳ペリサイトの関与

Takuro Iwao

Department of Pharmaceutical Care and Health Sciences, Faculty of Pharmaceutical Sciences, Fukuoka University

2023

Contents

Abbreviations

ABE: albumin-bound Evans blue

AD: Alzheimer's Disease

Ajs: adherens junctions-associated proteins

ALA: α-linolenic acid

BBB: blood–brain barrier

BMEC: brain microvessel endothelial cell

BSA: bovine serum albumin

CA: Cornu Ammonis

CBF: cerebral blood flow

Cdkn: cyclin-dependent kinase inhibitor

CNS: central nervous system

CO: corn oil

DAPI: 4',6-diamidino-2-phenylindole

DG: dentate gyrus

DHA: docosahexaenoic acid

D-PBS: Dulbecco's phosphate-buffered saline

EDTA: ethylenediaminetetraacetic acid

EPA: eicosapentaenoic acid

FABP5: fatty acid-binding protein 5

GFAP: glial fibrillary acidic protein

HBSS: Hanks' Balanced Salt Solution

HEPES: 4-(2-hydroxyethyl)-1-piperazineethanesulfonic acid

Iba1: ionized calcium-binding adapter molecule 1

IL: interleukin

LPC-DHA: lysophosphatidylcholine-DHA

MCP: monocyte chemoattractant protein,

MFSD2A: major facilitator superfamily domain-containing protein-2a

Na-F: sodium fluorescein

NE-DHA: non-esterified DHA

Pan-cad: pan-cadherin

PC: pericyte

PD: Parkinson’s disease

PDGF: platelet-derived growth factor

PDGFRβ: platelet-derived growth factor receptor β

PMSF: phenylmethylsulfonyl fluoride

RBEC, EC: rat brain endothelial cells

SASP: senescence-associated secretory phenotype

TBI: traumatic brain injury

TEER: transendothelial electrical resistance

Tjs: Tight junction-associated proteins

TNF: tumor necrosis factor

ZO-1: zonula occludens-1

αSMA: alpha-smooth muscle actin

General introduction

Aging increases the risk of developing neurodegenerative diseases, such as Alzheimer's Disease (AD) and Parkinson's disease (PD), which are closely associated with blood–brain barrier (BBB) dysfunction [1]. BBB disruption precedes the onset of AD and is an early biomarker of human cognitive dysfunction [2–3]. Furthermore, neurodegenerative diseases are implicated in age-related BBB impairment [4–7]. However, how BBB integrity alters gradually with aging is unclear.

BBB is formed by brain microvessel endothelial cells (BMECs), astrocytes, and pericytes. It restricts transport of substances in the blood for maintaining homeostasis of the central nervous system (CNS) [8]. BMECs, which are the basic unit of BBB, mainly control entry of various substances from blood to the brain. Tight junction-associated proteins (Tjs) spanning intracellular BMECs contribute to regulating paracellular permeability, and their disruption and loss result in the disruption of BBB integrity [8–9]. In addition, adherens junction-associated proteins (Ajs), such as cadherin proteins, contribute to holding the cells together, providing the tissue structural support, and are essential for formation of tight junctions [10]. Major facilitator superfamily domain-containing protein-2a (MFSD2A), which is exclusively expressed in BMEC, is a docosahexaenoic acid (DHA) transporter and can inhibit transcellular permeability by regulating endocytosis [11–14].

Pericytes are present at intervals along the walls of brain capillaries and play a key role in maintaining BBB integrity [15–18]. They induce formation of TJs in BMECs and regulate BBB permeability [15, 19]. Furthermore, their presence is required for the MFSD2A expression in BMECs [12].

The aim of the present study was to explore the characteristic changes in pericytes with aging and to ascertain whether or not pericytes are involved in age-related impairment of BBB. In the first chapter, we report age-related changes in DHA transport across BBB and the expression of DHA carrier proteins in young-adult, middle-aged, and aged mice. In the second chapter, we report the relationship between dynamic changes in BBB integrity with aging and cellular senescence in pericytes. Furthermore, we ascertained the relationship between BBB integrity and the inflammatory activation of microglia, which contributes to neuroinflammation. In the third chapter, we report the effect of senescence pericytes on the barrier function of BBB evaluated using an in vitro BBB model. In the fourth

chapter, we report how pericytes regulate the MFSD2A expression and whether or not pericytes affect the localization of MFSD2A in BMEC. In the fifth chapter, we report the effect of long-term dietary DHA supplementation for age-related BBB disruption and subsequent activation of microglia. Finally, we explore whether or not DHA regulated the barrier function of BBB in physiological condition in vitro.

The results of the present study would provide new insights into age-related impairment of BBB. Repairing age-related dysfunction of BBB can be a novel preventive strategy for neurological diseases.

References

1. Erickson MA, Banks WA. Age-Associated Changes in the Immune System and Blood–Brain Barrier Functions. Int J Mol Sci. 2019;20(7).

2. Sweeney MD, Sagare AP, Zlokovic BV. Blood-brain barrier breakdown in Alzheimer disease and other neurodegenerative disorders. Nat Rev Neurol. 2018;14(3):133-50.

3. Nation DA, Sweeney MD, Montagne A, Sagare AP, D'Orazio LM, Pachicano M, et al. Blood-brain barrier breakdown is an early biomarker of human cognitive dysfunction. Nat Med. 2019;25(2):270-6.

4. Verheggen ICM, de Jong JJA, van Boxtel MPJ, Gronenschild E, Palm WM, Postma AA, et al. Increase in blood-brain barrier leakage in healthy, older adults. Geroscience. 2020;42(4):1183-93.

5. Erdő F, Denes L, de Lange E. Age-associated physiological and pathological changes at the blood-brain barrier: A review. J Cereb Blood Flow Metab. 2017;37(1):4-24.

6. Montagne A, Barnes SR, Sweeney MD, Halliday MR, Sagare AP, Zhao Z, et al. Blood-brain barrier breakdown in the aging human hippocampus. Neuron. 2015;85(2):296-302.

7. Mooradian AD, Haas MJ, Chehade JM. Age-related changes in rat cerebral occludin and zonula occludens-1 (ZO-1). Mech Ageing Dev. 2003;124(2):143-6.

8. Abbott NJ, Patabendige AA, Dolman DE, Yusof SR, Begley DJ. Structure and function of the blood-brain barrier. Neurobiol Dis. 2010;37(1):13-25.

9. Correale J, Villa A. The blood-brain-barrier in multiple sclerosis: functional roles and therapeutic targeting. Autoimmunity. 2007;40(2):148-60.

10. Wolburg H, Lippoldt A. Tight junctions of the blood-brain barrier: development, composition and regulation. Vascul Pharmacol. 2002;38(6):323-37.

11. Angers M, Uldry M, Kong D, Gimble JM, Jetten AM. Mfsd2a encodes a novel major facilitator superfamily domain-containing protein highly induced in brown adipose tissue during fasting and adaptive thermogenesis. Biochem J. 2008;416(3):347-55.

12. Ben-Zvi A, Lacoste B, Kur E, Andreone BJ, Mayshar Y, Yan H, et al. Mfsd2a is critical for the formation and function of the blood-brain barrier. Nature. 2014;509(7501):507-11.

13. Nguyen LN, Ma D, Shui G, Wong P, Cazenave-Gassiot A, Zhang X, et al. Mfsd2a is a transporter for the essential omega-3 fatty acid docosahexaenoic acid. Nature. 2014;509(7501):503-6.

14. Eser Ocak P, Ocak U, Sherchan P, Zhang JH, Tang J. Insights into major facilitator superfamily domain-containing protein-2a (Mfsd2a) in physiology and pathophysiology. What do we know so far? J Neurosci Res. 2020;98(1):29-41.

15. Dalkara T, Gursoy-Ozdemir Y, Yemisci M. Brain microvascular pericytes in health and disease. Acta Neuropathol. 2011;122(1):1-9.

16. Attwell D, Mishra A, Hall CN, O'Farrell FM, Dalkara T. What is a pericyte? J Cereb Blood Flow Metab. 2016;36(2):451-5.

17. Nakagawa S, Deli MA, Kawaguchi H, Shimizudani T, Shimono T, Kittel A, et al. A new blood-brain barrier model using primary rat brain endothelial cells, pericytes and astrocytes. Neurochem Int. 2009;54(3-4):253-63.

18. Dohgu S, Takata F, Kataoka Y. [Brain pericytes regulate the blood-brain barrier function]. Nihon Yakurigaku Zasshi. 2015;146(1):63-5.

19. Daneman R, Zhou L, Kebede AA, Barres BA. Pericytes are required for blood-brain barrier integrity during embryogenesis. Nature. 2010;468(7323):562-6.

Chapter 1: Aging decreases docosahexaenoic acid transport across the blood-brain barrier in C57BL/6J mice

Introduction

Many essential nutrients are necessary to maintain physiological functions. A lack of essential nutrients can cause general disorders of the central nervous system (CNS), and proper functioning of the CNS requires adequate levels of essential nutrients in the brain. Maintaining the CNS microenvironment requires transporting various nutrients across the blood-brain barrier (BBB). The BBB comprises brain microvessel endothelial cells (BMECs) sealed with tight junctions; it restricts the paracellular transport of substances in the blood and selectively transports essential nutrients into the CNS via various specialized transporters located on BMECs [1].

It is increasingly recognized that the nutritional needs of the CNS vary in different diseases. In addition, the BBB is likely to be compromised under chronic inflammation, stroke, hypoxia, Alzheimer's disease (AD), and other neurological diseases [2], which can cause undernutrition of the brain [3]. These pathologies, as well as natural aging, induce dysfunction of the transporters and receptors and the loosening of tight junctions as well as other junctions at the BBB [4]. Indeed, chronic inflammation can lead to differential regulation of nutrient transporters [5], which contributes to the pathology of chronic inflammation-associated cognitive decline [6]. Therefore, low levels of several nutrients in the brain are associated with cognitive decline, likely due to changes in the functions of nutrient transporters at the BBB.

Docosahexaenoic acid (DHA) (22:6n-3), an n-3 polyunsaturated fatty acid (MW: 328), has attracted much attention because of its functional and structural importance in the brain. DHA is highly enriched in brain phospholipids and contributes to proper brain development and function. Moreover, many neurophysiological functions of DHA have been identified, including regulation of cell survival, neuroinflammation, neurogenesis, and participation in signal transduction [7]. It is controversial to state that the human brain’s capacity to biosynthesize DHA from its precursor, α-linolenic acid (ALA, 18:3n-3), is very low [8], because maternal dietary ALA given during pregnancy-lactation increased brain DHA levels in the offspring [9]. However, plasma DHA, which is obtained directly from dietary intake to maintain DHA levels in the brain, must be transported from the blood to the brain across the BBB [10].

Brain transport mechanisms of DHA vary based on its carrier form, non-esterified or esterified DHA [7]. Non-esterified DHA (NE-DHA) is mainly found in the blood as a complex with albumin [11]. NE-DHA disassociated from albumin is taken up into the brain

through passive diffusion [12]. In brain uptake of NE-DHA, fatty acid-binding protein 5 (FABP5) is directly involved in the intracellular trafficking of NE-DHA, which penetrates the luminal membrane of BMECs by passive diffusion, across BMECs [13,14]. Esterified DHA largely exists as phospholipids, in part triacylglycerol and cholesteryl ester pools [15]. Lysophosphatidylcholine-DHA (LPC-DHA) in circulating esterified fatty acid pools is bound to albumin or is sequestered within the phospholipid membrane of lipoproteins [15]. A previous study reported that the major transporter for LPC-DHA uptake by the brain is the major facilitator superfamily domain-containing protein 2a (MFSD2A) [16], which is exclusively expressed in BMECs. That study indicated that MFSD2A did not recognize DHA as a substrate because MFSD2A transported lysophosphatidylethanolamine, LPC-oleate and LPC-palmitate [16]. It remains unclear whether NE-DHA serves as a substrate for MFSD2a, although NE-DHA is the major plasma pool supplying the brain under normal physiological conditions [17]. Therefore, it is important to investigate the brain uptake mechanisms of NE-DHA and the effect of alteration of the milieu interieur on NE-DHA transport across the BBB.

Brain DHA levels decrease with age, and this reduced DHA is associated with age-related cognitive dysfunction [18]. DHA supplementation, which elevates NE-DHA levels in plasma [19], is likely to be beneficial when administered before or during the earliest stages of cognitive decline [20]. However, the mechanisms underlying the reduction of brain DHA levels with age are not well understood. Animal and clinical studies have evidenced age-related BBB dysfunction [21,22]; however, the impact of aging on brain DHA uptake at the BBB is currently unknown. In this study, we investigated age-related changes in NE-DHA transport across the BBB and expression of DHA carrier proteins in mice aged 2, 8, 12, and 24 months. We further examined whether brain uptake of [^{14}C]DHA is mediated by a transport carrier, such as MFSD2A, both, in vivo by transcardiac brain perfusion with excess DHA using 2-month-old mice and in vitro using BMECs with siRNA-mediated gene silencing.

Materials and Methods

Animals

All protocols involving experimental animals were approved by the Laboratory Animal Care and Use Committee of Fukuoka University (permit number: 2004001, 2204002). The 2- (young), 8- (adult), 12- (middle-aged), and 24 (aged)-months old male C57BL/6J mice and Wistar rats at 3 weeks old were purchased from Charles River Laboratory (Kanagawa, Japan) and Japan SLC, Inc. (Shizuoka, Japan). Mice and rats were housed under a controlled temperature (22 ± 2°C) and light-dark cycle (lights on from 7:00 to 19:00), with access to water and chow diet *ad libitum*. After habituation for 1 week, the mice underwent the experiments.

Measurement of Brain Uptake of [^{14}C]DHA, [^{3}H]Mannitol, and [^{14}C]Sucrose

Brain uptake of DHA was assessed in mice using an *in situ* transcardiac brain perfusion technique. This technique was previously used by Banks et al. [23]. The [1-^{14}C]DHA as NE-DHA (American Radiolabeled Chemicals, St. Louis, MO, USA; ARC0380), [^{3}H]mannitol (PerkinElmer, Waltham, MA, USA, NET101) and [^{14}C]sucrose (PerkinElmer, Waltham, MA, USA; NEC100X) were diluted to concentrations of 0.1 µCi/mL (DHA and sucrose) and 0.2 µCi/mL (mannitol) in a physiological buffer containing 141 mM NaCl (Sigma, St. Louis, MO, USA; 28–2270-5), 4 mM KCl (Wako, Osaka, Japan; 163-03545), 2.8 mM $CaCl_2$ (Sigma; 05-0580), 1 mM $MgSO_4 \cdot 7H_2O$ (Kishida Chemical Co., Ltd., Osaka, Japan; 000-46905), 1 mM $NaH_2PO_4 \cdot 2H_2O$ (Wako; 192-02815), 10 mM d-glucose (Wako; 041-00595), and 10 mM 4-(2-hydroxyethyl)-1-piperazineethanesulfonic acid (HEPES; Sigma; H4034); pH 7.4. In a competition assay, unlabeled NE-DHA (Sigma; D2534-100MG) was added to the perfusate (final concentration of unlabeled DHA: 100 µM) before infusion. Ethanol (Nacalai Tesque, Kyoto, Japan; 14713-95) was added to an equal volume of unlabeled DHA to the perfusate (final ethanol concentration: 0.001 %) as the vehicle control. Mice were anesthetized using an intraperitoneal injection of 25% urethane (Sigma; 94300). The heart was exposed, the left jugular vein was severed, and the descending aorta was ligated. Perfusate containing [^{14}C]DHA, [^{3}H]mannitol, or [^{14}C]sucrose was then infused into the left ventricle of the heart at a rate of 2 mL/min for 0.5 to 1.5 min using a 27

gauge butterfly needle. In the uptake experiment for aged mice, the perfusate was infused for 1 min. After perfusion, the brain was removed, dissected into six regions (the olfactory bulb, forebrain, cortex, hippocampus, thalamus and hypothalamus, and cerebellum), and weighed. Each brain region was mixed with 1 mL of tissue solubilizer (Solvable™; PerkinElmer; 6NE9100) and incubated at 60°C for 24 h. Samples were prepared for scintillation counting by the addition of 0.2 mL H_2O_2 (Sigma; 13-1910-5) and 10 mL of liquid scintillation cocktail (Pico-Fluor Plus; PerkinElmer; 6013699). The radioactivity in the samples was then measured using a liquid scintillation counter (Packard 2250CA; PerkinElmer). Brain/perfusate ratios were calculated by dividing the radioactivity in 1 g of brain tissue by the radioactivity in an mL of perfusate. Whole brain values were calculated by dividing the total radioactivity in each brain region by the total weight of each brain region. The unidirectional influx rate (Ki) was determined by the linear portion of the slope in the plot of brain/perfusate ratio against perfusion time.

Isolation of Brain Microvessels

Brian microvessels were isolated by the modified method of Yousif et al. [24]. Male mice aged 2, 8, 12, and 24 months were anesthetized before Dulbecco's phosphate-buffered saline (-) (D-PBS) (Wako; 045-29795;10 mL per mouse) was infused into the left ventricle of the heart. The brain tissue was triturated using a glass homogenizer coated with 1% bovine serum albumin (BSA)-Hanks' Balanced Salt Solution (HBSS; Thermo Fisher Scientific, Waltham, MA, USA; 14185-045) in 1 mL of Buffer A (HBSS containing 1% Phosphatase Inhibitor Cocktail [ethylenediaminetetraacetic acid (EDTA) free; Nacalai Tesque; 07575-51], 1% Protease Inhibitor Cocktail for use with mammalian and tissue extracts [Nacalai Tesque; 25955-11], 1 mM phenylmethylsulfonyl fluoride [PMSF; Sigma; P7626], and 15 µg/mL deoxyribonuclease I [Sigma; D4513]) on ice. This suspension was transferred into a 1.5 mL tube and centrifuged at 1,000 × g for 10 min at 4°C. Next, the supernatant was aspirated and the pellet was mixed with 1 mL of 17.5% dextran (Sigma; D8821)-HBSS. The suspension was then centrifuged at 4,400 × g for 15 min at 4°C. The supernatant with a lipid layer was removed and the pellet was resuspended in Buffer B (Buffer A containing 1% BSA). Next, the suspension was filtered using a 10 µm nylon mesh membrane to trap the residue, including microvessels, on the surface of the membrane. HBSS was then passed through the membrane to remove debris in the residue. The microvessels on the membrane were then washed into a 1.5 mL tube with Buffer A and

centrifuged at 20,000 × g for 5 min at 4°C. Finally, microvessels were obtained at the bottom of the tube and stored at -80°C until use. We confirmed that the obtained brain microvessels were enriched with brain endothelial cell-specific proteins (occludin and claudin-5).

Extraction of Total Protein from Brain Microvessels

The microvessels were homogenized in phosphoprotein lysis buffer containing 10 mM Tris-HCl (pH 6.8; Nacalai Tesque; 35434-34), 100 mM NaCl (Sigma; 28-2270-5), 1 mM EDTA (pH 8.0; Wako; 311-90075), 1 mM EGTA (Wako; 346-01312), 10% glycerol, 1% Triton-X100 (Sigma; X100), 0.1% sodium dodecyl sulfate (SDS; Nacalai Tesque; 02873-75), 0.5% sodium deoxycholate (Sigma; D6750), 20 mM sodium pyrophosphate (Sigma; S6422), 2 mM sodium orthovanadate (Sigma; S6508), 1 mM sodium fluoride (Wako; 196-01975), 1% protease inhibitor cocktail (Sigma; P2714), 1% phosphatase inhibitor cocktail 2 (Sigma; P5726), 1% Phosphatase Inhibitor Cocktail 3 (Sigma; P0044), and 1 mM PMSF (Sigma) using an electric mixer, and then sonicated on ice. Samples were centrifuged at 15,000 × g for 15 min at 4°C, and the supernatants were collected. The total protein concentration in the lysates obtained from microvessels was determined using a Pierce™ BCA Protein Assay Kit (Thermo Fisher Scientific; 23225).

Primary rat brain endothelial cell culture

The method of primary culture of rat brain endothelial cells (RBECs) is previously described [25]. The meninges and white matter were carefully removed from the forebrains, and the gray matter was minced using a scalpel and enzymatic digestion by DMEM (Wako; 048-29763), including collagenase type 2 (1 mg/mL, Worthington, Lakewood, NJ, USA; CLS2) for 75 min at 37°C with agitation in the water bath. After inactivation by adding cold DMEM, the suspension was centrifuged (1,000 × g, 8 min). The pellet was separated by centrifugation in 20% BSA, (Wako, 011-27055) - DMEM (1,000 × g, 20 min). The pellet containing microvessels were further digested with DMEM including collagenase/dispase (1 mg/mL, Roche, Mannheim, Germany; 11097113001) for 20 min at 37°C with agitation in the water bath. After inactivation, microvessel clusters were separated on a 33% continuous Percoll (GE Healthcare, Buckinghamshire, UK; 17-5445-01) gradient, collected

and plated on collagen type IV (0.1 mg/mL, Sigma; C5533) and fibronectin (0.075 mg/mL, Sigma; F1141-5MG) coated dishes. RBEC cultures were maintained in RBEC medium [DMEM/F12 (Wako; 042-30555) supplemented with 10% FBS (Biosera, Kansas, MO, USA; FB-1365/500), basic fibroblast growth factor (1.5 ng/mL, R&D, Minneapolis, MN, USA; 2099-FB-025), heparin (100 μg/mL, Sigma; H3149), insulin (5 μg/mL), transferrin (5 μg/mL), sodium selenite (5 ng/mL; insulin-transferrin-sodium selenite media supplement, Sigma; I1884), penicillin (100 units/mL), streptomycin (100 μg/mL; penicillin-streptomycin mixed solution, Nacalai Tesque; 09367-34) and gentamicin (50 μg/mL, Biowest, Riverside, MO, USA; L0012)] containing puromycin (4 μg/mL, Nacalai Tesque; 14861-84) at 37°C in a humidified atmosphere of 5% CO_2/95% air, for three days and typically reached 70–80 % confluency. RBECs were passaged to 35 mm dishes (30×10^4 cells/dish) and 24-well plates (10×10^4 cells/dish) and maintained in RBEC medium supplemented with 500 nM hydrocortisone (Sigma; H0135).

siRNA transfection

RBECs cultured on a 35-mm dish were transfected with the lipid complex, including Lipofectamine® RNAiMAX Transfection Reagent (4 μL; Invitrogen, 13778075) and Rat Mfsd2a Silencer® Select Pre-designed siRNA (50 nM; Life technologies, s151458) or Silencer Select Negative Control (50 nM; Life technologies, 4390843) in RBEC medium for 2 days. The MFSD2A protein levels in RBECs were assessed using Western blot and siMfsd2a-transfected RBECs were used for DHA cellular uptake assay.

Cellular uptake of [^{14}C]DHA

To measure the cellular uptake of DHA, RBECs cultured on a 24-well plate were incubated with 0.2 mL of physiological buffer containing 0.1 μCi/mL [^{14}C]DHA (incubation buffer) at 37°C for 30 s to 15 min. At the end of the experiment, RBECs were washed with D-PBS three times and incubated with 0.2 mL of 1M NaOH (Wako; 192-02175) at 37°C for 3 h for cell lysis. The total protein concentration in the cell lysates was determined using a Pierce™ BCA Protein Assay Kit. Samples were added to 10 mL of a liquid scintillation cocktail, then [^{14}C]DHA radioactivity in the cell lysate was measured using a liquid scintillation counter. The cellular uptake of [^{14}C]DHA by RBECs was expressed as

cell/medium ratios calculated by dividing the radioactivity in one milligram of protein by the radioactivity in one microliter of the incubation buffer. The rate of cellular uptake was determined by the linear portion of the slope of the cell/medium ratios against the incubation time (0.5, 2, 5, and 10 min) graph.

Western Blot Analysis

Equivalent amounts of protein from each sample were electrophoretically separated on 4–15% TGX Stain-Free gradient acrylamide gels (Bio-Rad, Hercules, CA; 4568084) or 12% TGX Stain-Free acrylamide gels (Bio-Rad; 161-0185) and transferred to low fluorescent polyvinylidene difluoride membranes (Bio-Rad; 1704274). Stain-Free technology using GelDoc go imaging system (Bio-Rad) was used for total protein normalization. Membranes were then blocked using Blocking One (Nacalai Tesque; 03953-95). MFSD2A, FABP5 and β-actin were detected using antibodies against MFSD2A (1:1,000; Sigma; SAB3500576), FABP5 (1:1,000; Sigma; SAB1401130) and β-actin (1:8,000; Sigma; A1978). After washing, the membranes were incubated in HRP–conjugated goat anti-rabbit IgG (Bio-Rad; 170-6515) or goat anti-mouse IgG (Bio-Rad; 170-6516), as appropriate. Immunoreactive bands were detected using Clarity Western ECL Substrate (Bio-Rad; 1705061). Images of the bands were digitally captured using a MultiImager II ChemiBOX (BioTools, Gunma, Japan), and band intensities were quantified using ImageJ software (National Institutes of Health Image, Bethesda, MD, USA). The relative intensity of each individual protein was expressed as the ratio of the corresponding protein to the total protein loading or β-actin.

Statistical Analysis

Results are expressed as the mean ± standard error of the mean (SEM). Statistical analyses were performed using GraphPad Prism 8.0 (GraphPad, San Diego, CA, USA). Simple linear regression analysis was used to evaluate the brain uptake rate of [^{14}C]DHA and [^{14}C]sucrose in competition assay using excess unlabeled DHA and the rate of cellular uptake of [^{14}C]DHA. Statistical differences in brain uptake of [^{14}C]DHA and [^{3}H]mannitol and expression levels of MFSD2A and FABP5 protein were analyzed using one-way analysis of variance (ANOVA) followed by Tukey's multiple comparison tests. A

two-way ANOVA (age × brain regions) was performed to analyze differences in the brain uptake of [^{14}C]DHA. An unpaired *t*-test was used to analyze the cellular uptake of [^{14}C]DHA and the expression levels of MFSD2A protein in RBECs transfected siMfsd2a. Differences were considered statistically significant for $P < 0.05$.

Results

Brain uptake of DHA decreased in 12- and 24-month-old mice

To evaluate the effects of aging on the brain uptake of DHA, [^{14}C]DHA brain/perfusate ratio was assessed in C57BL/6 mice at 2-, 8-, 12-, and 24 months of age. In the whole brains of mice aged 12 and 24 months, the brain uptake of [^{14}C]DHA decreased significantly compared with that of the 2-month-old group (Fig. 1a). In mice at 12 and 24 months of age, the [^{14}C]DHA brain/perfusate ratio in the whole brain was decreased by 0.03275 mL/g ($P = 0.0284$) and 0.03827 mL/g ($P = 0.0380$), respectively. Given that aging decreased brain uptake of DHA, we assessed [^{14}C]DHA uptake by six brain regions (olfactory bulb, forebrain, cortex, hippocampus, thalamus and hypothalamus, and cerebellum) of 2-, 8-, 12-, and 24-month-old mice, to determine whether aging affects specific brain regions. The uptake of [^{14}C]DHA in the olfactory bulb, hippocampus, thalamus and hypothalamus of 12- and 24-month-old mice was considerably lower than that of 2-month-old mice. Two-way ANOVA revealed the significant effects of age ($F(3,204) = 24.63$, $P < 0.0001$) and regions ($F(5,204) = 2.384$, $P = 0.0396$), but there was no significant interaction between age and regions ($F(15,204) = 0.5614$, $P = 0.9016$).

One-way ANOVA showed an effect for age in each region as follows: whole brain ($F = 4.422$, $P = 0.0099$), olfactory bulb ($F = 4.670$, $P < 0.0077$), forebrain ($F= 4.177$, $P = 0.0127$), hippocampus ($F = 9.209$, $P = 0.0001$) and thalamus and hypothalamus ($F = 6.458$, $P = 0.0014$). The differences of [^{14}C]DHA brain/perfusate ratio in each region of the 12- and 24-month-old mice were as follows: 0.04626 mL/g (2 vs. 24 months old, $P = 0.0042$) in the olfactory bulb, 0.04489 mL/g (2 vs. 12 months old, $P = 0.0299$) and 0.05294 mL/g (2 vs. 24 months old, $P = 0.0375$) in the forebrain, 0.03402 mL/g (2 vs. 12 months old, $P = 0.0101$) and 0.06034 mL/g (2 vs. 24 months old, $P = 0.0001$) in the hippocampus and 0.04306 mL/g (2 vs. 12 months old, $P = 0.0051$), 0.05106 mL/g (2 vs. 24 months old, $P = 0.0067$) in the thalamus and hypothalamus (Fig. 1b-g).

Brain uptake of mannitol did not decrease in 12- and 24-month-old mice

Next, we determined whether changes in BBB integrity during aging accounted for the decreased brain uptake of [^{14}C]DHA in mice aged 12- and 24- months. BBB integrity was evaluated using the brain/perfusate ratio of [^{3}H]mannitol at 1 min. We co-infused [^{14}C]DHA with [^{3}H]mannitol as a paracellular permeability marker as mannitol crosses the intact BBB poorly [26]. No significant changes in brain uptake of [^{3}H]mannitol were observed in the whole brain of 2-, 8-, 12-, and 24-month-old mice (Fig. 2a). In each brain region, there are no significant effects with age (Fig. 2b-g).

FABP5 protein expression in brain microvessels increased in 12- and 24-month-old mice

Following previous reports that brain NE-DHA uptake is mediated by passive membrane diffusion [12] and subsequent intracellular trafficking by an intracellular DHA carrier protein, FABP5 [14], we examined whether FABP5 expression is altered with aging. We evaluated the FABP5 protein expression levels in brain microvessels prepared from 2-, 8-, 12-, and 24-month-old mice using Western blot analysis. One-way ANOVA showed the effect of age on the FABP5 ($F = 3.246$, $P = 0.0448$) protein expression levels. The FABP5 protein expression in 24-month-old mice was significantly increased 4.6-fold ($P = 0.0412$) compared with that in the 2-month-old mice (Fig. 3). These results indicate that the decreased brain uptake of [^{14}C]DHA in aged mice was not caused by reduced FAPB5 expression. Since the previous study showed that the membrane permeability at the BBB did not change in 12- and 24-month-old mice [27], we ascertained whether NE-DHA is taken up into the brain by a transport carrier located on the luminal membrane of BMECs, such as MFSD2A.

The brain uptake rate of DHA was decreased by adding excess unlabeled DHA

To determine the brain transport mechanism of NE-DHA, we measured the brain/perfusate ratio of [^{14}C]DHA at 0.5–2.0 min using a perfusate containing unlabeled DHA 100 μM. Fig. 4 shows a linear relationship between the brain/perfusate ratio of

[^{14}C]DHA and perfusion time up to 1.5 min in the whole brain and each brain region. The brain uptake of [^{14}C]DHA plateaued at 1.5 min. The slope calculated by simple linear regression represents the brain uptake rate (Ki; mLg^{-1}min^{-1}) of [^{14}C]DHA. For the whole brain, Ki of the DHA 100 μM group (Ki = 0.2921 mLg^{-1}min^{-1}) was significantly decreased compared with that of the vehicle group (Ki = 0.5944 mLg^{-1}min^{-1}, F = 10.89, P = 0.0036) (Fig. 4a). In all brain regions, Ki of the DHA 100 μM group showed a significant reduction in comparison to the vehicle group (Fig. 4b–g). The data for all regions of the vehicle and DHA 100 μM groups are recorded below. Olfactory bulb (vehicle Ki: 0.6445 mLg^{-1}min^{-1}, DHA 100 μM Ki: 0.2848 mLg^{-1}min^{-1}, F = 6.959, P = 0.015), forebrain (vehicle Ki: 0.5712 mLg^{-1}min^{-1}, DHA 100 μM Ki: 0.2762 mLg^{-1}min^{-1}, F = 12.51, P = 0.021), cortex (vehicle Ki: 0.4516 mLg^{-1}min^{-1}, DHA 100 μM Ki: 0.2567 mLg^{-1}min^{-1}, F = 5.806, P = 0.0257), hippocampus (vehicle Ki: 0.5242 mLg^{-1}min^{-1}, DHA 100 μM Ki: 0.2478 mLg^{-1}min^{-1}, F = 7.369, P = 0.0133), thalamus and hypothalamus (vehicle Ki: 0.6684 mLg^{-1}min$^{-1,}$ DHA 100 μM Ki: 0.2848 mLg^{-1}min^{-1}, F = 7.766, P = 0.0114), and cerebellum (vehicle Ki: 0.6837 mLg^{-1}min^{-1}, DHA 100 μM Ki: 0.3547 mLg^{-1}min^{-1}, F = 10.89, P = 0.0036).

The BBB integrity was not altered by adding excess unlabeled DHA

Next, we determined whether changes in BBB integrity in the presence of excess unlabeled DHA accounted for the decreased brain uptake rate of [^{14}C]DHA in the competition assay. BBB integrity was evaluated using the brain uptake rate of [^{14}C]sucrose calculated by brain/perfusate ratio of [^{14}C]sucrose at the corresponding perfusion time of the brain uptake of [^{14}C]DHA, which revealed no differences between vehicle and DHA 100 μM groups (Fig. 5a-g). We paid attention to the concentration of the vehicle (ethanol) in the perfusate since a cerebral vascular volume (the y-intercept of a regression line of brain/perfusate ratio of [^{14}C]sucrose over perfusion time) enlarged by a high concentration of ethanol (> 0.001%) resulted in the uncertainty of the inhibition effect of unlabeled DHA.

MFSD2A mediated the cellular uptake of DHA by brain endothelial cells

To determine whether transport carriers mediate the brain uptake of NE-DHA and if MFSD2A is involved in the brain uptake of NE-DHA, we examined the effects of temperature and siMfsd2a on cellular uptake of [^{14}C]DHA by BMECs. Fig. 6a illustrates the

time course of cellular uptake of [^{14}C]DHA by RBECs. Because cellular uptake of [^{14}C]DHA by RBECs peaked at 10 min, the following experiments were performed at 10 min. The slope calculated by simple linear regression represents the rate of cellular uptake (μLmg protein^{-1} min^{-1}) of [^{14}C]DHA. The rate of cellular uptake of [^{14}C]DHA by RBECs at 4°C was significantly decreased by 60% (19.98 μLmg protein^{-1} min^{-1}) compared with the uptake rate at 37°C (50.13 μLmg protein^{-1} min^{-1}, $F = 112.8$, $P < 0.0001$) (Fig. 6b). The MFSD2A expression level in RBECs transfected with siMfsd2a was significantly down-regulated by 30% ($P = 0.0026$) compared with that of the cells transfected with negative control siRNA (Fig. 6c and 6d). The siMfsd2a-transfected RBECs showed a significant decrease of 17% ($P = 0.0108$) in cellular uptake of [^{14}C]DHA compared with negative control siRNA-transfected cells (Fig. 6e).

MFSD2A protein expression in brain microvessels decreased in 12- and 24-month-old mice

We determined the MFSD2A protein expression levels in brain microvessels prepared from 2-, 8-, 12-, and 24-month-old mice using Western blot analysis. A previous study showed that multiple MFSD2A immunoreactive bands of approximately 55 kDa are detected in lysates from mouse brains and neural stem cells [28]. Therefore, we considered all detected bands with an approximate size of 50 kDa as immunoreactive MFSD2A bands and quantified their intensity. One-way ANOVA showed the effect of age in the MFSD2A ($F = 5.171$, $P = 0.0109$) protein expression levels. The 12- and 24-month-old mice exhibited significant reductions in MFSD2A protein expression of 29% (12-month-old mice, $P = 0.0242$) and 26% (24-month-old mice, $P = 0.0432$), respectively, compared with 2-month-old mice (Fig. 7).

Discussion

An age-related decline in brain DHA is associated with cognitive decline [18,20]. Because brain DHA levels in adulthood are largely dependent on direct dietary intake, DHA in the peripheral circulation needs to be efficiently transported into the brain across the BBB [7]. DHA is present in plasma in a bound form; therefore, the cellular uptake of DHA depends on its affinity for plasma proteins [29]. In the present study, to exclude the influence of plasma protein binding to DHA, we used a transcardiac brain perfusion technique that is commonly used to evaluate BBB permeability [30]. The concentration of [^{14}C]DHA in the perfusate was the same as that reported in a previous study [31].

Using the perfusion technique, we demonstrated a significant decrease in the BBB transport of [^{14}C]DHA in the whole brains of 12- and 24-month-old mice compared with that in 2-month-old mice (Fig. 1). To evaluate region specificity in the brain uptake of [^{14}C]DHA, the brain was divided into six regions. There were age-related decreases in the brain uptake of [^{14}C]DHA in specific regions (Fig. 1). These data suggest that the availability of DHA is not influenced by aging in the cortex and cerebellum.

Furthermore, we evaluated the brain/perfusate ratio of [^{3}H]mannitol, a small hydrophilic molecule with low paracellular permeability across the BBB. The brain/perfusate ratio of [^{3}H]mannitol reflects the cerebral vascular volume, because [^{3}H]mannitol does not cross the BBB during a short period and remains within the intracerebral vasculature. There were no significant differences in brain uptake of [^{3}H]mannitol among the 2-, 8-, 12-, and 24-month-old groups. Our data is supported by a previous study that reported that BBB permeability did not alter in 28-month-old aged rats [32]. However, previous works showed the leakiness of human BBB in normal aging [33,34]. These discordances in age-related changes in BBB permeability probably depend on the evaluation methods used, including markers used for BBB permeability. Our findings suggest that the decreased brain uptake of [^{14}C]DHA in 12- and 24-month-old mice is not the result of changes in BBB integrity or cerebral vascular volume. These results indicate that the decreased DHA transport across the BBB in aged mice is predominantly attributable to changes in a transcellular pathway of DHA involving carrier-mediated transport and passive diffusion rather than a paracellular pathway.

Given that DHA crosses BMECs via a transcellular pathway, a possible explanation for the age-related decreased brain uptake of DHA is the decline in the FABP5-mediated intracellular trafficking of DHA. Interestingly, we observed that FABP5 protein

expression in the microvessel increased with age (Fig. 3). The highest level of FABP5 expression is detected during neonatal development and then declines after birth [35], indicating that FABP expression in the brain is altered with age [36]. Although further studies are needed to clarify whether the intracellular DHA transport activity of FABP5 is maintained during aging, our data suggest that the age-related decreased brain uptake of NE-DHA is likely due to compromised influx of NE-DHA through the luminal membrane of BMECs rather than the decline in the intracellular NE-DHA trafficking by FABP5. Therefore, we ascertained that NE-DHA is taken up into the brain by a transport carrier in the following experiments.

We demonstrated that the brain uptake of [^{14}C]DHA was inhibited by excess unlabeled NE-DHA (Fig.4) without changes in the brain/perfusate ratios of [^{14}C]sucrose (MW: 342.3), a small hydrophilic molecule with low paracellular permeability across the BBB, as a marker of cerebral vascular volume and BBB integrity, in all the brain regions (Fig. 5). Therefore, [^{14}C]DHA transport across the BBB is mediated by a saturable transport system. Our data are partly consistent with the findings of a previous study indicating that [^{14}C]DHA is transported across the BBB by passive diffusion [12], as the extent of inhibition by excess (55-fold) unlabeled DHA accounted for ~50% of the brain uptake rate of [^{14}C]DHA.

Next, we determined whether transport carriers mediate the brain uptake of [^{14}C]DHA and if MFSD2A is involved in the brain uptake of [^{14}C]DHA at the BBB using RBECs. We confirmed that RBECs expressed MFSD2A (Fig. 6c). In cellular uptake experiments, we used a physiological buffer containing [^{14}C]DHA without any proteins or phospholipids, indicating that [^{14}C]DHA was taken up by RBECs as the non-esterified form. We found that the cellular uptake of [^{14}C]DHA by RBECs was temperature-dependent (Fig. 6b). This result indicated that [^{14}C]DHA is taken up by transport carriers on BMECs and supported our data using the transcardiac brain perfusion technique (Fig. 4). MFSD2A knockdown by siRNA decreased MFSD2A protein levels and cellular uptake of [^{14}C]DHA by RBECs (Fig. 6c-e). Taking into account previous studies showing that LPC-DHA is a primary substrate for MFSD2A [16] and FABP5 contributes to the intracellular transport of NE-DHA, which penetrates the luminal membrane of BMECs [14], our results suggest that MFSD2A may also serve as a transporter for extracellular NE-DHA.

Considering our in vitro results that siRNA-mediated knockdown of MFSD2A decreased brain endothelial uptake of [^{14}C]DHA, another possible explanation for the decrease in DHA uptake in the aged brain is that MFSD2A protein expression on the luminal surface of the microvasculature is down-regulated. MFSD2A is expressed in CNS

vasculature in the entire brain [37]. In line with this concept, our results showed that the microvascular expression of MFSD2A is down-regulated in the 12- and 24-month-old brains (Fig. 7) which is consistent with the reduced [^{14}C]DHA uptake by the whole brain (Fig. 1a). In addition, we measured mRNA expression levels of MFSD2A in brain microvessels from 24-month-old mice and confirmed that they were down-regulated compared with those from 2-month-old mice (S1 Fig.). Our data is supported by a previous study demonstrating that MFSD2A protein expression levels of the brain endothelial cells decreased in aged mice [38]. Therefore, it is possible that FABP5 up-regulation in 12- and 24-month-old mice (Fig. 3) may play a crucial role in aged mice for maintaining brain DHA levels and regulating brain uptake of DHA. Further studies are required to clarify the mechanisms underlying age-related changes in MFSD2A and FABP5 expression. A limitation of our study is that we were forced to measure the expression levels of MFSD2A in microvessels obtained from the whole brain, but not the brain regions of interest due to a low yield of isolated microvessels from each brain region. We observed the regional variations of brain uptake of [^{14}C]DHA with aging (Fig. 1b-g). Therefore, the age-related decrease in the expression levels of MFSD2A in the olfactory bulb, hippocampus, and thalamus and hypothalamus might be greater than in the other regions. In addition, we cannot exclude the possibility that localization patterns of MFSD2A in BMECs are altered with aging, leading to impaired NE-DHA transport activity of MFSD2A. Future studies may shed light on the regional variations of the age-related down-regulation and/or impaired functional activity of MFSD2A.

There are technical limitations in this study. First, a transcardiac brain perfusion technique was optimized for fatty acids by Pan et al. [14]. Since the perfusion rate was given at 2 mL/min, without adding BSA in the perfusate, the cerebral vascular pressure was insufficient. The perfusion rate of 10 mL/min is more appropriate. The brain/perfusate ratio of [^{14}C]DHA in the present study is lower than that reported by Pan et al. [14]. Therefore, our results of the Kin value and/or brain/perfusate ratio of [^{14}C]DHA may be underestimated or not accurate due to insufficient cerebral vascular pressure caused by a lower perfusion rate. Of note, we found that the aged brain exhibited a decreased uptake of [^{14}C]DHA compared with the young brain even if the flow rate of 2 mL/min did not give sufficient cerebral vascular pressure. Therefore, further studies are needed to determine whether a higher perfusion rate (10 mL/min) would affect the obtained results. Second, in this study, we could not evaluate how the [^{14}C]DHA was processed. Therefore, it is unclear whether [^{14}C]DHA was transported across the BBB in the non-esterified form. Previous works using HPLC analysis showed that the majority of radioactivity was detected in total phospholipid fractions of [^{14}C]DHA-perfused brains corresponding to DHA in the perfusate and any

radiolabeled compounds associated with DHA were not detected after a 40 s brain perfusion [39,40]. In addition, capillary depletion of brain homogenates after brain perfusion showed that less than 10% of [^{14}C]DHA remained in endothelial cells of the brain vasculature [40]. Therefore, we considered that [^{14}C]DHA was probably transported across the BBB as NE-DHA. However, we cannot exclude the possibility that [^{14}C]DHA derivatives are also quantified.

Several studies have demonstrated the relationship between brain DHA levels and events that occur with increased age. For example, patients with dementia have decreased brain DHA [30,41], and DHA supplementation improves the accumulation of brain DHA in a dementia mouse model [42,43]. Further, higher DHA intake is inversely correlated with the relative risk of AD [44]. In addition, a decrease in DHA levels likely contributes to the cognitive impairment that is observed in individuals with AD [18]. MFSD2A expression levels in brain endothelial cells in AD patients were lower than those in healthy older adults [38], suggesting that insufficient transport of DHA across the BBB is one of the contributing factors underlying lower brain DHA levels in AD [45]. Indeed, the BBB transport of DHA is decreased in a mouse model for AD [46]. Notably, although 10–12 month-old mice do not exhibit cognitive impairment [47], we demonstrated a decrease in DHA transport across the BBB in the hippocampus at this age in the present study. Together, these findings suggest that deficient DHA transport across the BBB precedes age-related cognitive decline. Several clinical studies have indicated that DHA supplementation has benefits for cognitive health in aging [48], but the required oral dose of DHA supplementation for brain delivery remains unknown. The possibility that aging lowers the transport activity of DHA at the BBB should be considered when DHA supplementation is offered to older adults. An effective intervention that delivers DHA to the brain may be successful in improving brain DHA bioavailability in older adults.

Conclusions

In conclusion, we report reduced brain uptake of [^{14}C]DHA in middle-aged (12-month-old) and aged (24-month-old) mice. Furthermore, we demonstrated that [^{14}C]DHA is transported across the BBB by a saturable transport system and that MFSD2A partly mediates brain endothelial uptake of [^{14}C]DHA. Finally, we observed a decreased expression of MFSD2A in microvessels obtained from middle-aged and aged mice.

Therefore, these findings suggest that the reduced brain uptake of DHA in middle-aged and aged mice could be attributable to age-related down-regulation of MFSD2A, but not FABP5. These results suggest that improving deficient DHA transport across the BBB in older adults by DHA supplementation could be a new approach to enhance the therapeutic efficiency of treatment for AD or age-related cognitive decline.

Figures

Fig.1

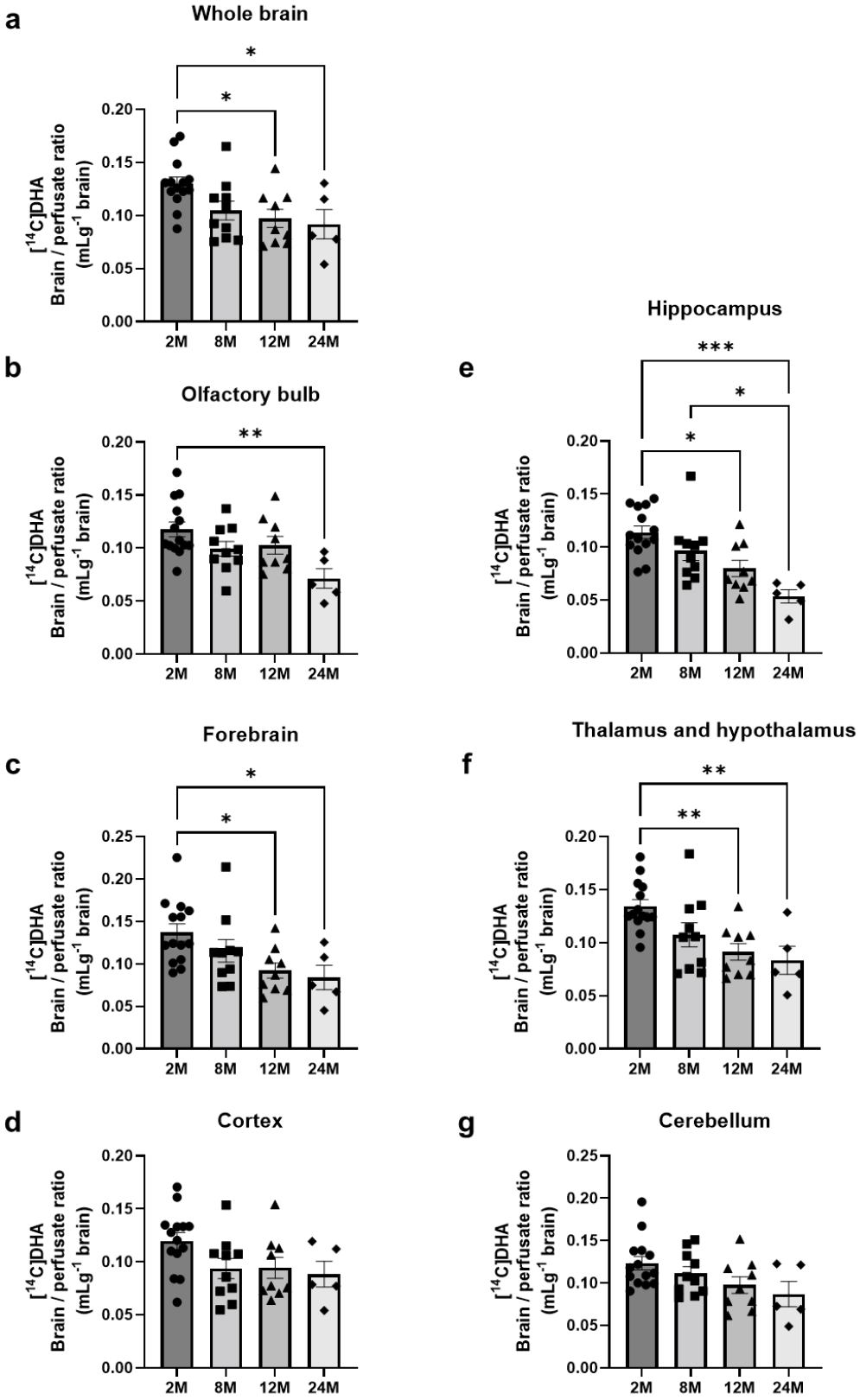

Fig 1. Brain uptake of [^{14}C]docosahexaenoic acid (DHA) in 2-, 8-, 12-, and 24-month-old mice.

Brain/perfusate ratio of [^{14}C]DHA as NE-DHA in the whole brain (a), olfactory bulb (b), forebrain (c), cortex (d), hippocampus (e), thalamus and hypothalamus (f), and cerebellum (g) of 2- (2M), 8- (8M), 12- (12M), and 24-month-old (24M) mice following in situ transcardiac brain perfusion for 1 min at 2 mL/min. Data are shown as the mean ± standard error of the mean (n = 4 - 15). Each closed symbol represents an individual value. *P < 0.05, **P < 0.01, ***P < 0.001, significantly different from 2-month-old group.

Fig.2

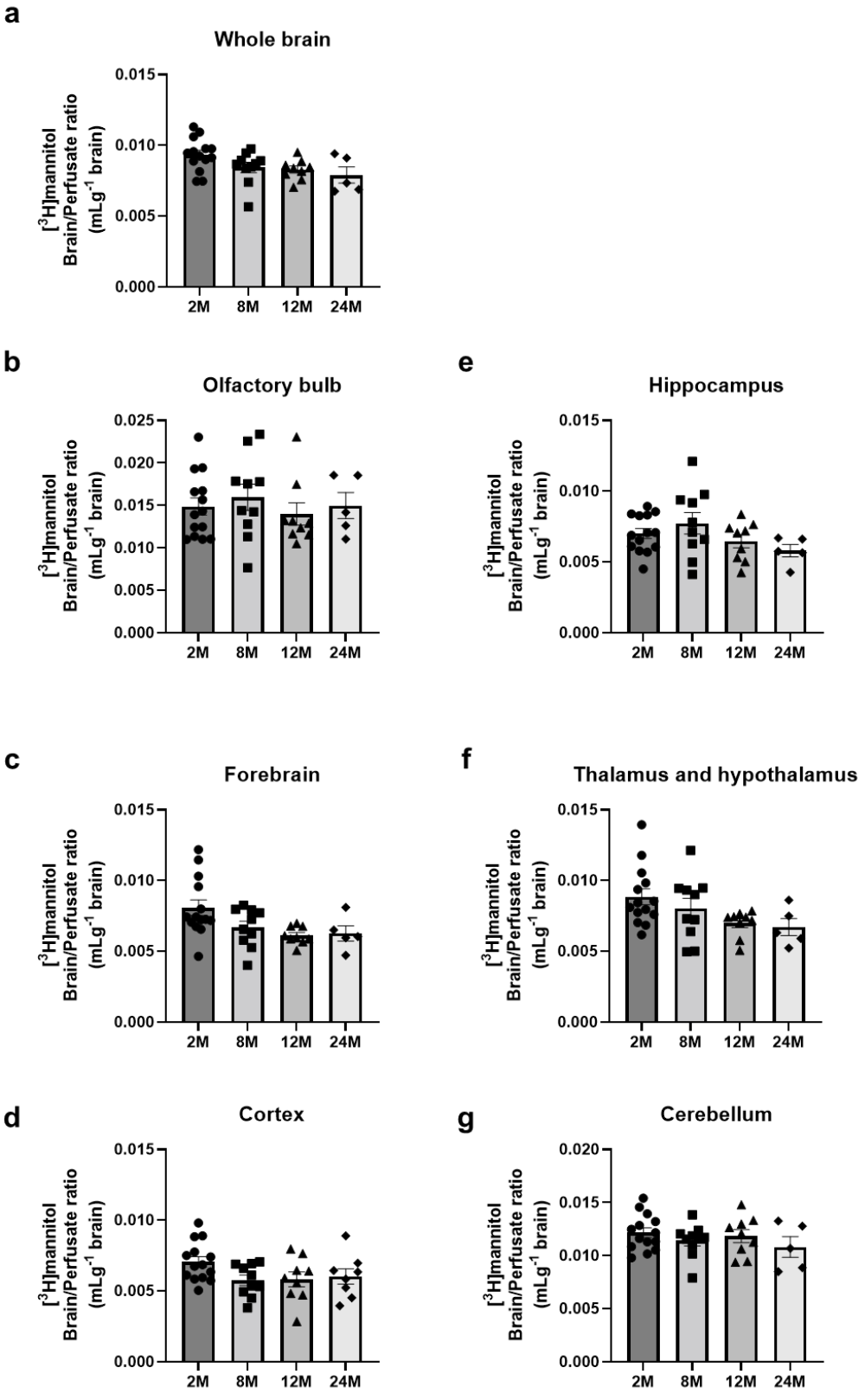
a
Whole brain
[3H]mannitol Brain/Perfusate ratio (mLg-1 brain)
0.015
0.010
0.005
0.000
2M
8M
12M
24M
b
Olfactory bulb
0.025
0.020
0.015
0.010
0.005
0.000
e
Hippocampus
c
Forebrain
f
Thalamus and hypothalamus
d
Cortex
g
Cerebellum
0.020

Fig 2. Brain uptake of [^{3}H]mannitol in 2-, 8-, 12-, and 24-month-old mice.

Brain/perfusate ratio of [^{3}H]mannitol in the whole brain (a), olfactory bulb (b), forebrain (c), cortex (d), hippocampus (e), thalamus and hypothalamus (f), and cerebellum (g), of 2- (2M), 8- (8M), 12- (12M), and 24-month-old (24M) mice following in situ transcardiac brain perfusion for 1 min at 2 mL/min. Data are shown as the mean ± standard error of the mean (n = 4 - 15). Each closed symbol represents an individual value.

Fig.3

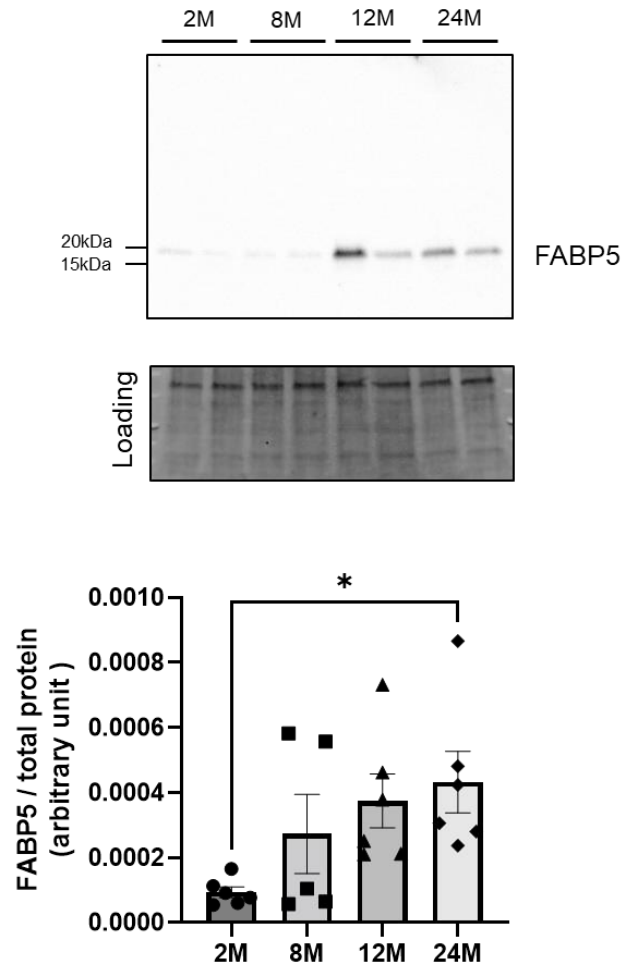

Fig 3. FABP5 expression levels in brain microvessels from 2-, 8-, 12-, and 24-month-old mice.

Representative Western blot images and band intensities quantified by densitometry in 2- (2M), 8- (8M), 12- (12M), and 24-month-old (24M) mice. Total protein levels measured by Stain-free technology were used as the loading controls for total protein normalization. Bars indicate the mean ± standard error of the mean (n = 5 - 6). Each closed symbol represents an individual value. *P < 0.05, significantly different from the 2-month-old group.

Abbreviations: FABP5, fatty acid-binding protein 5

Fig.4

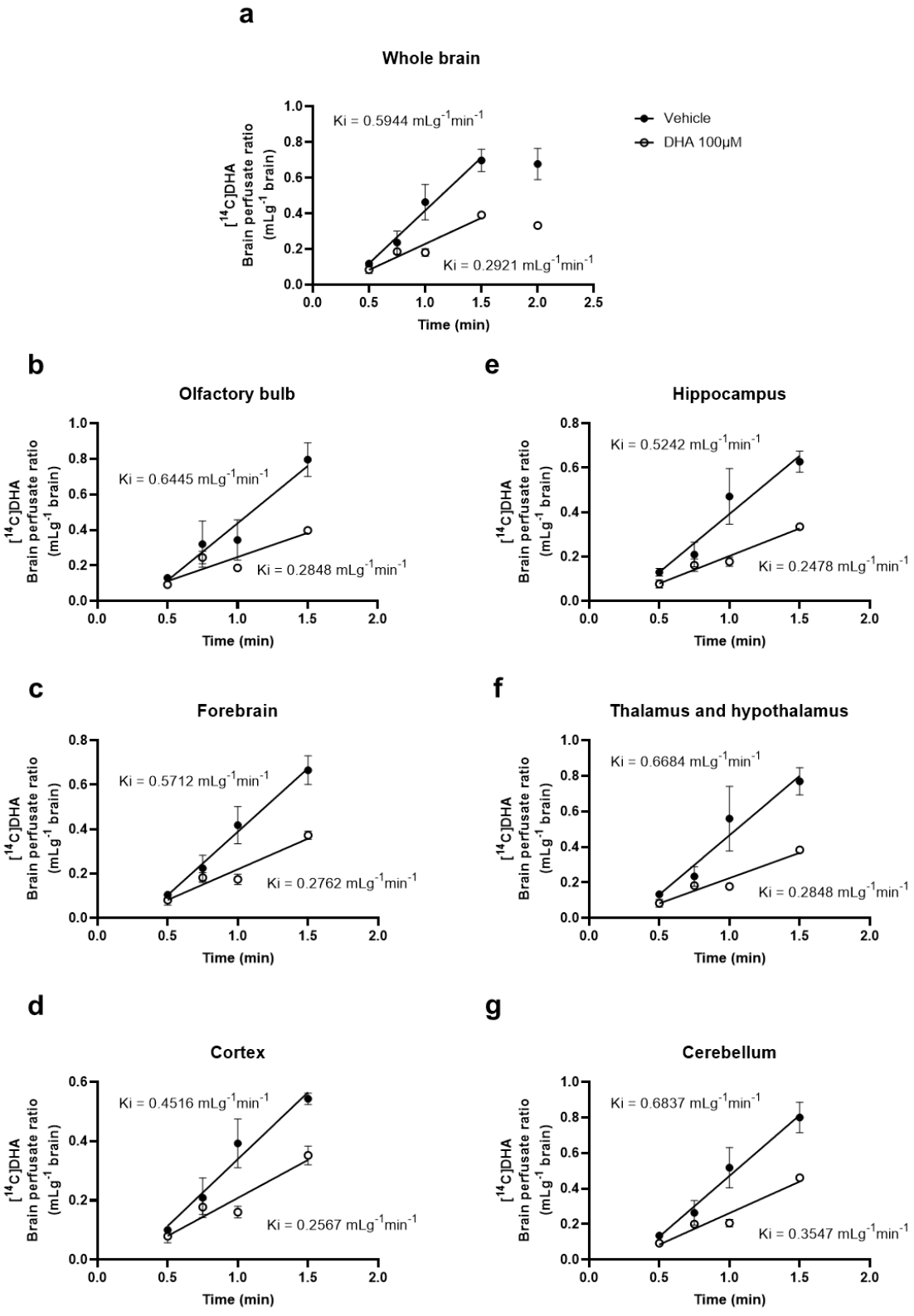
a
Whole brain
Ki = 0.5944 mLg-1min-1
Ki = 0.2921 mLg-1min-1
Vehicle
DHA 100μM
[14C]DHA Brain perfusate ratio (mLg-1 brain)
Time (min)
b
Olfactory bulb
Ki = 0.6445 mLg-1min-1
Ki = 0.2848 mLg-1min-1
e
Hippocampus
Ki = 0.5242 mLg-1min-1
Ki = 0.2478 mLg-1min-1
c
Forebrain
Ki = 0.5712 mLg-1min-1
Ki = 0.2762 mLg-1min-1
f
Thalamus and hypothalamus
Ki = 0.6684 mLg-1min-1
Ki = 0.2848 mLg-1min-1
d
Cortex
Ki = 0.4516 mLg-1min-1
Ki = 0.2567 mLg-1min-1
g
Cerebellum
Ki = 0.6837 mLg-1min-1
Ki = 0.3547 mLg-1min-1

Fig 4. Brain uptake rate of [^{14}C]docosahexaenoic acid (DHA) in the whole brain and each brain region.

Brain uptake of [^{14}C]DHA is expressed as brain/perfusate ratios following *in situ* transcardiac brain perfusion at 2 mL/min in 2-month-old mice. Linear regression of the mean brain/perfusate ratio of [^{14}C]DHA (mL/g brain) over perfusion time (0.5, 0.75, 1, and 1.5 min) in whole brain (a), olfactory bulb (b), forebrain (c), cortex (d), hippocampus (e), thalamus and hypothalamus (f), and cerebellum (g) of vehicle and DHA 100 μM groups yielded Ki (mL/g brain • min^{-1}). Ki represents the brain uptake rate of [^{14}C]DHA. Data are shown as the mean ± standard error of the mean (n = 3/time point).

Fig. 5

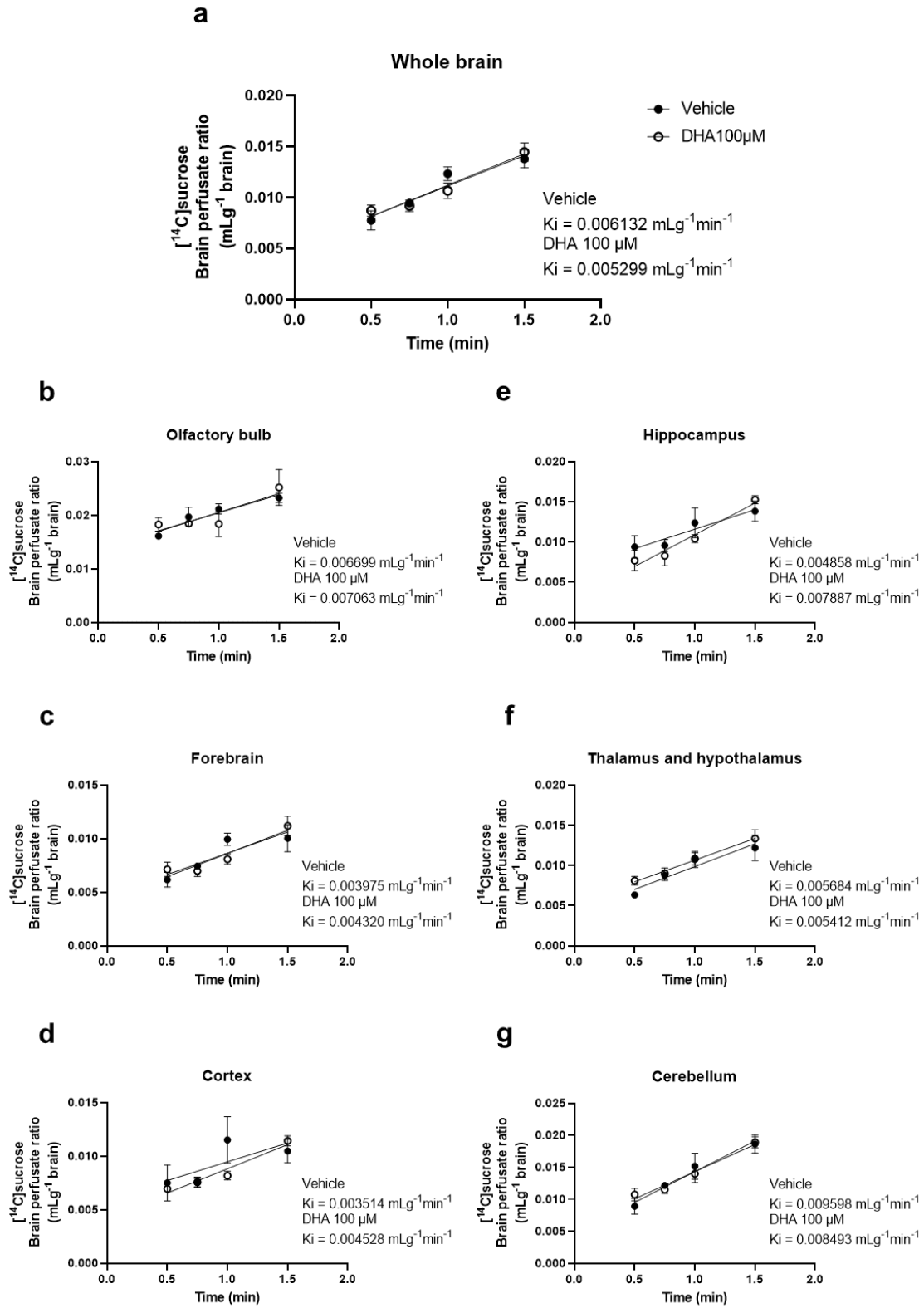
a
Whole brain
[14C]sucrose Brain perfusate ratio (mLg-1 brain)
Time (min)
Vehicle
DHA100μM
Vehicle
Ki = 0.006132 mLg-1min-1
DHA 100 μM
Ki = 0.005299 mLg-1min-1
b
Olfactory bulb
Vehicle
Ki = 0.006699 mLg-1min-1
DHA 100 μM
Ki = 0.007063 mLg-1min-1
e
Hippocampus
Vehicle
Ki = 0.004858 mLg-1min-1
DHA 100 μM
Ki = 0.007887 mLg-1min-1
c
Forebrain
Vehicle
Ki = 0.003975 mLg-1min-1
DHA 100 μM
Ki = 0.004320 mLg-1min-1
f
Thalamus and hypothalamus
Vehicle
Ki = 0.005684 mLg-1min-1
DHA 100 μM
Ki = 0.005412 mLg-1min-1
d
Cortex
Vehicle
Ki = 0.003514 mLg-1min-1
DHA 100 μM
Ki = 0.004528 mLg-1min-1
g
Cerebellum
Vehicle
Ki = 0.009598 mLg-1min-1
DHA 100 μM
Ki = 0.008493 mLg-1min-1

Fig 5. Brain uptake rate of [^{14}C]sucrose in the whole brain and individual brain regions.

Brain uptake of [^{14}C]sucrose is expressed as brain/perfusate ratios following *in situ* transcardiac perfusion at 2 mL/min in 2-month-old mice. Linear regression of the mean brain/perfusate ratio of [^{14}C]sucrose over perfusion time (0.5, 0.75, 1, and 1.5 min) in whole brain (a), olfactory bulb (b), forebrain (c), cortex (d), hippocampus (e), thalamus and hypothalamus (f), and cerebellum (g) of vehicle and DHA 100 μM groups yielded Ki (mL/g brain • min^{-1}). Ki represents the brain uptake rate of [^{14}C]sucrose. Data are shown as the mean ± standard error of the mean (n = 3/time point).

Fig. 6

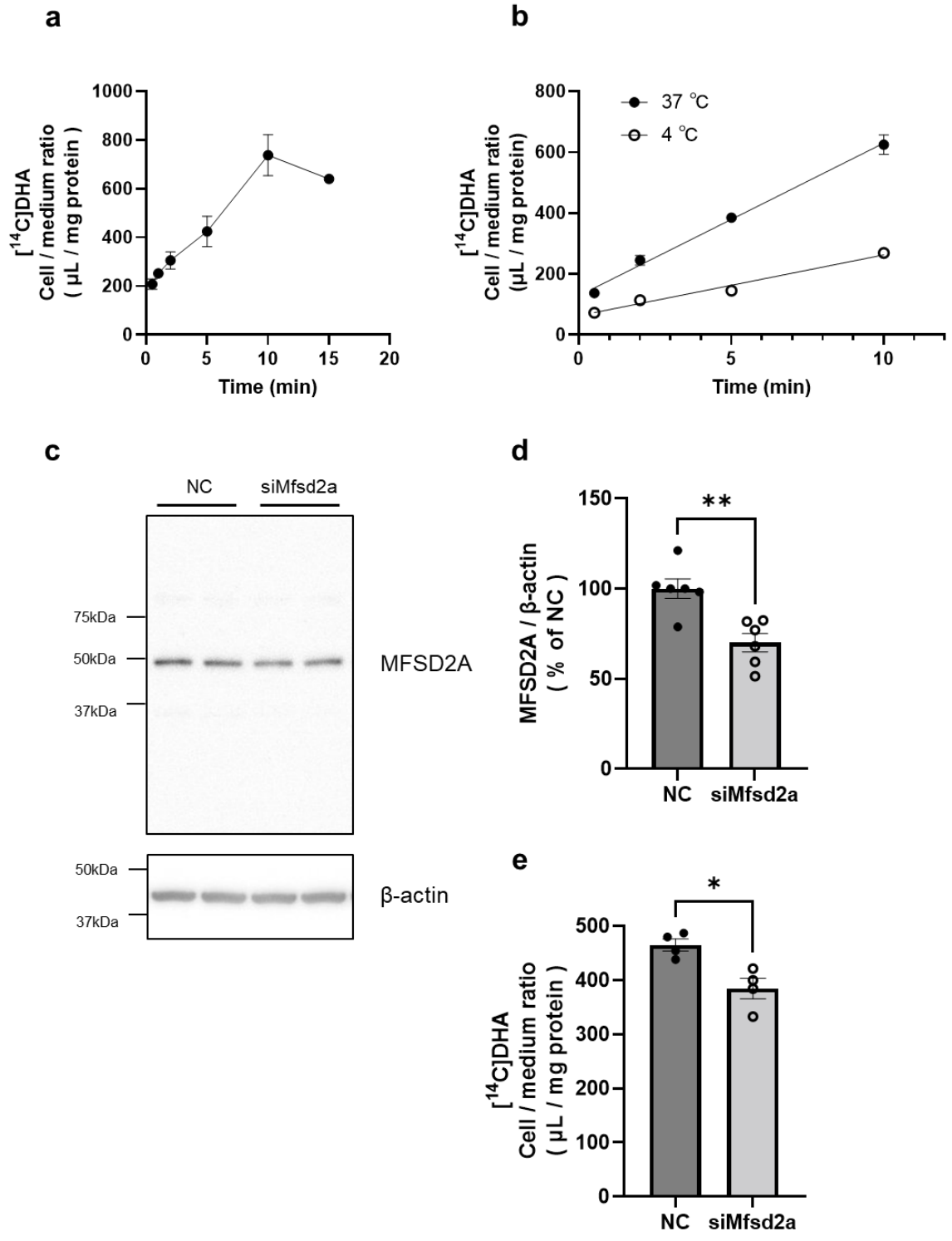
a
[14C]DHA
Cell / medium ratio
(µL / mg protein)
Time (min)
b
37 ℃
4 ℃
[14C]DHA
Cell / medium ratio
(µL / mg protein)
Time (min)
c
NC
siMfsd2a
75kDa
50kDa
37kDa
MFSD2A
50kDa
37kDa
β-actin
d
MFSD2A / β-actin
(% of NC)
**
NC
siMfsd2a
e
[14C]DHA
Cell / medium ratio
(µL / mg protein)
*
NC
siMfsd2a

Fig 6. Cellular uptake of [^{14}C]docosahexaenoic acid (DHA) by RBECs transfected with MFSD2A siRNA.

(a)Time course of cellular uptake of [^{14}C]DHA (μL/mg protein) by intact RBECs (n = 4 - 6). (b) Time course of cellular uptake of [^{14}C]DHA (μL/mg protein) by intact RBECs at 37°C and 4°C (n = 3). (c, d) Effect of Mfsd2a siRNA transfection on MFSD2A protein expression in RBECs. RBECs were treated with transfection reagent and 50 nM Mfsd2a siRNA for 48 h. Panel (c) shows representative Western blot images. Panel (d) shows the quantified band intensities corrected by β-Actin as the loading control in RBECs transfected with negative control siRNA (NC) and Mfsd2a siRNA (siMfsd2a). (n = 6) (e) Cellular uptake of [^{14}C]DHA by RBECs transfected with negative control (NC) and Mfsd2a siRNA (n = 4). The cellular uptake of [^{14}C]DHA for 2 min is expressed as cell/medium ratio (μL/mg protein). Data are shown as the mean ± standard error of the mean. Each closed symbol represents an individual value. *P < 0.05, **P < 0.01, significantly different from negative control siRNA-transfected RBECs.

Abbreviation: RBECs, rat brain endothelial cells. MFSD2A, major facilitator superfamily domain-containing protein 2A

Fig. 7

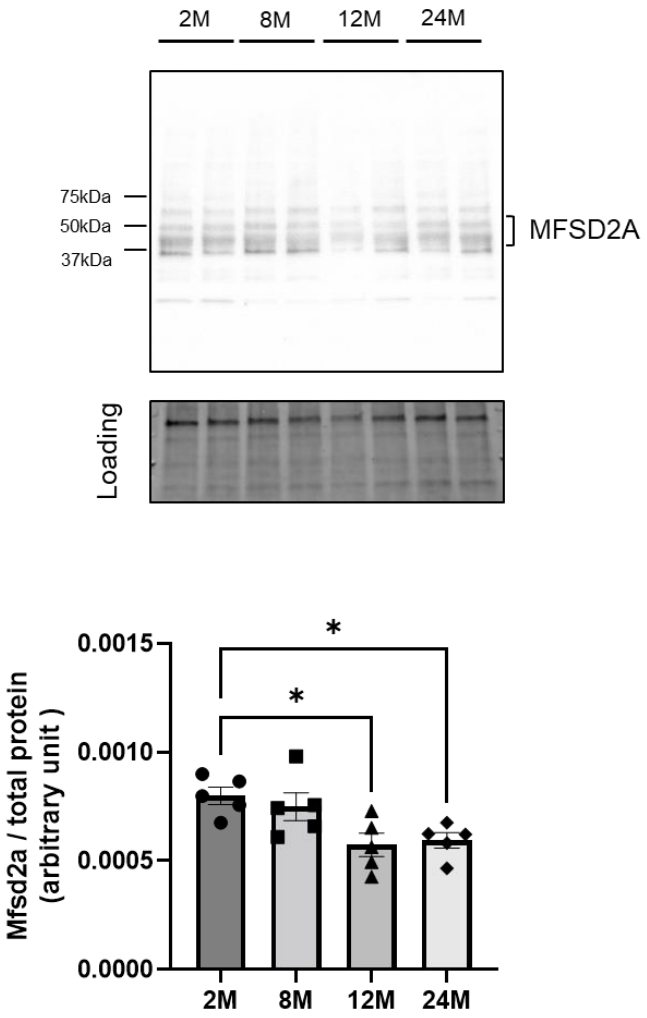

Fig 7. MFSD2A expression levels in brain microvessels from 2-, 8-, 12-, and 24-month-old mice.

Representative Western blot images and band intensities quantified by densitometry in 2- (2M), 8- (8M), 12- (12M), and 24-month-old (24M) mice. Total protein levels measured by Stain-free technology were used as the loading controls for total protein normalization. Bars indicate the mean ± standard error of the mean (n = 5 - 6). Each closed symbol represents an individual value. *P < 0.05, significantly different from 2-month-old group.

Supplementary Figure

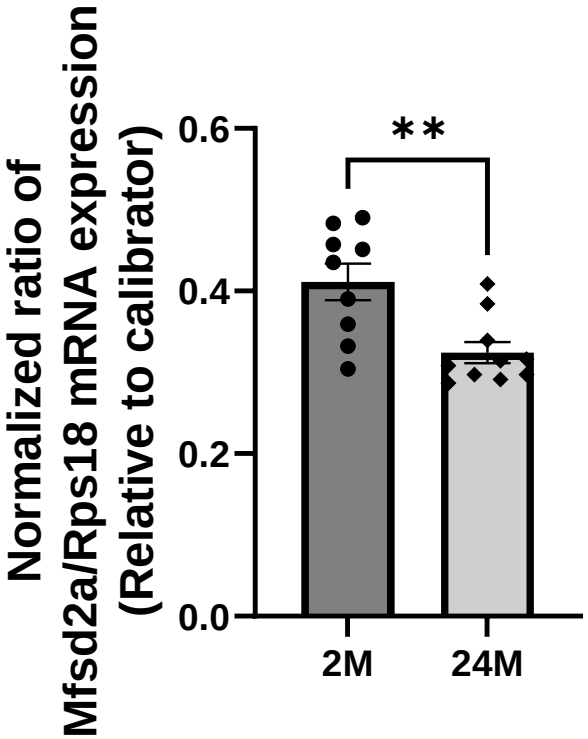

S1 Fig. The mRNA expression levels of Mfsd2a in brain microvessels from 2- and 24-month-old mice.

The mRNA expression levels for Mfsd2a in brain microvessels from 2- (2M) and 24-month-old (24M) mice were quantified by real-time quantitative PCR. Data are shown as the mean ± standard error of the mean. Each closed symbol represents an individual value (n = 9 - 10). **P < 0.01, significantly different from 2-month-old group.

References

1. Tiani KA, Stover PJ, Field MS. The role of brain barriers in maintaining brain vitamin levels. Annu Rev Nutr. 2019;39: 147-173. doi: 10.1146/annurev-nutr-082018-124235.

2. Liu WY, Wang ZB, Zhang LC, Wei X, Li L. Tight junction in blood-brain barrier: an overview of structure, regulation, and regulator substances. CNS Neurosci Ther. 2012;18: 609-615. doi: 10.1111/j.1755-5949.2012.00340.x.

3. Campos-Bedolla P, Walter FR, Veszelka S, Deli MA. Role of the blood-brain barrier in the nutrition of the central nervous system. Arch Med Res. 2014;45: 610-638. doi: 10.1016/j.arcmed.2014.11.018.

4. Zlokovic BV. The blood-brain barrier in health and chronic neurodegenerative disorders. Neuron. 2008;57: 178-201. doi: 10.1016/j.neuron.2008.01.003.

5. Varatharaj A, Galea I. The blood-brain barrier in systemic inflammation. Brain Behav Immun. 2017;60: 1-12. doi: 10.1016/j.bbi.2016.03.010.

6. Saedi E, Gheini MR, Faiz F, Arami MA. Diabetes mellitus and cognitive impairments. World J Diabetes. 2016;7: 412-422. doi: 10.4239/wjd.v7.i17.412.

7. Lacombe RJS, Chouinard-Watkins R, Bazinet RP. Brain docosahexaenoic acid uptake and metabolism. Mol Aspects Med. 2018;64: 109-134. doi: 10.1016/j.mam.2017.12.004.

8. Barceló-Coblijn G, Murphy EJ. Alpha-linolenic acid and its conversion to longer chain n-3 fatty acids: benefits for human health and a role in maintaining tissue n-3 fatty acid levels. Prog Lipid Res. 2009;48: 355-374. doi: 10.1016/j.plipres.2009.07.002.

9. Leikin-Frenkel A, Liraz-Zaltsman S, Hollander KS, Atrakchi D, Ravid O, Rand D, et al. Dietary alpha linolenic acid in pregnant mice and during weaning increases brain docosahexaenoic acid and improves recognition memory in the offspring. J Nutr Biochem. 2021;91: 108597. doi: 10.1016/j.jnutbio.2021.108597.

10. Echeverría F, Valenzuela R, Catalina Hernandez-Rodas M, Valenzuela A. Docosahexaenoic acid (DHA), a fundamental fatty acid for the brain: new dietary sources.

Prostaglandins Leukot Essent Fatty Acids. 2017;124: 1-10. doi: 10.1016/j.plefa.2017.08.001.

11. Goodman DS, Shafrir E. The interaction of human low density lipoproteins with long-chain fatty acid anions. J Am Chem Soc. 1959;81: 364-370. doi: 10.1021/ja01511a023.

12. Ouellet M, Emond V, Chen CT, Julien C, Bourasset F, Oddo S, et al. Diffusion of docosahexaenoic and eicosapentaenoic acids through the blood–brain barrier: an in situ cerebral perfusion study. Neurochem Int. 2009;55: 476-482. doi: 10.1016/j.neuint.2009.04.018.

13. Zhang W, Chen R, Yang T, Xu N, Chen J, Gao Y, et al. Fatty acid transporting proteins: roles in brain development, aging, and stroke. Prostaglandins Leukot Essent Fatty Acids. 2018;136: 35-45. doi: 10.1016/j.plefa.2017.04.004.

14. Pan Y, Scanlon MJ, Owada Y, Yamamoto Y, Porter CJ, Nicolazzo JA. Fatty acid-binding Protein 5 facilitates the blood-brain barrier transport of docosahexaenoic acid. Mol Pharm. 2015;12: 4375-4385. doi: 10.1021/acs.molpharmaceut.5b00580.

15. Browning LM, Walker CG, Mander AP, West AL, Madden J, Gambell JM, et al. Incorporation of eicosapentaenoic and docosahexaenoic acids into lipid pools when given as supplements providing doses equivalent to typical intakes of oily fish. Am J Clin Nutr. 2012;96: 748-758. doi: 10.3945/ajcn.112.041343.

16. Nguyen LN, Ma D, Shui G, Wong P, Cazenave-Gassiot A, Zhang X, et al. Mfsd2a is a transporter for the essential omega-3 fatty acid docosahexaenoic acid. Nature. 2014;509: 503-506. doi: 10.1038/nature13241.

17. Chen CT, Kitson AP, Hopperton KE, Domenichiello AF, Trépanier MO, Lin LE, et al. Plasma non-esterified docosahexaenoic acid is the major pool supplying the brain. Sci Rep. 2015;5: 15791. doi: 10.1038/srep15791.

18. Mohajeri MH, Troesch B, Weber P. Inadequate supply of vitamins and DHA in the elderly: implications for brain aging and Alzheimer-type dementia. Nutrition. 2015;31: 261-275. doi: 10.1016/j.nut.2014.06.016.

19. Conquer JA, Holub BJ. Effect of supplementation with different doses of DHA on the levels of circulating DHA as non-esterified fatty acid in subjects of Asian Indian background. J Lipid Res. 1998;39: 286-292. doi: 10.1016/S0022-2275(20)33890-6.

20. Jicha GA, Markesbery WR. Omega-3 fatty acids: potential role in the management of early Alzheimer's disease. Clin Interv Aging. 2010;5: 45-61. doi: 10.2147/cia.s5231.

21. Mooradian AD, Haas MJ, Chehade JM. Age-related changes in rat cerebral occludin and zonula occludens-1 (ZO-1). Mech Ageing Dev. 2003;124: 143-146. doi: 10.1016/s0047-6374(02)00041-6.

22. Goodall EF, Wang C, Simpson JE, Baker DJ, Drew DR, Heath PR, et al. Age-associated changes in the blood-brain barrier: comparative studies in human and mouse. Neuropathol Appl Neurobiol. 2018;44: 328-340. doi: 10.1111/nan.12408.

23. Banks WA, Niehoff ML, Zalcman SS. Permeability of the mouse blood-brain barrier to murine interleukin-2: predominance of a saturable efflux system. Brain Behav Immun. 2004;18: 434-442. doi: 10.1016/j.bbi.2003.09.013.

24. Yousif S, Marie-Claire C, Roux F, Scherrmann JM and Declèves X. Expression of drug transporters at the blood-brain barrier using an optimized isolated rat brain microvessel strategy. Brain Res. 2007;1134: 1-11. doi: 10.1016/j.brainres.2006.11.089.

25. Takata F, Dohgu S, Yamauchi A, Matsumoto J, Machida T, Fujishita K, et al. In vitro blood-brain barrier models using brain capillary endothelial cells isolated from neonatal and adult rats retain age-related barrier properties. PLOS ONE. 2013;8: e55166. doi: 10.1371/journal.pone.0055166.

26. Noorani B, Chowdhury EA, Alqahtani F, Ahn Y, Patel D, Al-Ahmad A, et al. LC-MS/MS-based in vitro and in vivo investigation of blood-brain barrier integrity by simultaneous quantitation of mannitol and sucrose. Fluids Barriers CNS. 2020;17: 61. doi: 10.1186/s12987-020-00224-1.

27. Kranz J, Petzinger E, Geyer J. Brain penetration of the OAB drug trospium chloride is not increased in aged mice. World J Urol. 2013;31: 219-224. doi: 10.1007/s00345-011-0803-z.

28. Chan JP, Wong BH, Chin CF, Galam DLA, Foo JC, Wong LC, et al. The lysolipid transporter Mfsd2a regulates lipogenesis in the developing brain. PLOS Biol. 2018;16: e2006443. doi: 10.1371/journal.pbio.2006443.

29. Tachikawa M, Akanuma SI, Imai T, Okayasu S, Tomohiro T, Hatanaka Y, et al. Multiple cellular transport and binding processes of unesterified docosahexaenoic acid in outer blood-retinal barrier retinal pigment epithelial cells. Biol Pharm Bull. 2018;41: 1384-1392. doi: 10.1248/bpb.b18-00185.

30. Yuki D, Sugiura Y, Zaima N, Akatsu H, Takei S, Yao I, et al. DHA-PC and PSD-95 decrease after loss of synaptophysin and before neuronal loss in patients with Alzheimer's disease. Sci Rep.. Sci Rep. 2014;4: 7130. doi: 10.1038/srep07130.

31. Low YL, Jin L, Morris ER, Pan Y, Nicolazzo JA. Pioglitazone increases blood-brain barrier expression of fatty acid-binding Protein 5 and docosahexaenoic acid trafficking into the brain. Mol Pharm. 2020;17: 873-884. doi: 10.1021/acs.molpharmaceut.9b01131.

32. Rapoport SI, Ohno K, Pettigrew KD. Blood-brain barrier permeability in senescent rats. J Gerontol. 1979;34: 162-169. doi: 10.1093/geronj/34.2.162.

33. Montagne A, Barnes SR, Sweeney MD, Halliday MR, Sagare AP, Zhao Z, et al. Blood-brain barrier breakdown in the aging human hippocampus. Neuron. 2015;85: 296-302. doi: 10.1016/j.neuron.2014.12.032.

34. Verheggen ICM, de Jong JJA, van Boxtel MPJ, Gronenschild E, Palm WM, Postma AA, et al. Increase in blood-brain barrier leakage in healthy, older adults. Geroscience. 2020;42: 1183-1193. doi: 10.1007/s11357-020-00211-2.

35. Pélerin H, Jouin M, Lallemand MS, Alessandri JM, Cunnane SC, Langelier B, et al. Gene expression of fatty acid transport and binding proteins in the blood-brain barrier and the cerebral cortex of the rat: differences across development and with different DHA brain status. Prostaglandins Leukot Essent Fatty Acids. 2014;91: 213-220. doi: 10.1016/j.plefa.2014.07.004.

36. Pu L, Igbavboa U, Wood WG, Roths JB, Kier AB, Spener F, et al. Expression of fatty acid binding proteins is altered in aged mouse brain. Mol Cell Biochem. 1999;198: 69-78. doi: 10.1023/a:1006946027619.

37. Ben-Zvi A, Lacoste B, Kur E, Andreone BJ, Mayshar Y, Yan H, et al. Mfsd2a is critical for the formation and function of the blood-brain barrier. Nature. 2014;509: 507-511. doi: 10.1038/nature13324.

38. Zhao L, Li Z, Vong JSL, Chen X, Lai HM, Yan LYC, et al. Pharmacologically reversible zonation-dependent endothelial cell transcriptomic changes with neurodegenerative disease associations in the aged brain. Nat Commun. 2020;11: 4413. doi: 10.1038/s41467-020-18249-3.

39. Chen CT, Liu Z, Ouellet M, Calon F and Bazinet RP. Rapid beta-oxidation of eicosapentaenoic acid in mouse brain: an in situ study. Prostaglandins Leukot Essent Fatty Acids. 2009;80: 157-63. doi: 10.1016/j.plefa.2009.01.005.

40. Ouellet M, Emond V, Chen CT, Julien C, Bourasset F, Oddo S, et al. Diffusion of docosahexaenoic and eicosapentaenoic acids through the blood–brain barrier: An in situ cerebral perfusion study. Neurochem Int. 2009:55; 476-482. doi: 10.1016/j.neuint.2009.04.018.

41. Snowden SG, Ebshiana AA, Hye A, An Y, Pletnikova O, O'Brien R, et al. Association between fatty acid metabolism in the brain and Alzheimer disease neuropathology and cognitive performance: A nontargeted metabolomic study. PLOS Med. 2017;14: e1002266. doi: 10.1371/journal.pmed.1002266.

42. Takeyama E, Islam A, Watanabe N, Tsubaki H, Fukushima M, Mamun MA, et al. Dietary intake of green nut oil or DHA ameliorates DHA distribution in the brain of a mouse model of dementia accompanied by memory recovery. Nutrients. 2019;11. doi: 10.3390/nu11102371.

43. Islam A, Takeyama E, Mamun MA, Sato T, Horikawa M, Takahashi Y, et al. Green nut oil or DHA supplementation restored decreased distribution levels of DHA containing phosphatidylcholines in the brain of a mouse model of dementia. Metabolites. 2020;10. doi: 10.3390/metabo10040153.

44. Freund-Levi Y, Eriksdotter-Jönhagen M, Cederholm T, Basun H, Faxén-Irving G, Garlind A, et al. Omega-3 fatty acid treatment in 174 patients with mild to moderate Alzheimer disease: OmegAD study: a randomized double-blind trial. Arch Neurol. 2006;63: 1402-1408. doi: 10.1001/archneur.63.10.1402.

45. Calon F. Omega-3 polyunsaturated fatty acids in Alzheimer's disease: key questions and partial answers. Curr Alzheimer Res. 2011;8: 470–478. doi: 10.2174/156720511796391881.

46. Pan Y, Choy KHC, Marriott PJ, Chai SY, Scanlon MJ, Porter CJH, et al. Reduced blood-brain barrier expression of fatty acid-binding protein 5 is associated with increased vulnerability of APP/PS1 mice to cognitive deficits from low omega-3 fatty acid diets. J Neurochem. 2018;144: 81-92. doi: 10.1111/jnc.14249.

47. Benice TS, Rizk A, Kohama S, Pfankuch T, Raber J. Sex-differences in age-related cognitive decline in C57BL/6J mice associated with increased brain microtubule-associated protein 2 and synaptophysin immunoreactivity. Neuroscience. 2006;137: 413-423. doi: 10.1016/j.neuroscience.2005.08.029.

48. Yurko-Mauro K, McCarthy D, Rom D, Nelson EB, Ryan AS, Blackwell A, et al. Beneficial effects of docosahexaenoic acid on cognition in age-related cognitive decline. Alzheimers Dement. 2010;6: 456-464. doi: 10.1016/j.jalz.2010.01.013.

Chapter 2: Age-related dynamic changes in the blood–brain barrier with cellular senescence in correlation with microglia activation

Introduction

The blood–brain barrier (BBB), which is formed by brain microvessel endothelial cells (BMECs), astrocytes, and pericytes, restricts transport of substances in blood for maintaining homeostasis of the central nervous system (CNS) [1]. BMECs, which are sealed with tight junctions (Tjs), restrict paracellular transport of substances in blood [2]. In addition, adherens junctions-associated proteins (Ajs), such as cadherin proteins, contribute to holding the cells together, providing the tissue structural support, and are essential for formation of Tjs [3]. Furthermore, major facilitator superfamily domain-containing protein-2a (MFSD2A) helps maintain a low-level permeability of BBB to regulate transcytosis in BMECs [4]. For maintenance of BBB functions, astrocytes and pericytes contribute to the formation of Tjs in BMEC with cell-to-cell interaction [5–6].

Disruption of BBB is related to various neurological diseases [7–9] and precedes the onset of Alzheimer's disease [10–11]. The mechanism of neurological diseases associated with BBB disruption is increasingly recognized as neuronal damage and neuroinflammation by plasma proteins derived from peripheral blood [12–13]. Fibrinogen is a marker of BBB disruption and plays a causative role in neurologic disease through the inflammatory activation of microglia [13–15].

BBB integrity is impaired in aging [16–19], which is related to cognitive decline in vascular mild cognitive impairment [20]. Accumulation of senescent cells in brain influences microenvironment and contributes to the pathogenesis of the age-related neurodegenerative diseases [21–22]. In relation to age-related BBB disruption, accumulation of senescent vascular cells is associated with compromised BBB integrity [23]. However, whether or not cellular senescence in cerebral microvessels is related to the BBB dysfunction in vivo is unclear.

The aim of the present study was to investigate the relationship between dynamic changes in BBB integrity with aging and cellular senescence in vivo. Furthermore, we evaluated the relationship between BBB integrity and inflammatory activation of microglia.

Material and Methods

Animals

All protocols involving experimental animals were approved by the Laboratory Animal Care and Use Committee of Fukuoka University (permit number: 2113105). The 2-, 4-, 8-, 12-, and 24-month-old male C57BL/6J mice were purchased from the Charles River Laboratory (Kanagawa, Japan) and housed under a controlled temperature (22°C ± 2°C) and light/dark cycle (lights on from 7:00 to 19:00), with access to water and chow diet *ad libitum*.

Isolation of brain microvessels

Male mice aged 2, 8, 12, and 24 months were anesthetized before Dulbecco's phosphate-buffered saline (-) (D-PBS) (Wako, Osaka, Japan; 045-29795;10 mL per mouse) was infused into the left ventricle of the heart. The brain tissue was triturated using a glass homogenizer coated with 1% bovine serum albumin (BSA)-Hanks' Balanced Salt Solution (HBSS; Thermo Fisher Scientific, Waltham, MA, USA; 14185-045) in 1 mL of Buffer A (HBSS containing 1% Phosphatase Inhibitor Cocktail [ethylenediaminetetraacetic acid (EDTA) free; Nacalai Tesque, Kyoto, Japan; 07575-51], 1% Protease Inhibitor Cocktail for use with mammalian and tissue extracts [Nacalai Tesque; 25955-11], 1 mM of phenylmethylsulfonyl fluoride [PMSF; Sigma, St. Louis, MO, USA; P7626], and 15 µg/mL of deoxyribonuclease I [Sigma; D4513]) on ice. Aliquots of this suspension were used as whole brain samples for western blotting. This suspension was transferred into a 1.5-mL tube and centrifuged at 1,000 × g for 10 min at 4°C. Next, the supernatant was aspirated, and the pellet was mixed with 1 mL of 17.5% dextran (Sigma; D8821)-HBSS. The suspension was then centrifuged at 4,400 × g for 15 min at 4°C. The supernatant with a lipid layer was removed, and the pellet was resuspended in Buffer B (Buffer A containing 1% BSA). Next, the suspension was filtered using a 10-µm nylon mesh membrane to trap the residue, including microvessels, on the surface of the membrane. HBSS was then passed through the membrane to remove debris from the residue. The microvessels on the

membrane were then washed into a 1.5-mL tube with Buffer A and centrifuged at 20,000 × g for 5 min at 4°C. Finally, microvessels were obtained at the bottom of the tube and stored at −80°C until use.

Extraction of total protein from brain microvessels and the whole brain

The microvessels were homogenized in a phosphoprotein lysis buffer containing 10 mM of Tris-HCl (pH 6.8; Nacalai Tesque; 35434-34), 100 mM of NaCl (Sigma; 28-2270-5), 1 mM of EDTA (pH 8.0; Wako; 311-90075), 1 mM of EGTA (Wako; 346-01312), 10% glycerol, 1% Triton-X100 (Sigma; X100), 0.1% sodium dodecyl sulfate (SDS; Nacalai Tesque; 02873-75), 0.5% sodium deoxycholate (Sigma; D6750), 20 mM of sodium pyrophosphate (Sigma; S6422), 2 mM of sodium orthovanadate (Sigma; S6508), 1 mM of sodium fluoride (Wako; 196-01975), 1% protease inhibitor cocktail (Sigma; P2714), 1% phosphatase inhibitor cocktail 2 (Sigma; P5726), 1% Phosphatase Inhibitor Cocktail 3 (Sigma; P0044), and 1 mM of PMSF (Sigma) using an electric mixer and then sonicated on ice. In the whole brain sample, 100 µL of the suspension was added with 50 µL of 3× sample buffer containing 0.03% Bromophenol Blue (Wako; 021-02911), 6% SDS, 30% glycerol, 187.5 mM of Tris-HCl (pH 6.8) and 15% 2-Mercaptoethanol (Sigma; M3148), homogenized using an electric mixer, and sonicated on ice. Samples were centrifuged at 15,000 × g for 15 min at 4°C, and the supernatants were collected. The total protein concentration in the lysates obtained from microvessels or the whole brain was determined using the Pierce™ BCA Protein Assay Kit (Thermo Fisher Scientific; 23225).

Western blotting

Equivalent amounts of protein from each sample were electrophoretically separated on 7.5% TGX Stain-Free gradient acrylamide gels (Bio-Rad, Hercules, CA; 161-0181) or 12% TGX Stain-Free acrylamide gels (Bio-Rad; 161-0185) and transferred to low fluorescent polyvinylidene difluoride membranes (Bio-Rad; 1704274). Stain-free technology using the GelDoc go imaging system (Bio-Rad) was used for total protein normalization.

Membranes were then blocked using Blocking One (Nacalai Tesque; 03953-95) and reacted with primary antibodies overnight. After washing, the membranes were incubated in HRP-conjugated goat anti-rabbit IgG (Bio-Rad; 170-6515) or goat anti-mouse IgG (Bio-Rad; 170-6516), as appropriate. Immunoreactive bands were detected using Clarity Western ECL Substrate (Bio-Rad; 1705061). Images of the bands were digitally captured using the MultiImager II ChemiBOX (BioTools, Gunma, Japan), and band intensities were quantified using ImageJ software (National Institutes of Health Image, Bethesda, MD, USA). The relative intensity of each individual protein was expressed as the ratio of the corresponding protein to the total protein loading.

Immunofluorescence staining

Male mice aged 2, 12, and 24 months were anesthetized before D-PBS (5 mL per mouse) was infused into the left ventricle of the heart. After D-PBS infusion, the brain was fixed by infusing 4% Paraformaldehyde Phosphate Buffer Solution (PFA; Wako; 163-20145; 5mL per mouse) into the left ventricle of the heart. The brain tissues were stored in 4% PFA overnight at 4°C and replaced by 20% sucrose (Wako; 196-00015) until embedding in O.C.T. Compound (Sakura Finetek Japan, Tokyo, Japan; 4583) at −80°C. The 20-μm frozen section of brain tissue was prepared using a cryostat. The brain tissue section on a microscope slide was washed and activated at 95°C, blocked using Blocking One Histo (Nacalai Tesque; 06349-64), and reacted with primary antibodies overnight. After washing, the brain tissue section was incubated overnight with Cy3-labeled Donkey Anti-goat IgG (1:100; Jackson ImmunoResearch, West Grove, PA, USA; 705-165-147), Alexa Fluor 488-labeled Donkey Anti-rabbit IgG (1:100; Thermo Fisher Scientific; A-21206), and DyLight 488-labeled Lectin (1:200, Vector Laboratories, Newark, CA, USA; DL-1174), as appropriate. After washing, the brain tissue section was encapsulated with the VECTASHIELD Mounting Medium with DAPI (Vector Laboratories, Newark, CA, USA; H-1200). All samples were imaged under a fluorescence microscope (BZ-X710, KEYENCE, Osaka, Japan).

Primary antibodies

Primary antibodies used for western blotting and immunofluorescence staining were as follows: ZO-1 (1:400; Invitrogen/Thermo Fisher Scientific; 61-7300), occludin (1:400; Invitrogen/Thermo Fisher Scientific; 33-1500), claudin-5 (1:1,000; Invitrogen/Thermo Fisher Scientific; 35-2500), cadherin (1:1,000; Cell Signaling Technology, Danvers, MA, USA; 4068S), PDGFRβ (1:1000; Cell Signaling Technology; 3169S), αSMA (1:1,000; PROGEN, Heidelberg, Germany; 65001), p53 (1:500; Santacruz, Dallas, TX, USA), p21 (1:500; Santacruz; sc-6246), and p16 (1:500; Santacruz; sc-1661) for western blotting; Fibrinogen (Dako Denmark/Agilent Technologies, Santa Clara, CA, USA; A0080), PDGFRβ (1:100; R&D Systems, Minneapolis, MN, USA; AF1042), GFAP (1:100; Merck Millipore, Darmstadt, Germany; AB5804), and Iba1 (1:100; Wako, 019-19741) for immunofluorescence staining.

Statistical analysis

Results are expressed as mean ± standard error of mean (SEM). Statistical analyses were performed using GraphPad Prism 8.0 (GraphPad, San Diego, CA, USA). Statistical differences between groups were analyzed using the one-way analysis of variance (ANOVA), followed by Tukey's multiple-comparisons tests. Statistical analyses for evaluating two factors between groups were performed using ANOVA, followed by Šídák's multiple-comparisons tests. Differences between means were considered to be statistically significant at a P-value < 0.05.

Results

Changes in protein expressions in Tjs and Ajs of microvessels with aging

To evaluate the effect of aging on the expression of Tjs and Ajs, we measured the protein expression levels of ZO-1, occludin, and claudin-5, which comprise Tjs, and pan-cadherin as Ajs in microvessels at 2-, 8-, 12-, and 24 months of age. The protein expression levels of ZO-1 and cadherin decreased significantly with aging (Fig. 1A, D). One-way ANOVA showed an effect for age on the protein expression levels of ZO-1 ($F(3,31) = 7.298$, $P = 0.0008$) and cadherin ($F(3,13) = 7.653$, $P = 0.0034$). The ZO-1 or cadherin expression showed no significant changes between 2 and 8 months of age. The protein expression levels of ZO-1 in 12- and 24-month-old mice decreased by 46.57% ($P = 0.0005$) and 31.85% ($P = 0.0131$) compared to that in 8-month-old mice, respectively. Pan-cadherin expressions in 12- and 24-month-old mice decreased by 50.22% ($P = 0.0448$) and 75.15% ($P = 0.0058$), respectively, compared to that in 2-month-old mice. In contrast, the protein expression levels of occludin increased significantly with aging (Fig. 1B). The one-way ANOVA showed an effect of age on the protein expression levels of occludin ($F(3,28) = 9.897$, $P = 0.0001$). The occludin expression in 12- and 24-month-old mice increased by 55.18% ($P = 0.0062$) and 81.81% ($P = 0.0002$) compared to that in 2-month-old mice, respectively. Claudin-5 levels increased significantly up to 12 months of age (Fig. 1C). The one-way ANOVA showed an effect of age on claudin-5 levels ($F(3,41) = 3.898$, $P = 0.0154$). The percentage increase in the protein expression levels of claudin-5 in 12-month-old mice was 44.05% (2 vs. 12 months old, $P = 0.0081$).

Changes in fibrinogen leakage in the brain with aging

To ascertain whether or not BBB integrity changed with aging, we evaluated the leakage of fibrinogen, a coagulation factor derived from circulating blood, in the hippocampus of 2-, 12-, and 24-month-old mice using immunofluorescence staining. Lectin was used to visualize the cerebral blood vessels. In the whole hippocampus, the fibrinogen-positive area and intensity tended to increase. CA1 in 24-month-old mice increased 6.4

folds (2 vs. 24 months old, $P = 0.0013$) and 3.2 folds (12 vs. 24 months old, $P = 0.0081$) in the positive area and by 7.2 folds (2 vs. 24 months old, $P = 0.0011$) and 3.2 folds (12 vs. 24 months old, $P = 0.0087$) in positive intensity (Fig. 2). The two-way ANOVA revealed significant effects of age and regions but not of interaction between age and regions. The two-way ANOVA showed the following: effects of age ($F(2, 24) = 6.178$, $P = 0.0068$), regions ($F(3, 24) = 3.583$, $P = 0.0285$), and interaction (age × regions) ($F(6, 24) = 1.923$, $P = 0.1181$) in the positive area and those of age ($F(2, 24) = 7.762$, $P = 0.0025$), regions ($F(3, 24) = 3.331$, $P = 0.0364$), and interaction (age × regions) ($F(6, 24) = 1.686$, $P = 0.1676$) in the positive intensity.

Changes in the protein expression of pericyte markers in microvessels with aging

In addition, we validated whether or not changes in pericytes in microvessels accounted for changes in Tjs and Ajs with aging. The protein expression levels of PDGFRβ and αSMA in 24-month-old mice were the lowest among the four age groups (Fig. 1A, B). The one-way ANOVA showed an effect of age on the protein expression levels of PDGFRβ ($F(3,32) = 18.59$, $P < 0.0001$) and αSMA ($F(3,26) = 4.295$, $P = 0.0137$). The protein expression levels of PDGFRβ peaked at 8 months of age (120.8% of 2-month-old level, $P < 0.05$) and then gradually decreased with age to 104.6% at 12 months of age 66.20% at 24 months of age ($P = 0.0003$ vs. 2-month-old level; $P < 0.0001$ vs. 8-month-old level; $P < 0.0001$ vs. 12-month-old level). αSMA levels increased to 150.1% at 12 months of age ($P < 0.05$) and decreased by 56.27% (12- vs. 24-month-old levels, $P = 0.0179$).

Changes in the protein expression of senescent cell markers in microvessels with aging

To determine whether or not cellular senescence occurred in microvessles with aging, we evaluated the protein expression levels of p53, p21, and p16, which are involved in cell cycle arrest as characteristics of senescent cells. The protein expression levels of p53, p21, and p16 tended to increase with aging (Fig. 3A–C). The one-way ANOVA

showed an effect of age on the protein expression levels of p53 ($F(3,16) = 4.687$, $P = 0.0156$), p21 ($F(3,20) = 3.111$, $P = 0.0494$), and p16 ($F(3,32) = 3.839$, $P = 0.0187$). The protein expression levels of p53 increased by 153.6% ($P = 0.0244$) and 142.5% ($P = 0.0385$) in 12- and 24-month-old mice compared to 2-month-old mice, respectively (Fig. 3A). In addition, the p21 expression in 12-month-old mice was increased by 68.75% compared to that in 2-month-old mice. Although the p16 expression levels in 24-month-old mice were significantly higher than those in 8-month-old mice ($P = 0.0127$), the difference was not statistically significant when compared with that in 2-month-old mice.

Elimination of pericytes from the hippocampus of 12- and 24-month-old mice

Furthermore, we investigated the impact of aging on the number and localization of pericytes using immunofluorescence staining. In the whole hippocampus, the PDGFRβ-positive cells, area, and intensity in 12-, and 24-month-old mice decreased significantly compared to 2-month-old mice (Fig. 5A–D). The two-way ANOVA revealed significant effects of age [positive cells ($F(2, 40) = 31.28$, $P < 0.0001$), area ($F(2, 40) = 19.20$, $P < 0.0001$), and intensity ($F(2, 40) = 22.88$, $P < 0.0001$)] but not of regions or interaction between age and regions.

Changes in astrocytes in the hippocampus of 12- and 24-month-old mice

In addition, we evaluated the impact of aging on the number and morphological features of astrocytes using immunofluorescence staining. Glial fibrillary acidic protein (GFAP) was used as a characteristic marker of astrocytes. Contrary to age-related changes in pericytes, GFAP-positive cells, area, and intensity in 12- and 24-month-old mice tended to increase in the whole hippocampus (Fig. 6A–D). Furthermore, astrocytes showed no morphological changes in 12- or 24-month-old mice.

Activation of microglia in the hippocampus of 24-month-old mice

Activation of microglia contributes to neuroinflammation, which is closely related to neurodegenerative disorders. Therefore, we ascertained whether or not microglia are activated with aging using immunofluorescence staining for Iba1 as a characteristic marker of microglia. In the whole hippocampus, the Iba1-positive cells, area, and intensity tended to increase in 24-month-old mice. In CA3, positive cells (2 vs. 24 months old, $P = 0.0487$), positive area (2 vs. 24 months old, $P = 0.0013$, 12 vs. 24 months old, $P = 0.0014$), and intensity (2 vs. 24 months old, $P = 0.0163$, 12 vs. 24 months old, $P = 0.0057$) increased significantly in 24-month-old mice (Fig. 7A–D). CA3 and CA2 increased significantly in the Iba-1-positive area (2 vs. 24 months old, $P = 0.0240$, 12 vs. 24 months old, $P = 0.0288$) and intensity (2 vs. 24 months old, $P = 0.0426$, 12 vs. 24 months old, $P = 0.0423$) in 24-month-old mice (Fig. 7A–D). The two-way ANOVA revealed significant effects of age [positive cells ($F(2, 40) = 6.756$, $P = 0.0030$), area ($F(2, 40) = 17.92$, $P < 0.0001$), and intensity ($F(2, 40) = 14.09$, $P < 0.0001$)] but not of age or interaction between age and regions.

Discussion

In this study, we focused on the relationship between age-related changes in BBB integrity and the cellular senescence marker expression in microvessels in vivo. Furthermore, we evaluated whether or not microglia are activated during aging accompanied with BBB disruption.

First, we demonstrated that expressions of Tjs- and Ajs-associated proteins in microvessels changed with aging (Fig. 1). Furthermore, fibrinogen leaked to brain parenchyma through microvasculature in 24-month-old mice (Fig. 2). The decrease in the Tj expression in the brain results in BBB disruption with aging. However, previous studies reported different findings regarding changes in expressions of ZO-1, occludin, and claudin-5 with aging [8, 24]. These discrepancies probably depend age, tissue, and model of animals used in experiments. Our results suggest that decreased ZO-1 and cadherin expressions in microvessels contribute to BBB disruption with aging. Furthermore, the ZO-1 expression decreased as a consequence of a decreased cadherin expression, because cadherin regulates the ZO-1 expression [3]. However, the occludin expression increased with aging, while the claudin-5 expression was not significantly influenced by aging (Fig. 1). A previous study using an in vitro senescent BBB model found that occludin showed disordered increases and disorganized membrane localization [23]. Therefore, increases in the occludin expression in microvessels could not contribute to BBB integrity in 24-month-old mice. Membrane localization of occludin is related with cadherin [25]. Reduced cadherin levels may disorder the occludin expression.

Fig. 3 shows that the expression of the pericyte marker in microvessels decreased with aging. Using αSMA and PDGFRβ, distinct morphologies of pericytes have been observed in the mouse brain [26, 27]. Our results suggested that pericytes on capillaries were more vulnerable, leading to pericyte loss, with aging than those on pre-capillaries.

Fig. 4 shows that the senescent cells in microvessels accumulated with natural aging. In particular, the increased p53 and p21 expressions preceded the increased p16 expression. Senescent BMECs upregulated the p21 expression, whereas senescent pericytes upregulated the p16 expression [23]. Our results and this report suggested that BMECs exhibit early senescence during aging, which do not directly cause the age-related BBB disruption. In contrast, cellular senescence in pericytes was delayed compared to that

in BMECs, and pericyte senescence was likely to be critical for BBB disruption with aging. However, the pathways of p16 and p53, which are upstream regulators of p21, closely regulated their expression levels through a feedback mechanism [28]. Therefore, identifying which cells increased the p53, p21, or p16 expression in this study is impossible.

Next, using Immunofluorescence staining, we evaluated the impact of aging on pericytes, astrocytes, and microglia in the hippocampus. Corresponding to the results of microvessels, pericytes were markedly decreased in the hippocampus of 12- and 24-month-old mice compared to 2-month-old mice (Fig. 5). Our results supported previous reports showing the loss of pericytes with aging [8, 29]. Moreover, the consequence of pericyte loss is related with aging-associated Tj dysregulation [30]. These reports and our results indicated that the loss of pericytes with aging probably contributed to aging-associated Tj dysregulation and BBB disruption.

Contrary to the loss of pericytes, astrocytes tended to increase but showed no significant changes with aging (Fig. 6). Our results support evidences that astrocytes accumulated in the normal aging brain increased in both number and size [31, 32]. Changes in astrocytes with aging may have compensated for the loss of pericytes.

Corresponding to the leakage of fibrinogen from BBB, microglia were activated with an amoeboid morphology in the hippocampus of 24-month-old mice (Fig. 7). Activated microglia produces high levels of neurotoxic and proinflammatory mediators, which result in cell injury and neuronal death [8, 33]. Because fibrinogen can induce the activation of microglia [14], leakage of fibrinogen caused by age-related BBB disruption may trigger the activation of microglia.

BBB disruption precedes the onset of Alzheimer’s disease [11] and is associated with the inflammatory activation of microglia [13]. Therefore, restoring age-related BBB dysfunction can be a preventive strategy for age-associated neurological disorders.

Figures

Fig. 1

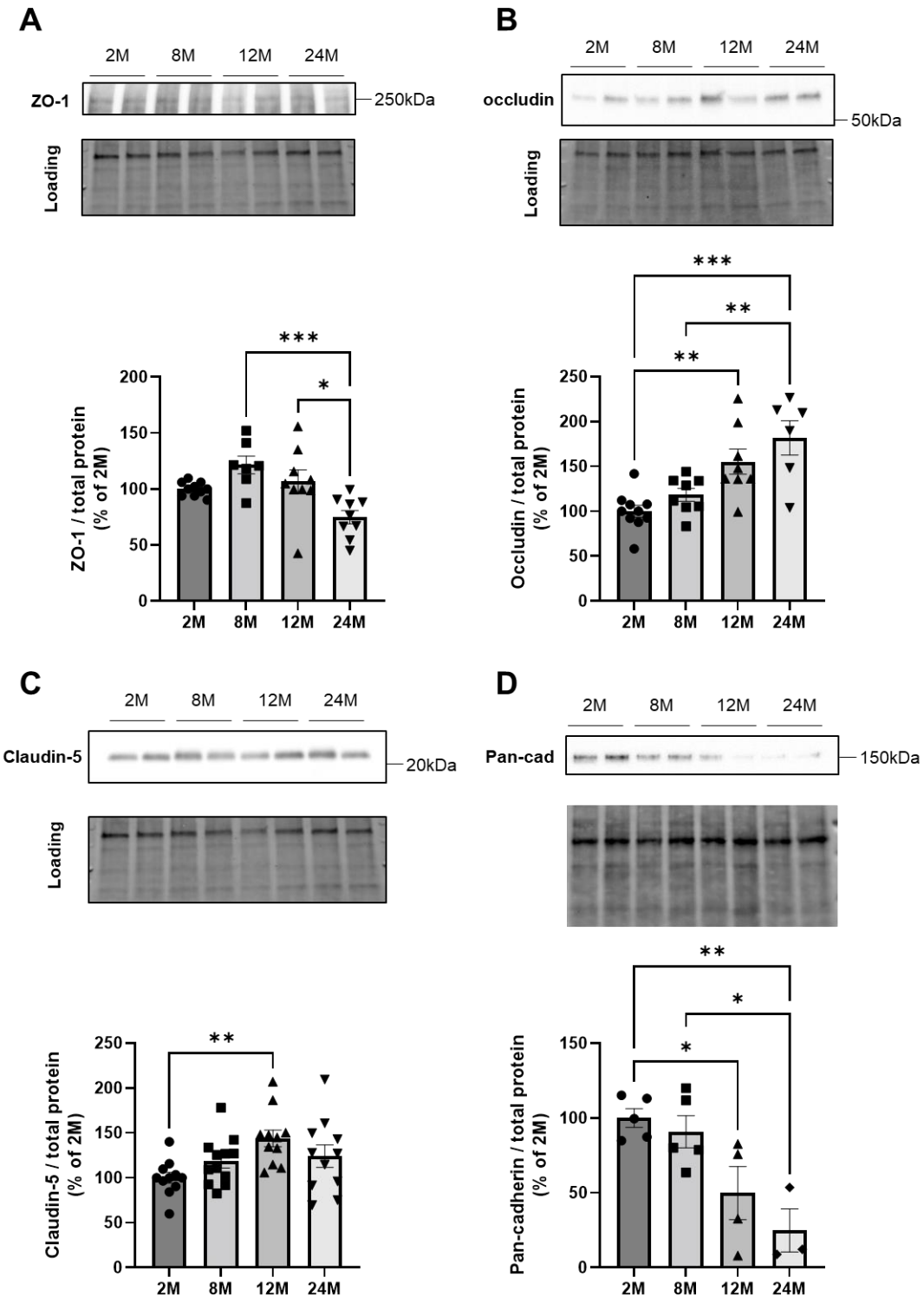

Fig 1. ZO-1, occludin, claudin-5, and pan-cadherin expression levels in brain microvessels of 2-, 8-, 12-, and 24-month-old mice

Representative western blotting images of ZO-1 (A), occludin (B), claudin-5 (C), and Pan-cadherin (D) in 2- (2M), 8- (8M), 12- (12M), and 24-month-old (24M) mice. Band intensities quantified by densitometry. Total protein levels measured by stain-free technology used as loading controls for total protein normalization. Data are expressed as percentages of the 2-month-old group's protein level. Bars indicate mean ± standard error of mean (n = 3–11). Each closed symbol represents an individual value. *$P < 0.05$, **$P < 0.01$, and ***$P < 0.001$, significantly different between groups.

Abbreviations: ZO-1, zonula occludens-1; Pan-cad, pan-cadherin

Fig. 2

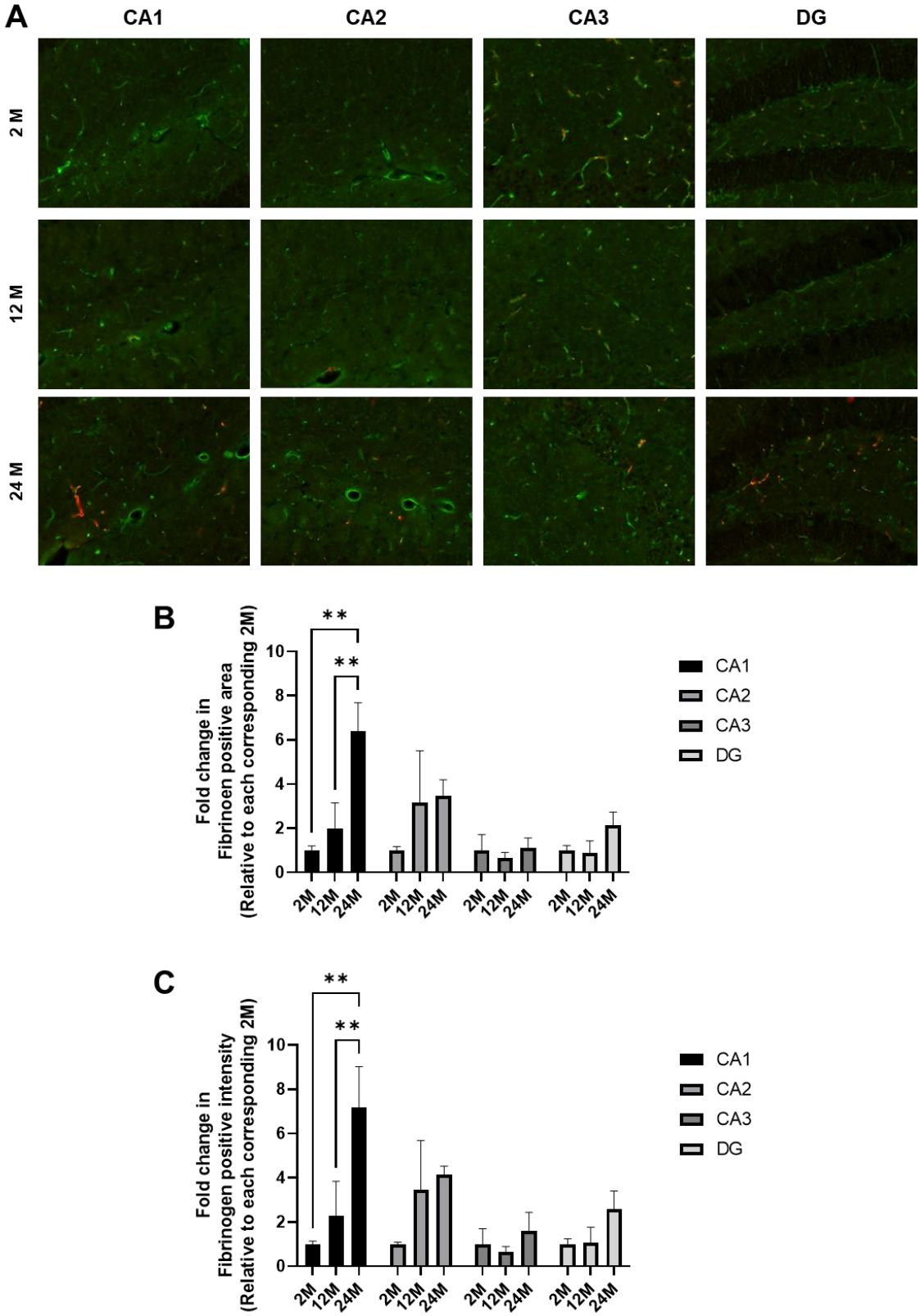
A
CA1
CA2
CA3
DG
2 M
12 M
24 M
B
Fold change in Fibrinoen positive area (Relative to each corresponding 2M)
**
**
10
8
6
4
2
0
2M
12M
24M
CA1
CA2
CA3
DG
C
Fold change in Fibrinogen positive intensity (Relative to each corresponding 2M)
**
**
10
8
6
4
2
0
2M
12M
24M
CA1
CA2
CA3
DG

Fig. 2 Fibrinogen extravasation in the hippocampus of 2-, 12-, and 24-month-old mice

Representative fluorescence images of fibrinogen (red) and lectin (green) in CA1, CA2, CA3, and DG of the hippocampus in 2- (2M), 12- (12M), and 24-month-old (24M) mice (A). Fibrinogen-positive areas (B) and intensity (C) detected and quantified by fluorescence microscopy. Data are expressed as fold changes in each corresponding 2M (n = 3). Bars indicate mean ± standard error of mean. $^{**}P < 0.01$, significantly different from each corresponding 2M.

Abbreviations: CA, Cornu Ammonis; DG, dentate gyrus

Fig. 3

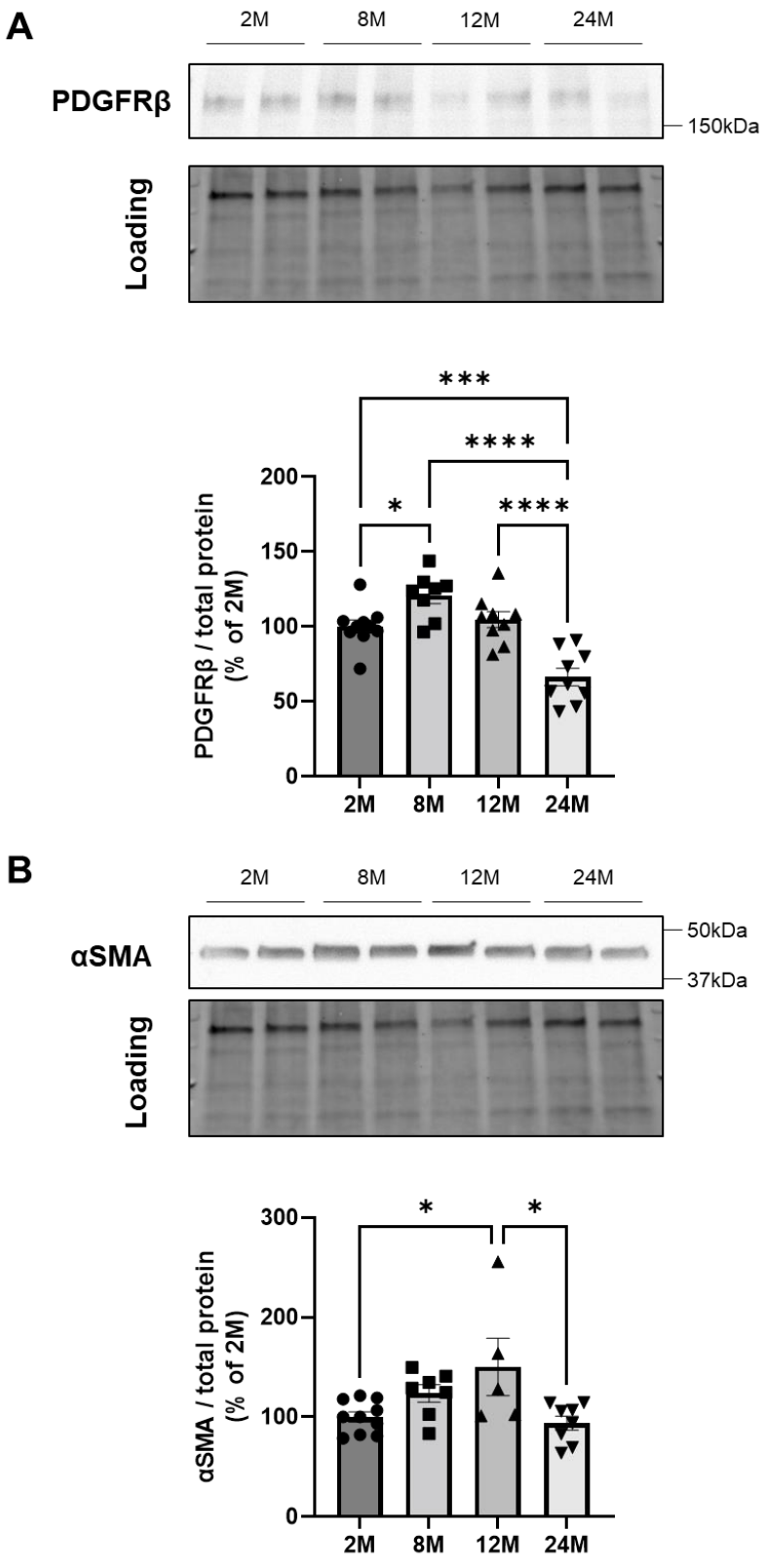
A
2M
8M
12M
24M
PDGFRβ
150kDa
Loading
***
****
*
****
PDGFRβ / total protein
(% of 2M)
200
150
100
50
0
2M
8M
12M
24M
B
2M
8M
12M
24M
αSMA
50kDa
37kDa
Loading
*
*
αSMA / total protein
(% of 2M)
300
200
100
0
2M
8M
12M
24M

Fig 3. PDGFRβ and αSMA expression levels in brain microvessels of 2-, 8-, 12-, and 24-month-old mice

Representative western blotting images of PDGFRβ (A) and αSMA (B) in 2- (2M), 8- (8M), 12- (12M), and 24-month-old (24M) mice. Band intensities quantified by densitometry. Total protein levels measured by stain-free technology used as the loading controls for total protein normalization. Data are expressed as percentages of the 2-month-old group's protein level. Bars indicate mean ± standard error of mean (n = 6–10). Each closed symbol represents an individual value. *P < 0.05, ***P < 0.001, and ****P < 0.0001, significantly different between each group.

Abbreviations: PDGFRβ, platelet-derived growth factor β; αSMA, α-smooth muscle actin

Fig. 4

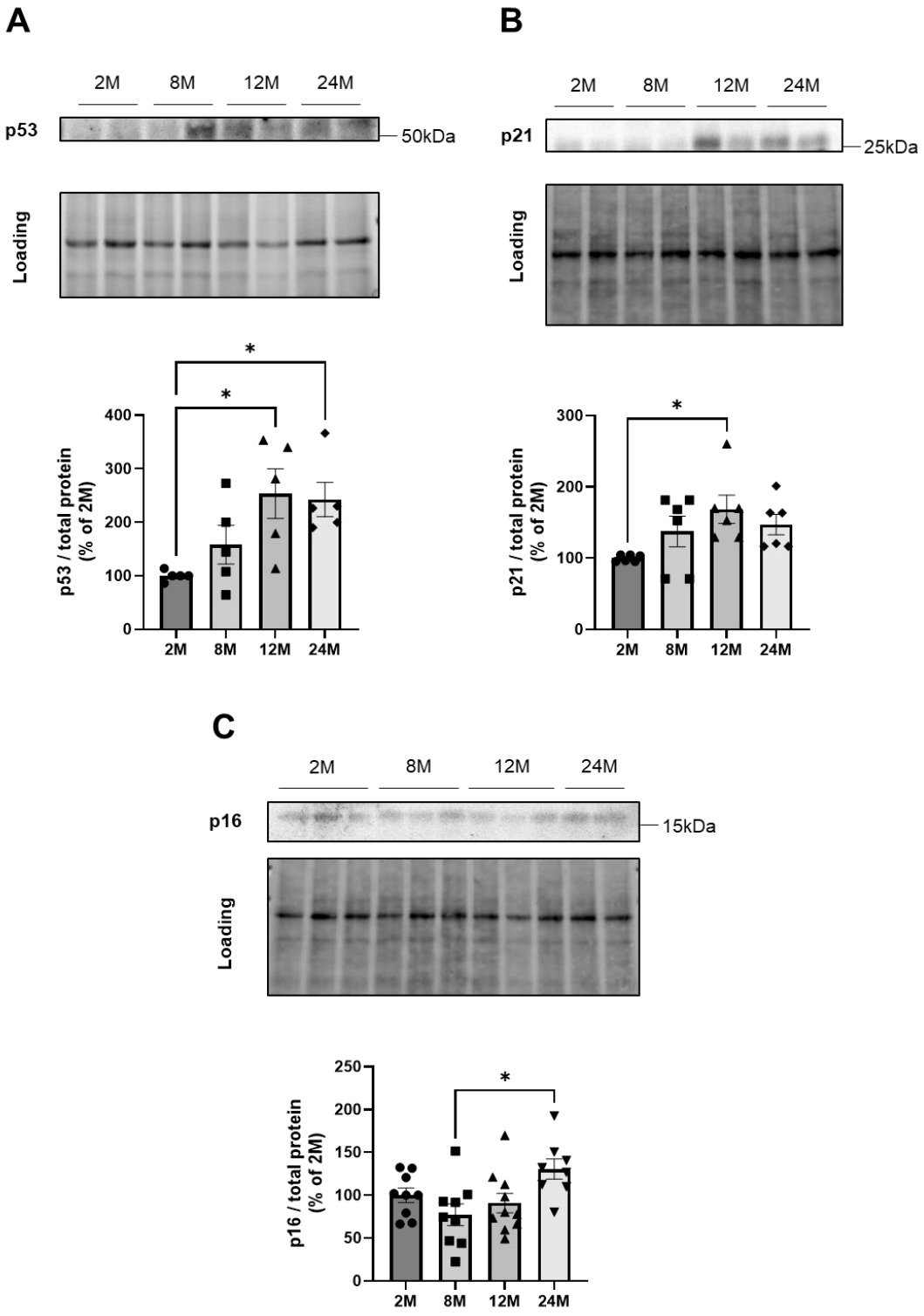
A
2M
8M
12M
24M
p53
50kDa
Loading
p53 / total protein (% of 2M)
400
300
200
100
0
*
*
B
2M
8M
12M
24M
p21
25kDa
Loading
p21 / total protein (% of 2M)
300
200
100
0
*
C
2M
8M
12M
24M
p16
15kDa
Loading
p16 / total protein (% of 2M)
250
200
150
100
50
0
*

Fig 4. p53, p21, and p16 expression levels in brain microvessels of 2-, 8-, 12-, and 24-month-old mice

Representative western blotting images of p53 (A), p21 (B), and p16 (C) in 2- (2M), 8- (8M), 12- (12M), and 24-month-old (24M) mice. Band intensities quantified by densitometry. Total protein levels measured by the stain-free technology used as the loading controls for total protein normalization. Data are expressed as percentages of the 2-month-old group's protein level. Bars indicate mean ± standard error of mean (n = 5–10). Each closed symbol represents an individual value. *$P < 0.05$, significantly different between each group.

Fig. 5

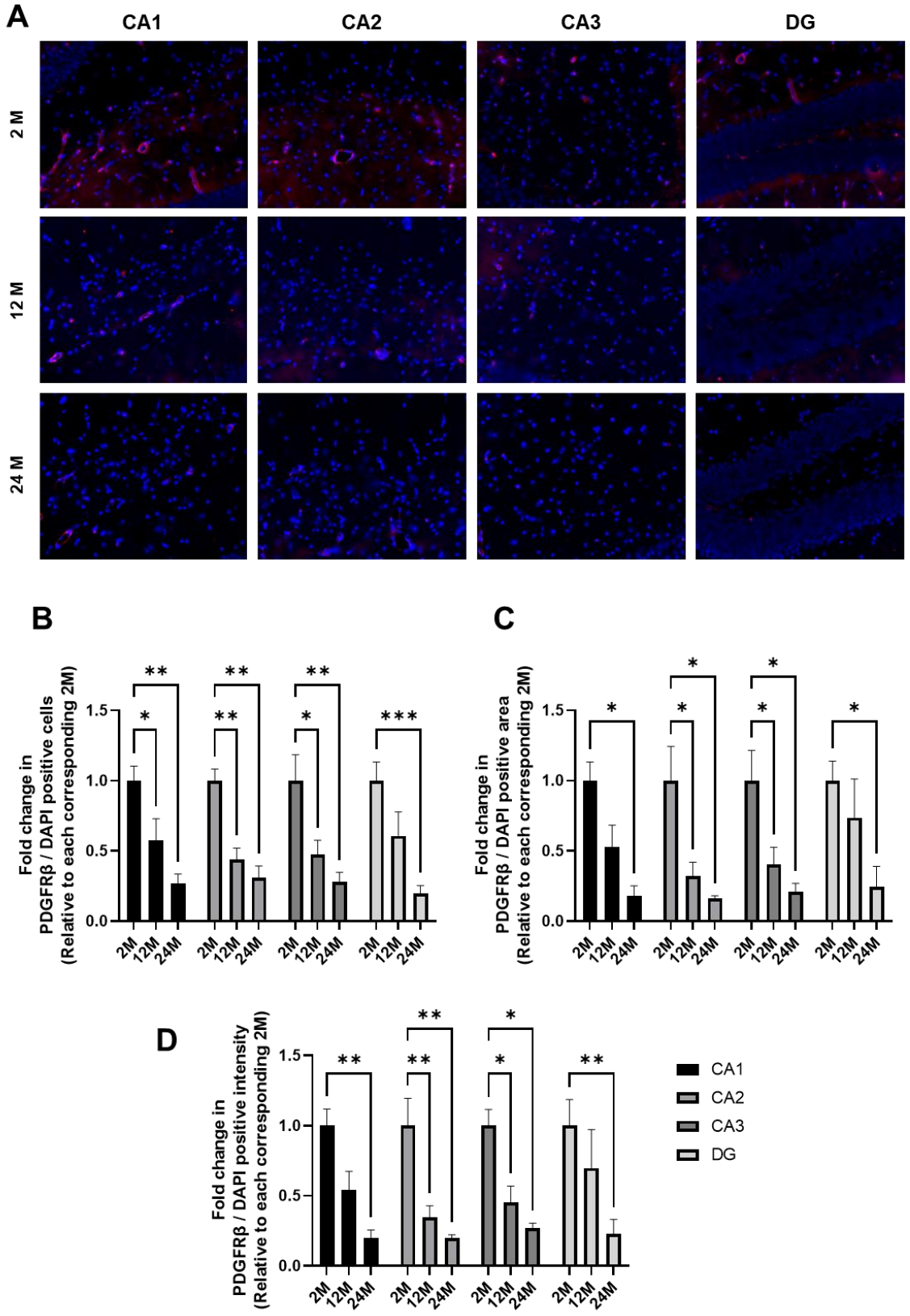
A
CA1
CA2
CA3
DG
2 M
12 M
24 M
B
Fold change in PDGFRβ / DAPI positive cells (Relative to each corresponding 2M)
C
Fold change in PDGFRβ / DAPI positive area (Relative to each corresponding 2M)
D
Fold change in PDGFRβ / DAPI positive intensity (Relative to each corresponding 2M)
2M
12M
24M
CA1
CA2
CA3
DG

Fig. 5 PDGFRβ expression levels in the hippocampus of 2-, 12-, and 24-month-old mice

Representative fluorescence images of PDGFRβ (red) and DAPI (blue) in CA1, CA2, CA3, and DG of the hippocampus of 2- (2M), 12- (12M), and 24-month-old (24M) mice (A). (B, C, D) PDGFRβ-positive cells (B), areas (C), and intensity (D) detected and quantified by fluorescence microscopy. Data are expressed as fold changes in each corresponding 2M (n = 3–5). Bars indicate mean ± standard error of mean. **P* < 0.05, ***P* < 0.01, and ****P* < 0.001, significantly different from each corresponding 2M.

Abbreviations: CA, Cornu Ammonis; DG, dentate gyrus; PDGFRβ, platelet-derived growth factor β; DAPI, 4',6-diamidino-2-phenylindole

Fig. 6

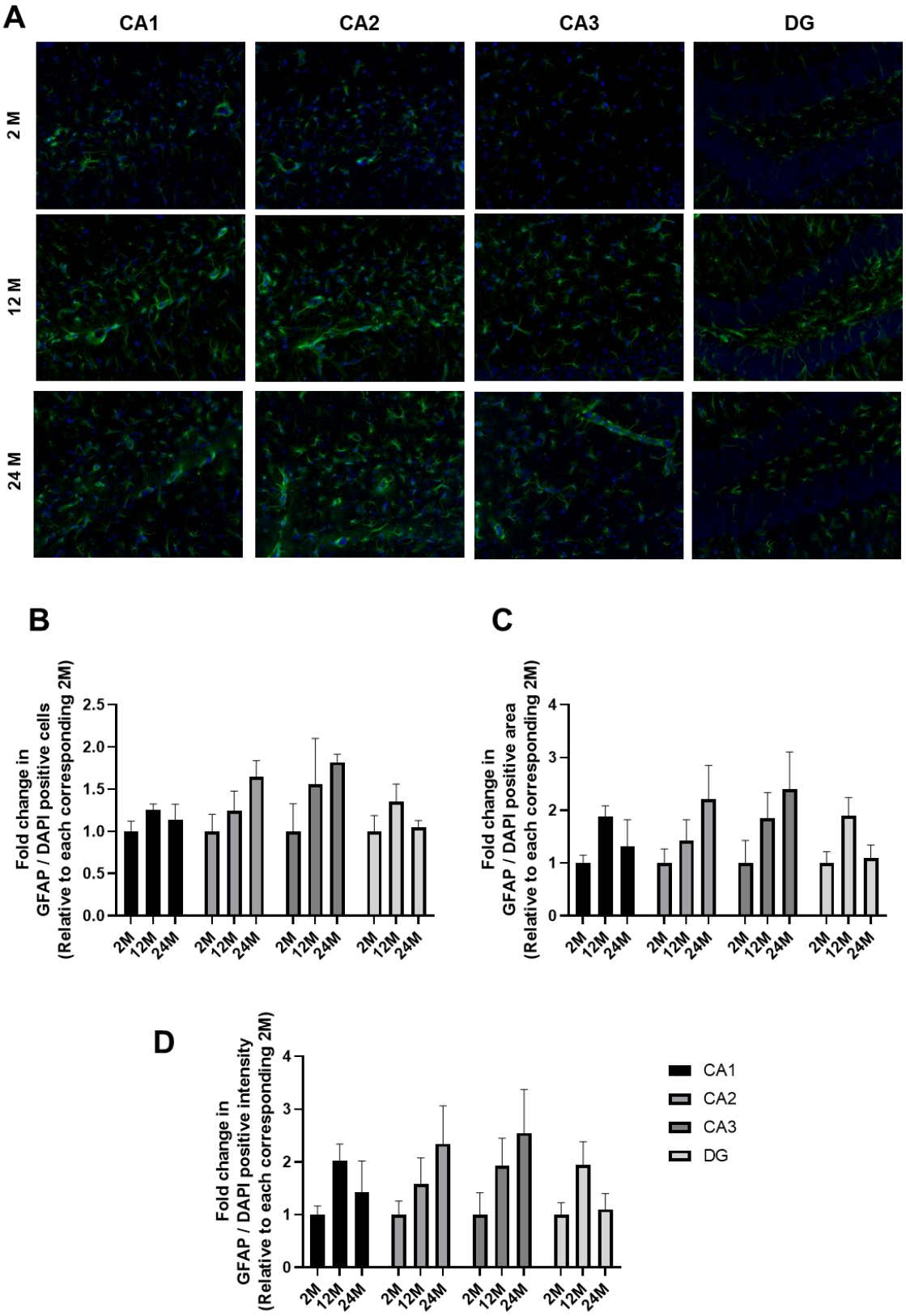
A
CA1
CA2
CA3
DG
2 M
12 M
24 M
B
Fold change in GFAP / DAPI positive cells (Relative to each corresponding 2M)
2.5
2.0
1.5
1.0
0.5
0.0
2M 12M 24M 2M 12M 24M 2M 12M 24M 2M 12M 24M
C
Fold change in GFAP / DAPI positive area (Relative to each corresponding 2M)
4
3
2
1
0
2M 12M 24M 2M 12M 24M 2M 12M 24M 2M 12M 24M
D
Fold change in GFAP / DAPI positive intensity (Relative to each corresponding 2M)
4
3
2
1
0
2M 12M 24M 2M 12M 24M 2M 12M 24M 2M 12M 24M
CA1
CA2
CA3
DG

Fig. 6 GFAP expression levels in the hippocampus of 2-, 12-, and 24-month-old mice

Representative fluorescence images of GFAP (green) and DAPI (blue) in CA1, CA2, CA3, and DG of the hippocampus of 2- (2M), 12- (12M), and 24-month-old (24M) mice (A). GFAP-positive cells (B), areas (C), and intensity (D) detected and quantified by fluorescence microscopy. Data are expressed as fold changes in each corresponding 2M (n = 3). Bars indicate mean ± standard error of mean.

Abbreviations: CA, Cornu Ammonis; DG, dentate gyrus; GFAP, glial fibrillary acidic protein; DAPI, 4',6-diamidino-2-phenylindole

Fig. 7

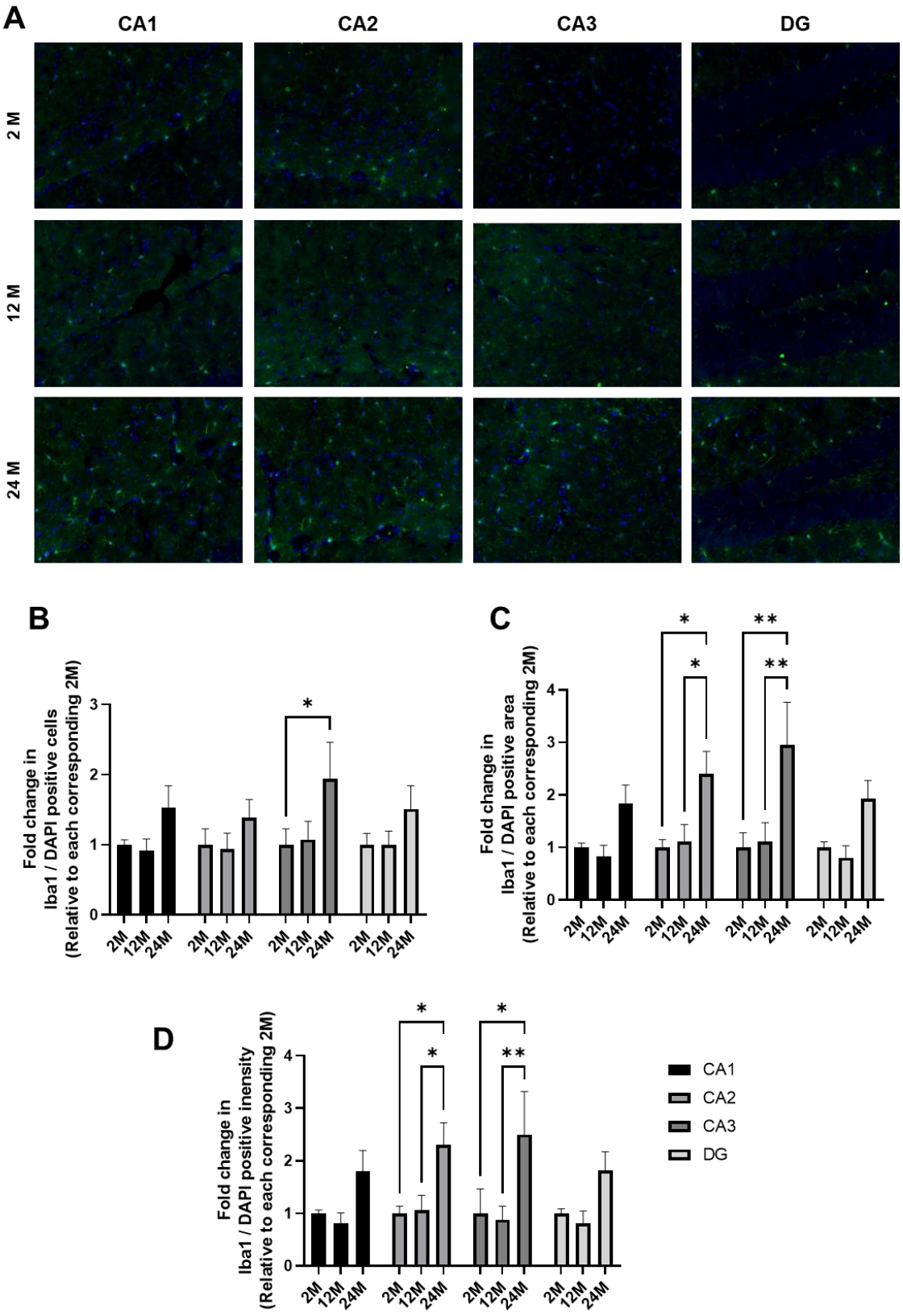
A
CA1
CA2
CA3
DG
2 M
12 M
24 M
B
Fold change in
Iba1 / DAPI positive cells
(Relative to each corresponding 2M)
C
Fold change in
Iba1 / DAPI positive area
(Relative to each corresponding 2M)
D
Fold change in
Iba1 / DAPI positive inensity
(Relative to each corresponding 2M)
2M
12M
24M
CA1
CA2
CA3
DG

Fig. 7 Iba1 expression levels in the hippocampus of 2-, 12-, and 24-month-old mice

Representative fluorescence images of Iba1 (green) and DAPI (blue) in CA1, CA2, CA3, and DG of the hippocampus of 2- (2M), 12- (12M), and 24-month-old (24M) mice (A). Iba1-positive cells (B), areas (C), and intensity (D) detected and quantified by fluorescence microscopy. Data are expressed as fold changes in each corresponding 2M (n = 4–5). Bars indicate mean ± standard error of mean. *P < 0.05 and **P < 0.01, significantly different from each corresponding 2M.

Abbreviations: CA, Cornu Ammonis; DG, dentate gyrus; Iba1, Ionized calcium-binding adapter molecule 1; DAPI, 4',6-diamidino-2-phenylindole

References

1. Abbott NJ, Patabendige AA, Dolman DE, Yusof SR, Begley DJ. Structure and function of the blood-brain barrier. Neurobiol Dis. 2010;37(1):13-25.

2. Correale J, Villa A. The blood-brain-barrier in multiple sclerosis: functional roles and therapeutic targeting. Autoimmunity. 2007;40(2):148-60.

3. Wolburg H, Lippoldt A. Tight junctions of the blood-brain barrier: development, composition and regulation. Vascul Pharmacol. 2002;38(6):323-37.

4. Andreone BJ, Chow BW, Tata A, Lacoste B, Ben-Zvi A, Bullock K, et al. Blood-Brain Barrier Permeability Is Regulated by Lipid Transport-Dependent Suppression of Caveolae-Mediated Transcytosis. Neuron. 2017;94(3):581-94.e5.

5. Abbott NJ. Astrocyte-endothelial interactions and blood-brain barrier permeability. J Anat. 2002;200(6):629-38.

6. Nakagawa S, Deli MA, Kawaguchi H, Shimizudani T, Shimono T, Kittel A, et al. A new blood-brain barrier model using primary rat brain endothelial cells, pericytes and astrocytes. Neurochem Int. 2009;54(3-4):253-63.

7. Desai BS, Monahan AJ, Carvey PM, Hendey B. Blood-brain barrier pathology in Alzheimer's and Parkinson's disease: implications for drug therapy. Cell Transplant. 2007;16(3):285-99.

8. Erdő F, Denes L, de Lange E. Age-associated physiological and pathological changes at the blood-brain barrier: A review. J Cereb Blood Flow Metab. 2017;37(1):4-24.

9. Li M, Li Y, Zuo L, Hu W, Jiang T. Increase of blood-brain barrier leakage is related to cognitive decline in vascular mild cognitive impairment. BMC Neurol. 2021;21(1):159.

10. Zlokovic BV. The blood-brain barrier in health and chronic neurodegenerative disorders. Neuron. 2008;57(2):178-201.

11. Nation DA, Sweeney MD, Montagne A, Sagare AP, D'Orazio LM, Pachicano M, et al. Blood-brain barrier breakdown is an early biomarker of human cognitive dysfunction. Nat Med. 2019;25(2):270-6.

12. Abbott NJ, Rönnbäck L, Hansson E. Astrocyte-endothelial interactions at the blood-brain barrier. Nat Rev Neurosci. 2006;7(1):41-53.

13. Ahn SJ, Anrather J, Nishimura N, Schaffer CB. Diverse Inflammatory Response After Cerebral Microbleeds Includes Coordinated Microglial Migration and Proliferation. Stroke. 2018;49(7):1719-26.

14. Piers TM, East E, Villegas-Llerena C, Sevastou IG, Matarin M, Hardy J, et al. Soluble Fibrinogen Triggers Non-cell Autonomous ER Stress-Mediated Microglial-Induced Neurotoxicity. Front Cell Neurosci. 2018;12:404.

15. Ryu JK, Davalos D, Akassoglou K. Fibrinogen signal transduction in the nervous system. J Thromb Haemost. 2009;7 Suppl 1(Suppl 1):151-4.

16. Lin Z, Sur S, Liu P, Li Y, Jiang D, Hou X, et al. Blood-Brain Barrier Breakdown in Relationship to Alzheimer and Vascular Disease. Ann Neurol. 2021;90(2):227-38.

17. Montagne A, Barnes SR, Sweeney MD, Halliday MR, Sagare AP, Zhao Z, et al. Blood-brain barrier breakdown in the aging human hippocampus. Neuron. 2015;85(2):296-302.

18. Mooradian AD, Haas MJ, Chehade JM. Age-related changes in rat cerebral occludin and zonula occludens-1 (ZO-1). Mech Ageing Dev. 2003;124(2):143-6.

19. Stamatovic SM, Keep RF, Andjelkovic AV. Brain endothelial cell-cell junctions: how to "open" the blood brain barrier. Curr Neuropharmacol. 2008;6(3):179-92.

20. Verheggen ICM, de Jong JJA, van Boxtel MPJ, Gronenschild E, Palm WM, Postma AA, et al. Increase in blood-brain barrier leakage in healthy, older adults. Geroscience. 2020;42(4):1183-93.

21. De Strooper B, Karran E. The Cellular Phase of Alzheimer's Disease. Cell. 2016;164(4):603-15.

22. Guerrero A, De Strooper B, Arancibia-Cárcamo IL. Cellular senescence at the crossroads of inflammation and Alzheimer's disease. Trends Neurosci. 2021;44(9):714-27.

23. Yamazaki Y, Baker DJ, Tachibana M, Liu CC, van Deursen JM, Brott TG, et al. Vascular Cell Senescence Contributes to Blood-Brain Barrier Breakdown. Stroke. 2016;47(4):1068-77.

24. Costea L, Mészáros Á, Bauer H, Bauer HC, Traweger A, Wilhelm I, et al. The Blood-Brain Barrier and Its Intercellular Junctions in Age-Related Brain Disorders. Int J Mol Sci. 2019;20(21).

25. Dejana E, Lampugnani MG, Martinez-Estrada O, Bazzoni G. The molecular organization of endothelial junctions and their functional role in vascular morphogenesis and permeability. Int J Dev Biol. 2000;44(6):743-8.

26. Grant RI, Hartmann DA, Underly RG, Berthiaume AA, Bhat NR, Shih AY. Organizational hierarchy and structural diversity of microvascular pericytes in adult mouse cortex. J Cereb Blood Flow Metab. 2019;39(3):411-25.

27. Smyth LCD, Rustenhoven J, Scotter EL, Schweder P, Faull RLM, Park TIH, et al. Markers for human brain pericytes and smooth muscle cells. J Chem Neuroanat. 2018;92:48-60.

28. Leong WF, Chau JF, Li B. p53 Deficiency leads to compensatory up-regulation of p16INK4a. Mol Cancer Res. 2009;7(3):354-60.

29. Stewart PA, Magliocco M, Hayakawa K, Farrell CL, Del Maestro RF, Girvin J, et al. A quantitative analysis of blood-brain barrier ultrastructure in the aging human. Microvasc Res. 1987;33(2):270-82.

30. Bell RD, Winkler EA, Sagare AP, Singh I, LaRue B, Deane R, et al. Pericytes control key neurovascular functions and neuronal phenotype in the adult brain and during brain aging. Neuron. 2010;68(3):409-27.

31. Chisholm NC, Sohrabji F. Astrocytic response to cerebral ischemia is influenced by sex differences and impaired by aging. Neurobiol Dis. 2016;85:245-53.

32. Middeldorp J, Hol EM. GFAP in health and disease. Prog Neurobiol. 2011;93(3):421-43.

33. Ronaldson PT, Davis TP. Blood-brain barrier integrity and glial support: mechanisms that can be targeted for novel therapeutic approaches in stroke. Curr Pharm Des. 2012;18(25):3624-44.

Chapter 3: Senescence in brain pericytes attenuates blood-brain barrier function in vitro: A comparison of serially passaged and isolated pericytes from aged rat brains

Introduction

The Blood-brain barrier (BBB) formed by brain microvascular endothelial cells (BMECs), astrocytes, and pericytes, regulates the exchange of substances, including various molecules and ions, between the blood and brain to maintain the homeostasis of the central nervous system (CNS)[1]. BMECs that are sealed with tight junctions (Tjs), restrict the paracellular transport of substances in the blood [2]. Disruption of this barrier system causes various neurological diseases including Parkinson's disease (PD), Alzheimer's disease (AD), and multiple sclerosis [3–5]. Moreover, BBB integrity is impaired with aging [6–9], which is related to cognitive decline in vascular mild cognitive impairment [10] and precedes the onset of Alzheimer's disease [11,12]. However, the mechanism that induces altered BBB integrity during aging remains unclear.

Recently, it has been recognized that aging induces the accumulation of senescent cells in tissues of various organs [13,14]. Cellular senescence is caused by stress responses to molecular damage, such as replicative exhaustion, aberrant oncogene activation, or chemotherapeutic-based treatments, which result in a permanent cell cycle arrest [15,16]. Furthermore, senescent cells, showing the senescence-associated secretory phenotype (SASP), exhibit a complex secretome, and undergo characteristic changes including transcriptional, epigenetic, morphological, and metabolic alterations [16,17]. SASP influences the microenvironment and contributes to the pathogenesis of age-related neurodegenerative diseases [18,19].

Accumulation of senescent vascular cells is associated with compromised BBB integrity [20]. Pericytes are present at intervals along the walls of the brain capillaries and play a key role in maintaining BBB integrity [21–24]. Pericytes induce the formation of tight junctions (Tjs) in BMECs and regulate the permeability of BBB [21,25]. Pericyte coverage and the number of brain capillaries are downregulated in patients with AD, which is associated with BBB breakdown [26,27], suggesting that pericyte loss with aging results in progressive vascular-mediated neurodegeneration [28]. However, the ability of pericytes to support BBB integrity and their characteristic changes during cellular senescence or aging need to be explored. In this study, we used BBB models comprising intact brain endothelial cells co-cultured with senescent pericytes that were obtained through a serial passage or isolated from 18-month-old rats to evaluate their impact on BBB integrity and the differences between replicative senescence and natural aging in pericytes. Furthermore, we evaluated SASP in tested senescent pericytes and a distinct mRNA expression profile of pericyte markers in them.

Materials and Methods

Animals

All experimental protocols involving animals were approved by the Laboratory Animal Care and Use Committee of Fukuoka University (permit number 2204002). Male and female Wistar rats (3–4 weeks, and 18 months old) were purchased from Japan SLC Inc. (Shizuoka, Japan). Rats were housed under a controlled temperature (22 ± 2 °C) and light and dark cycle (light from 7:00 to 19:00); they were provided access to water and a chow diet ad libitum.

Primary culture of rat brain endothelial cells and pericytes

The primary culture of rat brain endothelial cells (ECs) and pericytes (PCs) was maintained as previously described [29,30]. PCs were isolated from 3–4-week-old and 18-month-old Wistar rats.

Passage culture of rat brain pericytes for inducing cellular senescence

Replicative senescence can be induced by serial passage, a classical laboratory protocol [20,31]. The primary cultures of PCs were passaged using Cellmatrix Collagen Type I-C (0.1 mg/mL, Nitta Gelatin Inc., Osaka, Japan; 637-00773)-coated flasks (50 × 104 cells/flask) once a week up to nine times. In the second passage, PCs isolated from 3- to 4-week-old rats were used as lower-passage PCs (P2 PCs) and young PCs. In the fourth, seventh, and tenth passages (i.e., after 3, 6, and 9 repeated passages), PCs isolated from 3- to 4-week-old rats were used as higher-passaged (P4, 7, and 10) PCs. PCs isolated from 18-month-old rats, in their second passage, were used as aged PCs.

In vitro evaluation of the barrier function of the BBB

ECs isolated from 3-week-old Wistar rats were seeded (5 × 104 cells/well) into 24-well transwell inserts (0.4-μm pore size; Corning, Midland, MI, USA; 3470) coated with collagen type IV (0.1 mg/mL, Nitta Gelatin Inc.; 638-05921) and fibronectin (0.025 mg/mL, Sigma) and maintained in EC medium supplemented with 500 nM hydrocortisone (Sigma; H0135). PCs were seeded in Cellmatrix Collagen Type I-C (0.1 mg/mL, Nitta Gelatin Inc.)-coated 24-well plate (2.5 × 104 cells/well) and cultured in the PC medium. The inserts with ECs were placed in a 24-well plate containing cultured PCs at the bottom of the plate (PC co-culture group). Inserts with ECs were placed into a 24-well plate without PCs, which served as the control group (EC monolayer group). Both groups were cultured for 3 days in an EC medium supplemented with 500 nM hydrocortisone. To evaluate the barrier function in EC monolayer and PC co-culture groups, the permeability coefficients of sodium fluorescein (Na-F) and transendothelial electrical resistance (TEER) values were measured as reported previously [32,33].

Experimental conditions

For β-galactosidase staining, real-time quantitative PCR and Western Blot Analysis, PCs were seeded on Cellmatrix Collagen Type I-C (0.1 mg/mL)-coated 35-mm dishes and cultured using PC medium. On the next day, the medium was replaced with serum-free PC medium and incubated for 16 h. Subsequently, real-time quantitative RT-PCR and Western Blotting were performed to analyze PCs, and the cell culture-conditioned medium was collected for the MILLIPLEX assay.

β-Galactosidase staining

We further analyzed PCs using a Senescence β-galactosidase Staining Kit (Cell Signaling Technology, Danvers, MA, USA; 9860S). For this purpose, PCs were washed

with Dulbecco's phosphate-buffered saline (-) (D-PBS) (Nacalai Tesque, 14249-24) once, fixed with 1 × fixative solution for 15 min, and washed twice with D-PBS. Subsequently, the PCs were incubated with β-galactosidase Staining Solution at 37 °C overnight in a dry incubator. The β-galactosidase-positive staining on PCs was detected using a phase contrast microscope (Nikon, Tokyo, Japan). The stained area of the cells that were β-galactosidase-positive was calculated using the ImageJ software (National Institutes of Health Image, Bethesda, MD, USA). Results were expressed in terms of percentage of β-galactosidase-positive area [(stained area/total area in investigated microscopic fields) x 100].

Real-time quantitative RT-PCR

Total RNA was extracted from PCs using the FastGene RNA Basic Kit (FastGene Co, Ltd., Tokyo, Japan; FG-80250). Equivalent amounts of RNA from each sample were reverse-transcribed with FastGene cDNA Synthesis 5× ReadyMix OdT (FastGene Co, Ltd., NE-LS65) following the protocol provided by the manufacturer. Real-time PCR was conducted in a Light Cycler 96 System (F. Hoffmann-La Roche, Ltd., Basel, Switzerland) using KAPA SYBR Fast qPCR Kit (Kapa Biosystems, Inc., Bath, UK) according to the protocol provided by the manufacturer. After pre-incubation at 95 °C for 3 min, PCR was performed through 45 cycles of 95 °C for 10 s, 60 °C for 20 s, and 72 °C for 1 min, using specific primers of the genes of interest purchased from Takara Bio Inc. (Shiga, Japan) and Integrated DNA Technologies, Inc. (Coralville, IA, USA). The genes of interest and their primer sequences are listed in Supplementary Table 1. GAPDH was used as the reference gene, and hence, the threshold cycle value (Cq) of each target gene was normalized to that of GAPDH. Total RNA sample isolated from rats was purchased from QIAGEN (XpressRef Rat Universal Total RNA, Venlo, Netherlands; 338116) and used as a calibrator for relative quantification of altered gene expression.

Western Blot Analysis

PCs were scraped and lysed using a lysis buffer containing 10 mM Tris-HCl (pH 6.8; Nacalai Tesque; 35434-34), 100 mM NaCl (Sigma; 28-2270-5), 1 mM EDTA (pH 8.0; Wako; 311-90075), 1 mM EGTA (Wako; 346-01312), 10% glycerol, 1% Triton-X100 (Sigma; X100), 0.1% sodium dodecyl sulfate (SDS; Nacalai Tesque; 02873-75), 0.5% sodium deoxycholate (Sigma; D6750), 20 mM sodium pyrophosphate (Sigma; S6422), 2 mM sodium orthovanadate (Sigma; S6508), 1 mM sodium fluoride (Wako; 196-01975), 1% protease inhibitor cocktail (Sigma; P2714), 1% phosphatase inhibitor cocktail 2 (Sigma; P5726), 1% Phosphatase Inhibitor Cocktail 3 (Sigma; P0044), and 1 mM phenylmethylsulfonyl fluoride (Sigma; P7626). To determine the total protein concentration, cell lysates were analyzed using a Pierce™ BCA Protein Assay Kit (23225; Thermo Fisher Scientific). Equivalent amounts of protein from each sample were electrophoretically separated on 7.5% TGX Stain-Free gradient acrylamide gels (Bio-Rad, Hercules, CA; 161-0181) or 12% TGX Stain-Free acrylamide gels (Bio-Rad; 161-0185), and subsequently, they were transferred to low fluorescent polyvinylidene difluoride membranes (Bio-Rad; 1704274). For the stain-free method of total protein normalization, the GelDoc Go imaging system (Bio-Rad) was used. The membranes were then blocked using Blocking One (Nacalai Tesque; 03953-95). Antibodies developed against p16 (1:500; Santa Cruz Biotechnology, Dallas, TX, USA; sc-1661) and p21 (1:500; Santa Cruz Biotechnology; sc-6246) were used to detect p16 and p21. After washing, the membranes were incubated with HRP–conjugated goat anti-rabbit IgG (Bio-Rad; 170-6515) or goat anti-mouse IgG (Bio-Rad; 170-6516), as appropriate. Immunoreactive bands were detected using Clarity Western ECL Substrate (Bio-Rad; 1705061). Digital images of the bands were recorded using a MultiImager II ChemiBOX (BioTools, Gunma, Japan), and quantitatively analyzed using ImageJ software (National Institutes of Health Image, Bethesda, MD, USA). The relative protein band intensity was expressed as the ratio to the corresponding total protein.

MILLIPLEX assay

Cell culture conditioned medium (1,000 µL) was centrifuged to remove all debris and then concentrated using Amicon Ultra-0.5 PLBC ultracel-3 membrane 3kDa (Merck Millipore; UFC5003) following the protocol provided by the manufacturer. Cytokine and chemokine levels in the cell culture conditioned medium were measured using the MILLIPLEX MAP Rat Cytokine/Chemokine Magnetic Bead Panel (Merck Millipore, Darmstadt, Germany; RECYTMAG-65K) and Luminex 200 xPONENT 3.1 System (Merck Millipore) following the instructions provided by the manufacturer.

Statistical Analysis

Results are expressed as the mean ± standard error of the mean (SEM). Statistical analyses of data were performed using GraphPad Prism 8.0 (GraphPad Software, San Diego, CA, USA). The unpaired t-test was applied to compare the two groups. Statistical differences between groups were analyzed using one-way analysis of variance (ANOVA), followed by Tukey's multiple comparison test. Differences between the means were considered statistically significant at $P < 0.05$.

Results

Ability of pericytes to upregulate the barrier function of BBB was attenuated by serial passages and aging

To evaluate the effects of serial passage and aging on the ability of pericytes to enhance BBB function, we evaluated the permeability coefficients of Na-F and TEER values of ECs co-cultured with or without PCs. Schematic diagrams of BBB models developed using ECs co-cultured with or without PCs are shown in Fig. 1A. TEER values of ECs co-cultured with P2 or P4 PCs were significantly increased by 2.1 ($P < 0.0001$) and 1.9 ($P = 0.0017$) folds, respectively, compared to that of the EC monolayer. However, the increase in TEER values of ECs co-cultured with P7 and P10 PCs was less than that of P2 PCs (Fig. 1B). In P2, P4 and P7 PC cocultures, significantly lower permeability coefficients of Na-F for ECs were detected, showing reductions by 59.15% ($P < 0.0001$), 42.32% ($P = 0.0131$), and 30.54% ($P = 0.0261$) in P2, P4 and P7, respectively, compared with those recorded in the EC monolayer (Fig. 1C); however, the permeability coefficients of Na-F did not decrease significantly in the P10 set (Fig. 1C). In contrast to the young PCs, the aged PCs were incapable of increasing the TEER values (Fig.1D) and decreasing the permeability coefficients of Na-F in ECs (Fig.1E).

Serial passage induced enhanced β-Galactosidase activity, and expressions of senescent cell markers in pericytes

We investigated whether serial passage induced cellular senescence in PCs using β-galactosidase staining, real-time quantitative RT-PCR, and western blotting. Two characteristic features of senescent cells were evaluated: (1) the expression of senescence-associated β-galactosidase reflecting the change in lysosomal mass of senescent cells, and (2) an increase in the expressions of Cdkn2a (p16) and Cdkn1a (p21), which act as cyclin-dependent kinase inhibitors and mediate permanent cell cycle arrest [17,34]. The β-galactosidase-positive area in the PCs increased with the passage number. The β-galactosidase-positive area in P7 and P10 PCs significantly increased compared with that in P2 and P4 PCs ($P < 0.0001$ for all pairwise comparisons) (Fig. 2A, B). Cdkn2a (p16) and Cdkn1a (p21) are characteristic markers of cellular senescence. In P4, P7, and

P10 PCs, Cdkn2a mRNA and p16 protein were highly expressed compared with that in P2 PCs (Fig. 2C, D). Moreover, P7 PCs showed a significantly increased Cdkn1a mRNA expression compared to that in P2 and other PCs ($P < 0.01$ vs. P2, P4, and P10) (Fig. 2E). However, p21 protein expression increased in P4, P7, and P10 PCs by 102.4%, 153.7% ($P = 0.0249$), and 192.7% ($P = 0.0327$), respectively, compared with that in P2 PCs (Fig. 2F).

β-Galactosidase activity and senescent marker expression were increased in pericytes isolated from aged rats

Furthermore, cellular senescence in PCs isolated from 18-month-old rats were assessed. The β-galactosidase-positive area in aged PCs was 2.5-fold higher ($P < 0.0001$) than in young PCs (Fig. 3A, B); however, at the transcript level, Cdkn2a and Cdkn1a expressions did not increase in aged PCs (Fig. 3C, E). Results revealed significantly increased p16 protein expression [49.1% ($P < 0.0445$)] in aged PCs than in young PCs (Fig. 3D), while no significant change was observed in p21 protein expression (Fig. 3F).

Serial passage and aging induced altered mRNA expression and release of SASP factors in pericytes

To examine whether the production of SASP factors in PCs is facilitated by serial passage and aging, we measured the mRNA levels of IL-6, IL-1β, TNFα, and MCP-1 as SASP factors in PCs. We also assessed these cytokines secreted in PC-conditioned media using multiplex ELISA. In serially passaged PCs, IL-6 mRNA expression was significantly increased at P7 compared to that in P2 and the other groups (Fig. 4A). P7 PCs released significantly more IL-6 than that secreted by P2 ($P < 0.001$) and P4 ($P < 0.05$) PCs (Fig. 4D). Higher level of IL-6 released by P10 PCs was detected to be than that secreted by P2 PCs; however, the difference was not statistically significant. Aged PCs secreted significantly higher IL-6 (2.2-fold, $P = 0.0009$) (Fig 4J) than young PCs did, however, such difference was not evident in the IL-6 mRNA expression (Fig.4G). TNFα mRNA expressed significantly more in P4 PCs than that in P2 ($P < 0.05$) and P7 ($P < 0.01$) PCs (Fig. 4B), whereas P10 PCs exhibited the highest release of TNFα (Fig. 4E). TNFα mRNA expression was increased 2.9-fold in aged PCs compared to that in young PCs (Fig. 4H). However,

TNF-α release in young and aged PCs did not significantly vary (Fig. 4K). IL-1β mRNA expression was significantly decreased in P4, P7, and P10 PCs compared with that in P2 PCs ($P < 0.0001$ vs. P4, P7, and P10) (Fig. 4C), while it was 5-fold increased ($P = 0.0237$) in aged PCs compared with young ones (Fig. 4I). The concentration of secreted IL-1β was undetectable in media. MCP-1 release by P7 PCs was significantly higher than that by P2 PCs ($P = 0.0025$), whereas lower level of MCP-1 was released by P4 and P10 PCs than that in P2 set (Fig. 4F). Aged PCs released a 2.9-fold higher MCP-1 ($P = 0.0068$) than young PCs (Fig. 4I).

Serial passage and aging affected mRNA expression of pericyte markers

We characterized the phenotype of senescent pericytes by assessing mRNA expression levels of 13 common pericyte markers in serially passaged and aged PCs. Pericytes are characterized by various biochemical markers [35,36]. Of the 13 markers studied, Des, Nes, Acta2, Abcc9, Cspg4, Mcam (CD146), Myh11, Myl9, and Rgs5 mRNA expression levels were significantly downregulated after serial passage (Fig. 5A). Of these, seven markers (Des, Nes, Acta2, Cspg4, Mcam, Myh11, and Myl9) were significantly decreased in P4, P7, and P10 PCs compared with that recorded in P2 PCs. Contrastingly, no downregulated markers was detected in aged PCs. Des, Pdgfrb, Acta2, Abcc9, Mcam, Myh11, Kcnj8, and Myl9 mRNA expression levels were significantly upregulated in aged PCs compared to that in young PCs (Fig. 5B).

Discussion

Previous reports demonstrated that BBB integrity is impaired during aging [6–9], but the mechanism of age-related BBB disorders remained unclear. In particular, the correlation of aging with pericytes, crucial members of the BBB, was unknown. In this study, we investigated whether senescent brain pericytes affect the barrier function of the BBB and exhibit the SASP. We focused on the differences between serial passage-induced cellular senescence and natural aging in PCs.

We demonstrated that both serially passaged and aged PCs did not enhance the barrier properties of ECs as indicated by the permeability to Na-F and TEER in comparison with the young/P2 PCs (Fig. 1). These data indicate attenuated ability of PCs to upregulate BBB barrier function, which was induced by senescence under both serial passage and natural aging conditions. Aged PCs were less effective on the barrier function of ECs than serially passaged PCs.

Next, we characterized serially passaged and aged PCs in terms of cellular senescence. The β-galactosidase activity and expression analyses of senescent cell markers distinctly indicated the characteristic features of senescence in serially passaged cells, which was partly insignificant in naturally aged cells. For in vitro studies of senescent cells, methods of stress-induced senescence involving reagents such as hydrogen peroxide and serial passages are commonly considered; this cannot clarify whether stress- or serial passage-induced cellular senescence can be reproduced in vivo. To address this question, we studied PCs isolated from intact 18-month-old rats which may be considered as naturally aged PCs and demonstrated that they retain characteristic features of senescent cells in contrast to PCs induced using oxidative stress or multiple passages; similar to the current experimental outcomes, p16 levels increase during aging of most mammalian tissues [37,38], while the senescence-specific phenotype showed dynamic changes at varying intervals after inducing senescence [39]. Moreover, a previous study suggested that p53, an upstream regulator of p21, regulates p16 expression through a negative feedback mechanism [40]. The increase in p16 levels is attributable to its decreased degradation rather than an increased rate of synthesis [41]. These mechanisms may be associated with our results showing the dynamic variation in Cdkn2a (p16) and Cdkn1a (p21) levels in PCs during cellular senescence.

Senescent cells are characterized by not only cell cycle arrest but also senescence-associated secretory phenotype (SASP) [31]. We demonstrated the synthesis

and release of SASP factors induced by serially passaged and aged PCs (Fig. 4). However, the expression patterns of SASP factors differed between serially passaged and aged PCs. Moreover, our data indicated that PCs secrete SASP after changing the cell cycle, and the secretion of IL-6 by PCs precedes that of TNFα during senescence. It has been reported that senescent vascular smooth muscle cells, which have the same cell lineage as pericytes, contribute to the proinflammatory environment through IL-6 and CCL2 productions [42]. Although pericytes can stabilize the BBB under normal physiological conditions, the production of inflammatory mediators under pathological conditions induces BBB dysfunction [43]. Moreover, IL-6 modulates the expression of claudin-5 and occludin in cerebral cortical microvessels [44], and age-related BBB breakdown is associated with elevated TNFα expression and disruption of assembly of tight junction complexes [45]. Therefore, the SASP released by senescent PCs likely contributes to age-related BBB disruption. Moreover, PCs interact with ECs, astrocytes, microglia, oligodendrocytes, and neurons to maintain brain function through neurovascular units [46]. Therefore, further studies are required to clarify the impact of SASP of senescent PCs on other cellular components of the neurovascular units during aging.

Finally, we evaluated the mRNA expression of pericyte markers to characterize the phenotypes of senescent PCs. Both serially passaged and aged PCs isolated from 18-month-old rats showed a similar pattern of mRNA expression in 13 markers of PCs explored. Notably, PCs exhibit different morphologies depending on their location in cerebral capillaries [22]. A previous single-cell RNA sequencing study indicated that capillary PCs expressed high levels of Vtn, Cspg4, Pdgfrβ, Anpep, Rgs5, Kcnj8, and Abcc9 and low levels of Acta2, Myl9, and Myh11 [36], suggesting that our primary cultures of PCs are heterogeneous because were derived from various types of brain capillaries (precapillary arterioles, capillaries, and venules). Changes in mRNA expression levels were inconsistent in serially passaged and aged PCs (Fig. 5). Serial passage induced a significant decrease in Des, Nes, Acta2, Abcc9, Cspg4, Mcam, Myh11, and Myl9 expression in PCs. Interestingly, aged PCs isolated from 18-month-old rats showed a significant increase in Des, Pdgfrb, Acta2, Abcc9, Mcam, Myh11, Kcnj8, and Myl9. Therefore, it is unlikely that serially passaged and aged PCs share a common phenotype characterized by similarly expressed PC markers. These discrepancies may be explained by the differences in culture conditions that are important in determining the in vitro phenotype. A long-term culture in the serial passage method possibly affects the expression levels of PC markers [35,47]. The results of aged PCs potentially aid characterization of the phenotypes observed in senescent PCs of aged animals. The

discrepancies between serially passaged and aged PCs should be considered when studying senescent brain pericytes in vitro.

In conclusion, we demonstrated that serially passaged PCs and aged PCs isolated from 18-month-old rats failed to maintain and enhance the barrier integrity of brain endothelial cells. Furthermore, serially passaged and aged PCs showed characteristic features of senescent cells, including cell cycle arrest as well as the synthesis and release of SASP factors. These results suggest that senescent PCs contribute to age-related BBB dysfunction. Although different expression patterns of senescence- and PC-associated markers were detected in serially passaged and aged PCs, our results indicate that PCs isolated from aged animals retain the properties of senescent cells and can be replaced with PCs undergoing replicative or stress-induced senescence by serial passage or oxidative stress, respectively, for in vitro evaluation of the impact of senescent PCs on BBB function. Impaired BBB integrity during aging is related to the pathogenesis of age-related neurodegeneration such as Alzheimer's disease. Therefore, the application of senolysis to repair BBB function to selectively eliminate senescent PCs could be a new approach for preventing age-related neurodegeneration.

Figures

Fig. 1

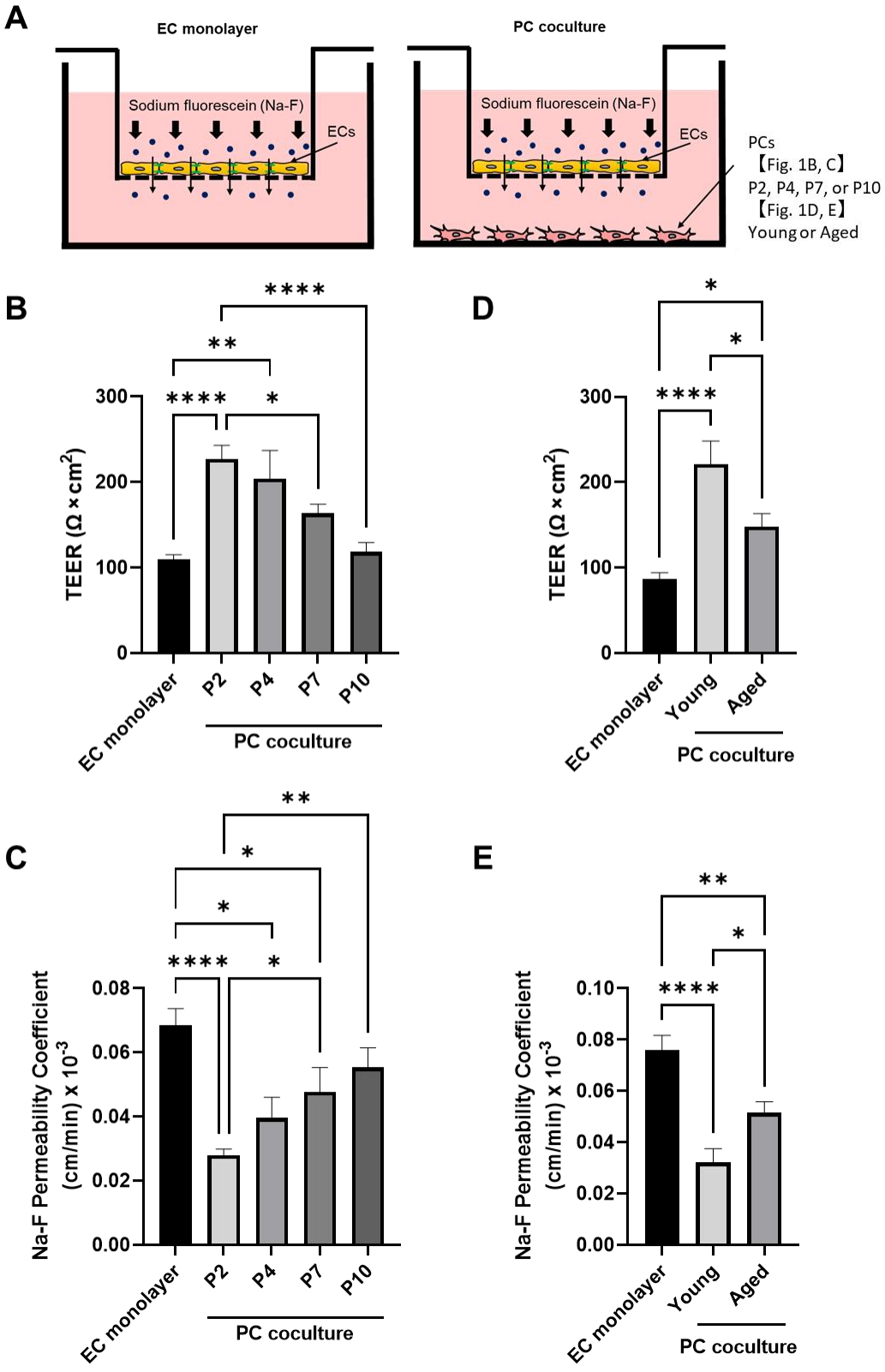

Fig. 1. Influence of brain pericytes, which were serially passaged or isolated from 18-month-old rats, on the endothelial barrier function of BBB.

(A) Schematic showing the in vitro BBB models using rat brain endothelial cells (ECs) co-cultured with or without rat brain pericytes (PCs), which were serially passaged or isolated from 18-month-old rats. (B, D) TEER values and (C, E) permeability coefficients of sodium fluorescein (Na-F) for the EC monolayer were measured after culturing for 3 days. Bar graph represents the mean ± SEM (n = 7–24). *P < 0.05, **P < 0.01, and ****P < 0.0001.

Fig. 2

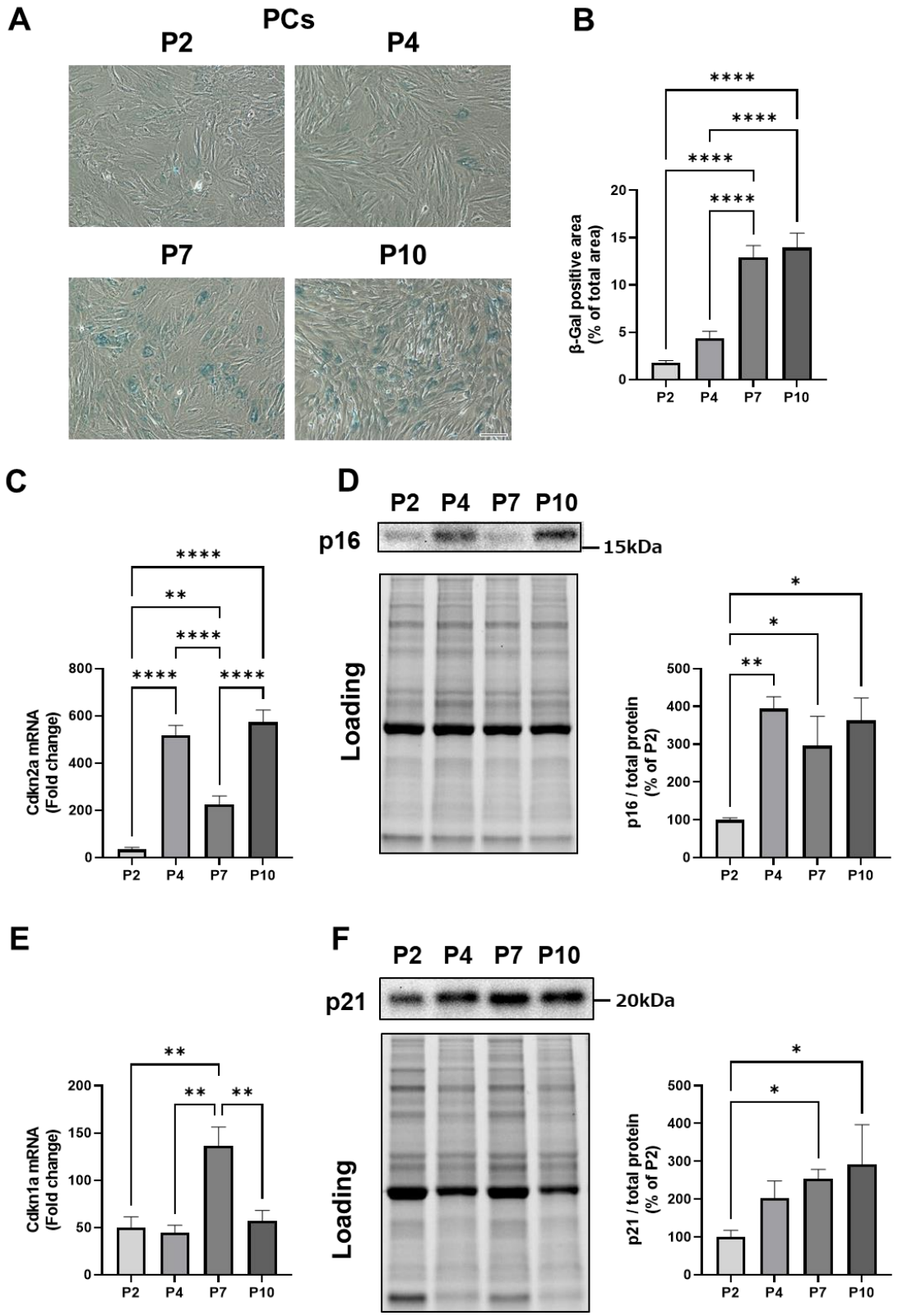
A
PCs
P2
P4
P7
P10
B
β-Gal positive area (% of total area)
C
Cdkn2a mRNA (Fold change)
D
p16
15kDa
Loading
p16 / total protein (% of P2)
E
Cdkn1a mRNA (Fold change)
F
p21
20kDa
Loading
p21 / total protein (% of P2)

Fig. 2 Effect of serial passage on β-Galactosidase activities, Cdkn2a and Cdkn1a mRNA expression, and p16 and p21 protein expression in pericytes.

(A) Representative microscopic images of β-galactosidase (β-Gal) staining in the P2, P4, P7, and P10 PCs. Scale bar: 100 μm. (B) β-galactosidase-positive area was quantified and compared between each group. (C, E) mRNA expression levels of Cdkn2a and Cdkn1a in P2, P4, P7, and P10 PCs. The results are expressed as fold-change relative to a calibrator (rat universal RNA). The representative western blot images of p16 (D) and p21 (F) in the P2, P4, P7, and P10 PCs. Densitometric quantification of the bands were done (right panel – D, F). Total protein levels measured using stain-free technology were considered as loading controls. The data were expressed as the percentage of corresponding data recorded for P2 PCs. Bar graphs indicate mean ± SEM (n = 3–7). *P < 0.05, **P < 0.01, ***P < 0.001, and ****P < 0.0001.

Fig. 3

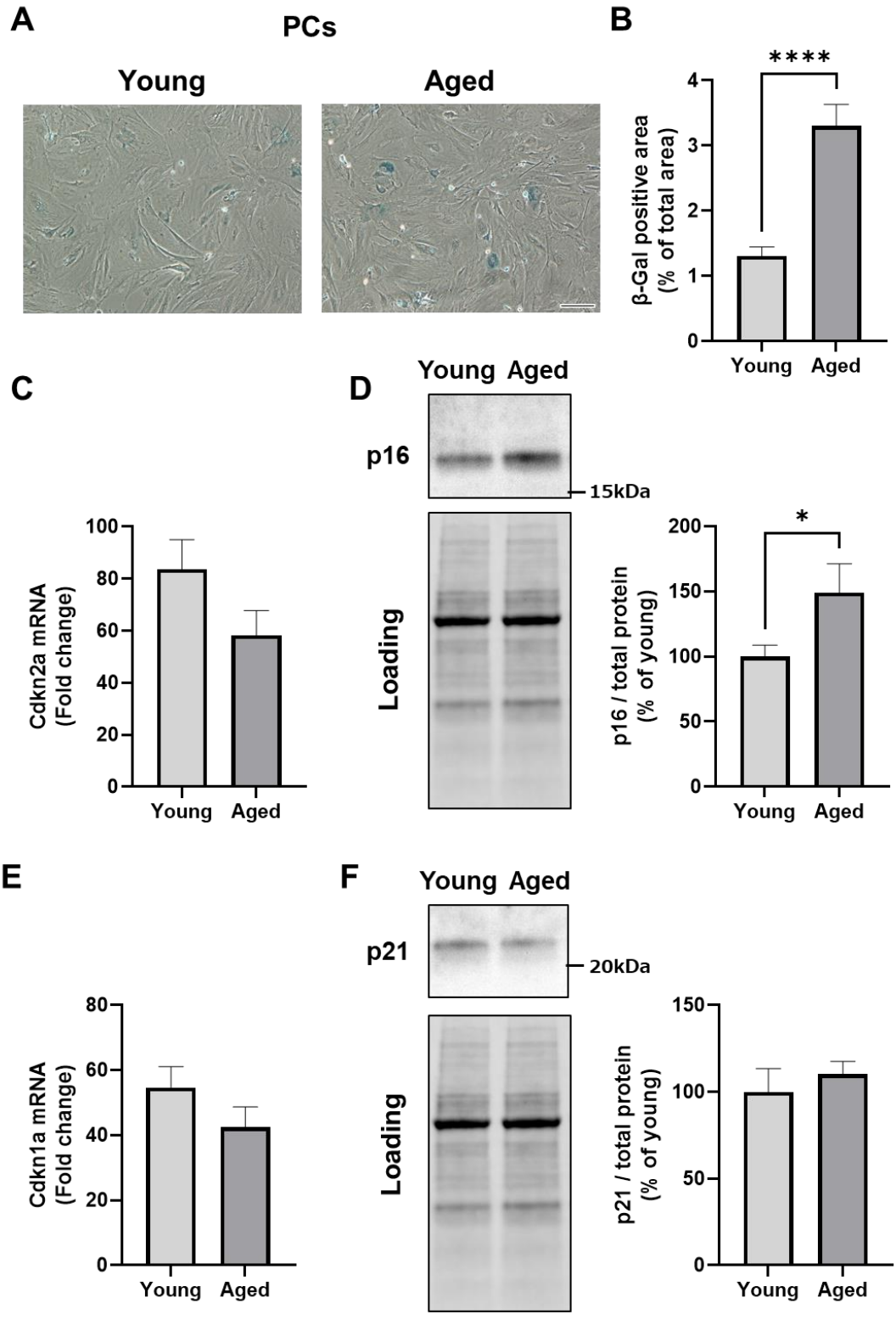
A
PCs
Young
Aged
B
****
β-Gal positive area
(% of total area)
Young
Aged
C
Cdkn2a mRNA
(Fold change)
Young
Aged
D
Young Aged
p16
15kDa
Loading
*
p16 / total protein
(% of young)
Young
Aged
E
Cdkn1a mRNA
(Fold change)
Young
Aged
F
Young Aged
p21
20kDa
Loading
p21 / total protein
(% of young)
Young
Aged

Fig. 3 Effect of aging on β-Galactosidase activities, Cdkn2a and Cdkn1a mRNA expression, and p16 and p21 protein expression in pericytes.

(A) Representative images of β-galactosidase (β-Gal) staining in PCs isolated from young (3–4-week-old) and aged (18-month-old) rats. Scale bar: 100 μm. (B) β-galactosidase-positive area was quantified and compared between the groups. (C, E) mRNA expression of Cdkn2a and Cdkn1a in young and aged PCs. The results are expressed as fold-change relative to a calibrator (rat universal RNA). The left panel shows representative western blot images of p16 (D) and p21 (F) in young and aged PCs. The band intensities were quantified using densitometry (right panel – D and F). Total protein was used as loading controls in the stain-free technology. Data are expressed as the percentage of data obtained for young PCs. Bar graphs indicate mean ± SEM (n = 3–6). *P < 0.05 and ****P < 0.0001, significantly different from young PCs.

Fig. 4

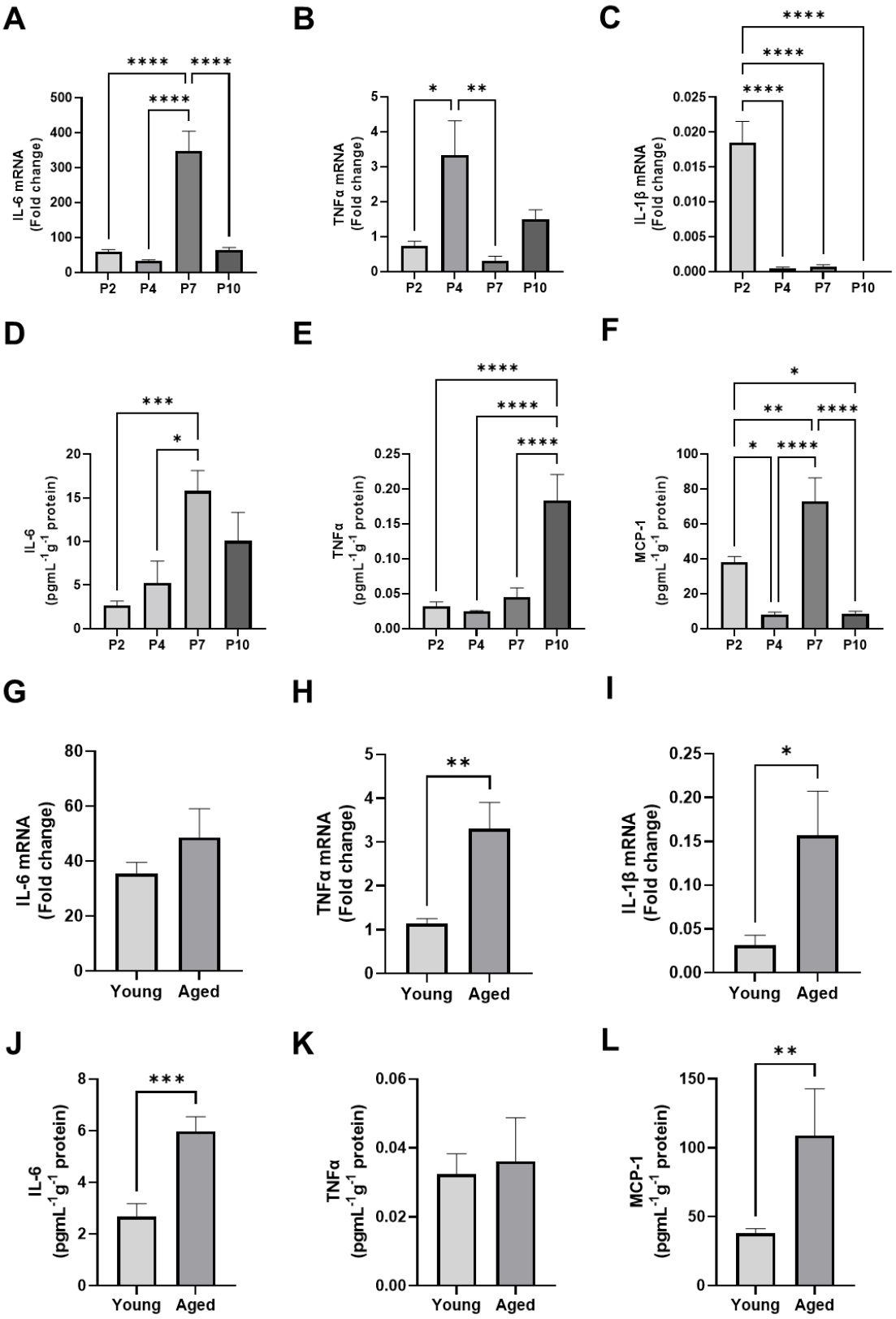
A
IL-6 mRNA (Fold change)
B
TNFα mRNA (Fold change)
C
IL-1β mRNA (Fold change)
D
IL-6 (pgmL-1g-1 protein)
E
TNFα (pgmL-1g-1 protein)
F
MCP-1 (pgmL-1g-1 protein)
G
IL-6 mRNA (Fold change)
H
TNFα mRNA (Fold change)
I
IL-1β mRNA (Fold change)
J
IL-6 (pgmL-1g-1 protein)
K
TNFα (pgmL-1g-1 protein)
L
MCP-1 (pgmL-1g-1 protein)
P2
P4
P7
P10
Young
Aged

Fig. 4 mRNA expression and release of senescence-associated secretory phenotype (SASP) factors in serial passaged and aged pericytes.

The mRNA expression levels of IL-6, TNFα, and IL-1β considered as senescence-associated secretory phenotype (SASP) factors in P2, P4, P7, and P10 PCs (A, B, C) and young and naturally aged PCs (G, H, I). The results are expressed as fold-change relative to a calibrator (rat universal RNA). The concentrations of IL-6, TNFα, and MCP-1 in conditioned media obtained from P2, P4, P7, and P10 PCs (D, E, F) and young and aged PCs (J, K, L). Data are shown as mean ± SEM (n = 3 – 8). *P < 0.05, **P < 0.01, ***P < 0.001, and ****P < 0.0001.

Fig. 5

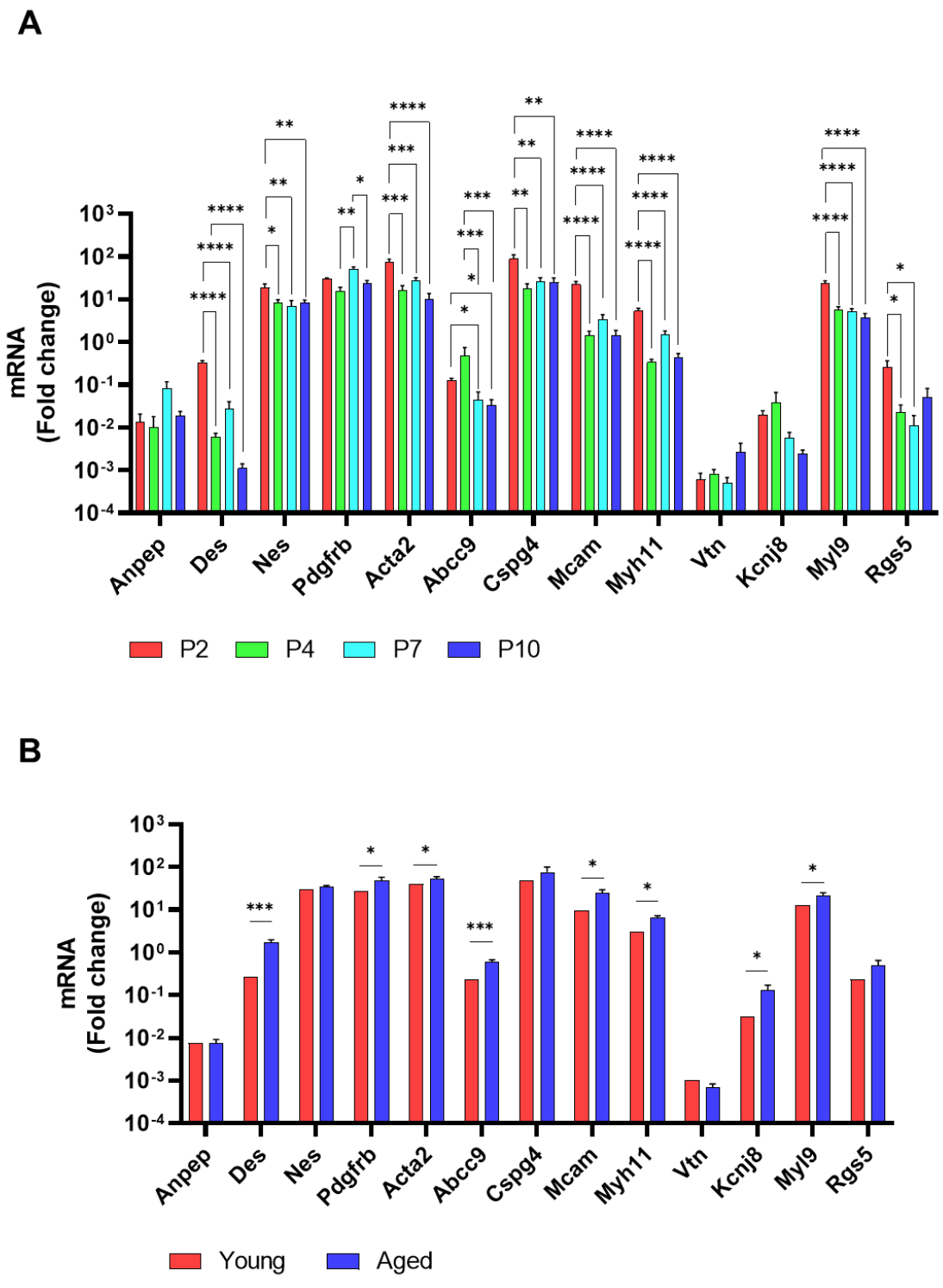
A
mRNA (Fold change)
Anpep
Des
Nes
Pdgfrb
Acta2
Abcc9
Cspg4
Mcam
Myh11
Vtn
Kcnj8
Myl9
Rgs5
P2
P4
P7
P10
B
mRNA (Fold change)
Young
Aged

Fig. 5 mRNA expression of pericyte markers in serially passaged and aged pericytes.

(A) mRNA expression levels of Anpep (N-aminopeptidase, CD13), Des (desmin), Nes (nestin), Pdgfrb, Acta2 (α-smooth muscle actin), Abcc9 (SUR2 subunit of K+-ATP channel), Cspg4 (chondroitin sulfate proteoglycan neuron-glial antigen 2, NG2), Mcam (melanoma cell adhesion molecule, CD146), Myh11 (myosin heavy chain 11), Vtn (vitronectin), Kcnj8 (Kir6.1), Myl9 (myosin light chain 9), and Rgs5 (regulator of G protein signaling 5) considered as brain pericyte markers in P2, P4, P7, and P10 PCs; (B) and PCs isolated from young (3–4-week-old) and aged (18-month-old) rats. The results are expressed as fold-change relative to a calibrator (rat universal RNA). Data are shown as mean ± SEM (n = 5 – 8). *P < 0.05, **P < 0.01, ***P < 0.001, and ****P < 0.0001.

References

[1] N.J. Abbott, A.A. Patabendige, D.E. Dolman, et al., Structure and function of the blood-brain barrier, Neurobiol. Dis. 37 (2010) 13–25. https://doi.org/10.1016/j.nbd.2009.07.030.

[2] S.M. Stamatovic, R.F. Keep, A.V. Andjelkovic, Brain endothelial cell-cell junctions: How to “open” the blood brain barrier, Curr. Neuropharmacol. 6 (2008) 179–192. https://doi.org/10.2174/157015908785777210.

[3] B.S. Desai, A.J. Monahan, P.M. Carvey, et al., Blood-brain barrier pathology in Alzheimer’s and Parkinson’s disease: Implications for drug therapy, Cell Transplant. 16 (2007) 285–299. https://doi.org/10.3727/000000007783464731.

[4] B.V. Zlokovic, The blood-brain barrier in health and chronic neurodegenerative disorders, Neuron. 57 (2008) 178–201. https://doi.org/10.1016/j.neuron.2008.01.003.

[5] J. Correale, A. Villa, The blood-brain-barrier in multiple sclerosis: Functional roles and therapeutic targeting, Autoimmunity. 40 (2007) 148–160. https://doi.org/10.1080/08916930601183522.

[6] I.C.M. Verheggen, J.J.A. de Jong, M.P.J. van Boxtel, et al., Increase in blood-brain barrier leakage in healthy, older adults, GeroScience. 42 (2020) 1183–1193. https://doi.org/10.1007/s11357-020-00211-2.

[7] A. Montagne, S.R. Barnes, M.D. Sweeney, et al., Blood-brain barrier breakdown in the aging human hippocampus, Neuron. 85 (2015) 296–302. https://doi.org/10.1016/j.neuron.2014.12.032.

[8] A.D. Mooradian, M.J. Haas, J.M. Chehade, Age-related changes in rat cerebral occludin and zonula occludens-1 (ZO-1), Mech. Ageing Dev. 124 (2003) 143–146. https://doi.org/10.1016/s0047-6374(02)00041-6.

[9] F. Erdő, L. Denes, E. de Lange, Age-associated physiological and pathological changes at the blood-brain barrier: A review, J. Cereb. Blood Flow Metab. 37 (2017) 4–24. https://doi.org/10.1177/0271678X16679420.

[10] M. Li, Y. Li, L. Zuo, et al., Increase of blood-brain barrier leakage is related to cognitive decline in vascular mild cognitive impairment, BMC Neurol. 21 (2021) 159. https://doi.org/10.1186/s12883-021-02189-6.

[11] Z. Lin, S. Sur, P. Liu, et al., Blood-brain barrier breakdown in relationship to Alzheimer and vascular disease, Ann. Neurol. 90 (2021) 227–238. https://doi.org/10.1002/ana.26134.

[12] D.A. Nation, M.D. Sweeney, A. Montagne, et al., Blood-brain barrier breakdown is an early biomarker of human cognitive dysfunction, Nat. Med. 25 (2019) 270–276. https://doi.org/10.1038/s41591-018-0297-y.

[13] J.C. Jeyapalan, M. Ferreira, J.M. Sedivy, et al., Accumulation of senescent cells in mitotic tissue of aging primates, Mech. Ageing Dev. 128 (2007) 36–44. https://doi.org/10.1016/j.mad.2006.11.008.

[14] A. Calcinotto, J. Kohli, E. Zagato, et al., Cellular senescence: Aging, cancer, and injury, Physiol. Rev. 99 (2019) 1047–1078. https://doi.org/10.1152/physrev.00020.2018.

[15] S. Courtois-Cox, S.L. Jones, K. Cichowski, Many roads lead to oncogene-induced senescence, Oncogene. 27 (2008) 2801–2809. https://doi.org/10.1038/sj.onc.1210950.

[16] J. Birch, J. Gil, Senescence and the SASP: Many therapeutic avenues, Genes Dev. 34 (2020) 1565–1576. https://doi.org/10.1101/gad.343129.120.

[17] V. Gorgoulis, P.D. Adams, A. Alimonti, et al., Cellular senescence: Defining a path forward, Cell. 179 (2019) 813–827. https://doi.org/10.1016/j.cell.2019.10.005.

[18] B. De Strooper, E. Karran, The cellular phase of Alzheimer's disease, Cell. 164 (2016) 603–615. https://doi.org/10.1016/j.cell.2015.12.056.

[19] A. Guerrero, B. De Strooper, I.L. Arancibia-Cárcamo, Cellular senescence at the crossroads of inflammation and Alzheimer's disease, Trends Neurosci. 44 (2021) 714–727. https://doi.org/10.1016/j.tins.2021.06.007.

[20] Y. Yamazaki, D.J. Baker, M. Tachibana, et al., Vascular cell senescence contributes to blood-brain barrier breakdown, Stroke. 47 (2016) 1068–1077. https://doi.org/10.1161/STROKEAHA.115.010835.

[21] T. Dalkara, Y. Gursoy-Ozdemir, M. Yemisci, Brain microvascular pericytes in health and disease, Acta Neuropathol. 122 (2011) 1–9. https://doi.org/10.1007/s00401-011-0847-6.

[22] D. Attwell, A. Mishra, C.N. Hall, et al., What is a pericyte?, J. Cereb. Blood Flow Metab. 36 (2016) 451–455. https://doi.org/10.1177/0271678X15610340.

[23] S. Nakagawa, M.A. Deli, H. Kawaguchi, et al., A new blood-brain barrier model using primary rat brain endothelial cells, pericytes and astrocytes, Neurochem. Int. 54 (2009) 253–263. https://doi.org/10.1016/j.neuint.2008.12.002.

[24] S. Dohgu, F. Takata, Y. Kataoka, Brain pericytes regulate the blood-brain barrier function, Nihon Yakurigaku Zasshi. 146 (2015) 63–65. https://doi.org/10.1254/fpj.146.63.

[25] R. Daneman, L. Zhou, A.A. Kebede, et al., Pericytes are required for blood-brain barrier integrity during embryogenesis, Nature. 468 (2010) 562–566. https://doi.org/10.1038/nature09513.

[26] J.D. Sengillo, E.A. Winkler, C.T. Walker, et al., Deficiency in mural vascular cells coincides with blood-brain barrier disruption in Alzheimer's disease, Brain Pathol. 23 (2013) 303–310. https://doi.org/10.1111/bpa.12004.

[27] M.D. Sweeney, A.P. Sagare, B.V. Zlokovic, Blood-brain barrier breakdown in Alzheimer disease and other neurodegenerative disorders, Nat. Rev. Neurol. 14 (2018) 133–150. https://doi.org/10.1038/nrneurol.2017.188.

[28] R.D. Bell, E.A. Winkler, A.P. Sagare, et al., Pericytes control key neurovascular functions and neuronal phenotype in the adult brain and during brain aging, Neuron. 68 (2010) 409–427. https://doi.org/10.1016/j.neuron.2010.09.043.

[29] S. Dohgu, F. Takata, J. Matsumoto, et al., Monomeric α-synuclein induces blood-brain barrier dysfunction through activated brain pericytes releasing inflammatory mediators in vitro, Microvasc. Res. 124 (2019) 61–66. https://doi.org/10.1016/j.mvr.2019.03.005.

[30] F. Takata, S. Dohgu, A. Yamauchi, et al., In vitro blood-brain barrier models using brain capillary endothelial cells isolated from neonatal and adult rats retain age-related barrier properties, PLOS ONE. 8 (2013) e55166. https://doi.org/10.1371/journal.pone.0055166.

[31] A. Hernandez-Segura, J. Nehme, M. Demaria, Hallmarks of cellular senescence, Trends Cell Biol. 28 (2018) 436–453. https://doi.org/10.1016/j.tcb.2018.02.001.

[32] F. Takata, S. Dohgu, J. Matsumoto, et al., Oncostatin M-induced blood-brain barrier impairment is due to prolonged activation of STAT3 signaling in vitro, J. Cell. Biochem. 119 (2018) 9055–9063. https://doi.org/10.1002/jcb.27162.

[33] S. Dohgu, N. Sumi, T. Nishioku, et al., Cyclosporin A induces hyperpermeability of the blood-brain barrier by inhibiting autocrine adrenomedullin-mediated up-regulation of endothelial barrier function, Eur. J. Pharmacol. 644 (2010) 5–9. https://doi.org/10.1016/j.ejphar.2010.05.035.

[34] F. Rodier, J. Campisi, Four faces of cellular senescence, J. Cell Biol. 192 (2011) 547–556. https://doi.org/10.1083/jcb.201009094.

[35] L.C.D. Smyth, J. Rustenhoven, E.L. Scotter, et al., Markers for human brain pericytes and smooth muscle cells, J. Chem. Neuroanat. 92 (2018) 48–60. https://doi.org/10.1016/j.jchemneu.2018.06.001.

[36] M. Vanlandewijck, L. He, M.A. Mäe, et al., A molecular atlas of cell types and zonation in the brain vasculature, Nature. 554 (2018) 475–480. https://doi.org/10.1038/nature25739.

[37] J. Krishnamurthy, C. Torrice, M.R. Ramsey, et al., Ink4a/Arf expression is a biomarker of aging, J. Clin. Invest. 114 (2004) 1299–1307. https://doi.org/10.1172/JCI22475.

[38] H. Rayess, M.B. Wang, E.S. Srivatsan, Cellular senescence and tumor suppressor gene p16, Int. J. Cancer. 130 (2012) 1715–1725. https://doi.org/10.1002/ijc.27316.

[39] A. Hernandez-Segura, T.V. de Jong, S. Melov, et al., Unmasking transcriptional heterogeneity in senescent cells, Curr. Biol. 27 (2017) 2652–2660.e4. https://doi.org/10.1016/j.cub.2017.07.033.

[40] W.F. Leong, J.F. Chau, B. Li, p53 Deficiency leads to compensatory up-regulation of p16INK4a, Mol. Cancer Res. 7 (2009) 354–360. https://doi.org/10.1158/1541-7786.MCR-08-0373.

[41] D. Tsygankov, Y. Liu, H.K. Sanoff, N.E. Sharpless, et al., A quantitative model for age-dependent expression of the p16INK4a tumor suppressor, Proc. Natl Acad. Sci. U. S. A. 106 (2009) 16562–16567. https://doi.org/10.1073/pnas.0904405106.

[42] Y. Song, H. Shen, D. Schenten, et al., Aging enhances the basal production of IL-6 and CCL2 in vascular smooth muscle cells, Arterioscler. Thromb. Vasc. Biol. 32 (2012) 103–109. https://doi.org/10.1161/ATVBAHA.111.236349.

[43] F. Takata, S. Nakagawa, J. Matsumoto, et al., Blood-brain barrier dysfunction amplifies the development of neuroinflammation: Understanding of cellular events in brain microvascular endothelial cells for prevention and treatment of BBB dysfunction, Front. Cell. Neurosci. 15 (2021) 661838. https://doi.org/10.3389/fncel.2021.661838.

[44] S.S. Cohen, M. Min, E.E. Cummings, et al., Effects of interleukin-6 on the expression of tight junction proteins in isolated cerebral microvessels from yearling and adult sheep, Neuroimmunomodulation. 20 (2013) 264–273. https://doi.org/10.1159/000350470.

[45] M. Elahy, C. Jackaman, J.C. Mamo, et al., Blood-brain barrier dysfunction developed during normal aging is associated with inflammation and loss of tight junctions but not with leukocyte recruitment, Immun. Ageing. 12 (2015) 2. https://doi.org/10.1186/s12979-015-0029-9.

[46] L.S. Brown, C.G. Foster, J.M. Courtney, et al., Pericytes and neurovascular function in the healthy and diseased brain, Front. Cell. Neurosci. 13 (2019) 282. https://doi.org/10.3389/fncel.2019.00282.

[47] J. Rustenhoven, L.C. Smyth, D. Jansson, et al., Modelling physiological and pathological conditions to study pericyte biology in brain function and dysfunction, BMC Neurosci. 19 (2018) 6. https://doi.org/10.1186/s12868-018-0405-4.

Chapter 4: Brain pericytes induce the expression and plasma membrane localization of MFSD2A in brain endothelial cells through the PDGFB/PDGFRβ signaling pathway.

Introduction

The central nervous system (CNS) has a blood–brain barrier (BBB), which is composed of brain microvessel endothelial cells (BMECs), astrocytes, and pericytes, to maintain brain homeostasis by restricting penetration of substances from blood to the brain. Tight junction (Tj)-associated proteins in BMECs play an important role in regulating paracellular permeability. Moreover, BBB restricts a paracellular permeability and regulates transcellular permeability, such as transport of ions, neurotransmitters, and nutrients, between blood and the brain by various transporters expressed on BMECs [1,2]. The functional and structural breakdown of BBB occurs in various neurological diseases, including chronic Alzheimer's disease and Parkinson's disease, acute ischemic stroke, traumatic brain injury, epileptic seizures, and brain tumor [3,4].

Major facilitator superfamily domain-containing protein-2a (Mfsd2a) is a major facilitator superfamily (MFS) of membrane proteins and exclusively expressed in BMECs [5,6]. The major transporter for LPC-DHA uptake by the brain is MFSD2A [7]. Moreover, MFSD2A mediates the cellular uptake of NE-DHA through brain endothelial cells (ECs; Chapter 1). In addition, the proper localization of MFSD2A in BMECs is required for transport activity [6,7]. MFSD2A is involved in brain DHA transport and contributes to the formation and functioning of BBB [6,8]. In particular, it helps maintain a low-level permeability of BBB to regulate transcytosis in BMECs [9]. It is associated with pathological processes of nervous system diseases by regulating BBB integrity [10,11].

Pericytes are present at intervals along the walls of capillaries and surround BMECs in CNS. They interact with neighboring cells, including BMECs and astrocytes, and contribute to maintaining homeostasis of CNS by regulating cerebral blood flow, stabilizing BBB integrity, and mediating immune responses [12,13]. Furthermore, their presence is required for the MFSD2A expression in BMECs [6]. However, how pericytes regulate the MFSD2A expression in BMECs is unclear.

The aim of the present study was to investigate how pericytes regulate the expression and localization of MFSD2A in BMECs.

Materials and Methods

Animals

All protocols involving experimental animals were approved by the Laboratory Animal Care and Use Committee of Fukuoka University (permit number: 2204002). The 3- to 4-week-old male and female Wistar rats were purchased from Japan SLC, Inc. (Shizuoka, Japan), and housed under a controlled temperature (22°C ± 2°C) and light/dark cycle (lights on from 7:00 to 19:00), with access to water and chow diet *ad libitum*.

Primary cultures of rat brain ECs and pericytes

The method of primary culture of ECs and pericytes was as previously described [14,15]. Primary cultured ECs were plated on 100-mm dishes coated with collagen type IV (0.1 mg/mL, Sigma, St. Louis, MO, USA; C5533) and fibronectin (0.075 mg/mL, Sigma; F1141-5MG) for ECs. Primary cultured pericytes were plated on an uncoated 75-cm^2 flask. Primary cultured ECs were maintained in the EC medium (Dulbecco's Modified Eagle Medium [DMEM]/F12 [Wako; 042-30555]) supplemented with 10% fetal bovine serum (FBS; Biosera, Kansas, MO, USA; FB-1365/500), a basic fibroblast growth factor (1.5 ng/mL, R&D, Minneapolis, MN, USA; 2099-FB-025), heparin (100 μg/mL, Sigma; H3149), insulin (5 μg/mL), transferrin (5 μg/mL), sodium selenite (5 ng/mL; insulin-transferrin-sodium selenite media supplement, Sigma; I1884), penicillin (100 units/mL), streptomycin (100 μg/mL; penicillin–streptomycin mixed solution, Nacalai Tesque, Kyoto, Japan; 09367-34) and gentamicin (50 μg/mL, Biowest, Riverside, MO, USA; L0012) containing puromycin (4 μg/mL, Nacalai Tesque; 14861-84) at 37°C in a humidified atmosphere of 5% CO_2/95% air, for 3 days and typically reaching 70%–80% confluency. Pericyte cultures were maintained in the pericyte medium DMEM (Wako, 048-29763) supplemented with 20% FBS (Gibco/Thermo Fisher Scientific, Waltham, MA, USA; A3160602), penicillin (100 units/mL), streptomycin (100 μg/mL; penicillin–streptomycin mixed solution, Nacalai Tesque, 09367-34) and gentamicin (50 μg/mL, Biowest, Riverside; L0012)] at 37°C in a

humidified atmosphere of 5% CO_2/95% air, for 9 days with exchanging fresh culture media once 3 days and typically reaching 70%–80% confluency.

Non-contact coculture models using rat brain ECs and pericytes

Rat brain ECs were seeded to the bottom of a 6-well plate (30×10^4 cells/well), the inside of 24-well transwell inserts (5×10^4 cells/transwell, 0.4-μm pore size; Corning, Midland, MI; 3470) and the bottom of a 24-well plate (10×10^4 cells/well) coated with collagen type IV (0.1 mg/mL, Nitta Gelatin Inc.; 638-05921) and fibronectin (0.025 mg/mL, Sigma) and maintained in the EC medium supplemented with 500 nM of hydrocortisone (Sigma; H0135). Rat brain pericytes were seeded to the inside of 6-well transwell inserts (0.1 to 10×10^4 cells/transwell), 35-mm dishes (10×10^4 cells/dish), the bottom of a 24-well plate (2.5×10^4 cells/well) and the inside of 24-well transwell inserts (1 to 4×10^4 cells/transwell, 0.4-μm pore size; Corning; 3470) coated with Cellmatrix Collagen Type I–C (0.1 mg/mL, Nitta Gelatin Inc.) and cultured in the pericyte medium. Cell cultures of non-contact cocultured models, structuring ECs on the bottom of a plate and pericytes in the transwell inserts or ECs in the transwell inserts and pericytes on the bottom of a plate, were maintained in the EC medium supplemented with 500 nM of hydrocortisone for 1–3 days in vitro.

Treatment of rat brain ECs with a conditioned medium derived from pericytes

Rat brain pericytes on 35-mm dishes were cultured in the rat brain EC medium supplemented with 500 nM of hydrocortisone for 3 days in vitro and collected in tubes. In parallel, to obtain a cell-free conditioned medium, the EC medium supplemented with 500 nM of hydrocortisone without pericytes was incubated in 35-mm dishes for the same period and collected in tubes. Subsequently, ECs were cultured in a pericyte-conditioned medium or cell free-conditioned medium for 3 days in vitro.

Small interfering RNA (siRNA) transfection

Pericytes cultured on 35-mm dishes or the inside of 6-well transwell inserts were transfected with the lipid complex, including Lipofectamine® RNAiMAX Transfection Reagent (4 μL; Invitrogen/Thermo Fisher Scientific, 13778075) and Rat Pdgfrb Silencer® Select Pre-designed siRNA (50 nM; Life technologies/Thermo Fisher Scientific, 4390771) or Silencer Select Negative Control (50 nM; Life technologies/Thermo Fisher Scientific, 4390843) in the pericyte medium for 1–3 days in vitro. PDGFRβ protein levels in pericytes were assessed using western blotting. In addition, pericytes were transfected with the lipid complex, including siPdgfrb or a negative control, in the pericyte medium for 1 day and cultured by replacing with the EC medium for 3 days in vitro. Subsequently, PDGFRβ protein levels in pericytes were assessed using western blotting.

Non-contact coculture models using rat brain ECs and siPdgfrb-transfected pericytes

Rat brain pericytes cultured on inside of 6-well transwell inserts were transfected with the lipid complex, including siPdgfrb or a negative control, in the pericyte medium for 1 day and cocultured with rat brain ECs seeded to the bottom of a 6-well plate for 3 days in vitro by the EC medium supplemented with 500 nM of hydrocortisone. In parallel, ECs were cultured without pericytes for 3 days in vitro by the EC medium supplemented with 500 nM of hydrocortisone as control groups.

Non-contact coculture models using rat brain ECs and AG1296-treated pericytes

The bottoms of 24-well plates with or without rat brain pericytes were pre-incubated with a vehicle (0.1% dimethyl sulfoxide [Wako, 045-24511]) or AG1296 10 μM (Santacruz, Dallas, TX, USA; sc-200631) in the rat brain EC medium supplemented with 500 nM of hydrocortisone for 15 min. Subsequently, ECs seeded on the inside of 24-well

transwell inserts were cocultured with or without pericytes pre-treated with a vehicle or AG1296 10 μM for 3 days in vitro in the EC medium supplemented with 500 nM of hydrocortisone.

Western blotting

Rat brain ECs and pericytes were scraped and lysed in a lysis buffer containing 10 mM Tris-HCl (pH 6.8; Nacalai Tesque; 35434-34), 100 mM NaCl (Sigma; 28-2270-5), 1 mM of ethylenediaminetetraacetic acid (pH 8.0; Wako; 311-90075), 1 mM of egtazic acid (Wako; 346-01312), 10% glycerol, 1% Triton-X100 (Sigma; X100), 0.1% sodium dodecyl sulfate (Nacalai Tesque; 02873-75), 0.5% sodium deoxycholate (Sigma; D6750), 20 mM of sodium pyrophosphate (Sigma; S6422), 2 mM of sodium orthovanadate (Sigma; S6508), 1 mM of sodium fluoride (Wako; 196-01975), 1% protease inhibitor cocktail (Sigma; P2714), 1% phosphatase inhibitor cocktail 2 (Sigma; P5726), 1% Phosphatase Inhibitor Cocktail 3 (Sigma; P0044), and 1 mM of phenylmethylsulfonyl fluoride (Sigma; P7626). The total protein concentration in cell lysates was determined using the Pierce™ BCA Protein Assay Kit (Thermo Fisher Scientific; 23225). Equivalent amounts of protein from each sample were electrophoretically separated on 7.5% TGX Stain-Free gradient acrylamide gels (Bio-Rad, Hercules, CA; 161-0181) or 12% TGX Stain-Free acrylamide gels (Bio-Rad; 161-0185) and transferred to low fluorescent polyvinylidene difluoride membranes (Bio-Rad; 1704274). Membranes were then blocked using Blocking One (Nacalai Tesque; 03953-95). MFSD2A, PDGFRβ, and β-actin were detected using antibodies against MFSD2A (1:1,000; Sigma; SAB3500576), PDGFRβ (1:1,000; Cell Signaling Technology, Danvers, MA, USA; 3169S), and β-actin (1:8,000; Sigma; A1978). After washing, the membranes were incubated in horseradish peroxidase-conjugated goat anti-rabbit IgG (Bio-Rad; 170-6515) or goat anti-mouse IgG (Bio-Rad; 170-6516), as appropriate. Immunoreactive bands were detected using the Clarity Western ECL Substrate (Bio-Rad; 1705061). Images of the bands were digitally captured using the MultiImager II ChemiBOX (BioTools, Gunma, Japan), and band intensities were quantified using ImageJ software (National Institutes of Health Image, Bethesda, MD, USA). The relative intensity of each individual protein was expressed as the ratio of the corresponding protein to the β-actin.

Immunofluorescence staining

Rat brain ECs cultured on the inside of 24-well transwell inserts were fixed with 99.8% methanol (Nacalai Tesque, 21915-93) for 2 min at −20°C. ECs were permealized and blocked with 0.3% Triton™ X-100 (Sigma; X100) in Blocking One for 30 min and incubated with primary antibodies against occludin (1:100; Invitrogen/Thermo Fisher Scientific; 33-1500) and MFSD2A (1:100; Sigma; SAB3500576) overnight at 4°C. Subsequently, they were incubated with CF488-labeled goat anti-mouse IgG (1:1,000; Nacalai Tesque) for occludin and Cy3-labeled donkey anti-rabbi IgG (1:1,000; Jackson ImmunoResearch, West Grove, PA, USA) for MFSD2A for 1 h at 20-25°C. The membrane of the transwell inserts was cut and mounted on a slide glass and then encapsulated with the VECTASHIELD Mounting Medium with 4',6-diamidino-2-phenylindole (Vector Laboratories, Newark, CA, USA; H-1200). All samples were imaged using a fluorescence microscope (BZ-X710, KEYENCE, Osaka, Japan).

Cellular uptake of [^{14}C]DHA by brain ECs cocultured with pericytes

The method of cellular uptake of DHA was as previously described (Chapter 1). Rat brain ECs seeded to the bottom of a 24-well plate were cocultured with or without pericytes seeded to the inside of 24-well transwell inserts for 3 days in vitro. Subsequently, ECs were incubated with 0.2 mL of a physiological buffer containing 0.1 μCi/mL [^{14}C]DHA (incubation buffer; American Radiolabeled Chemicals, St. Louis, MO, USA; ARC0380) at 37°C for 2 min. Subsequently, they were washed with D-PBS thrice and incubated with 0.2 mL of 1M NaOH (Wako; 192-02175) at 37°C for 3 h for cell lysis. The total protein concentration in cell lysates was determined using the Pierce™ BCA Protein Assay Kit. Samples were added to 10 mL of a liquid scintillation cocktail (Pico-Fluor Plus; PerkinElmer; 6013699), and [^{14}C]DHA radioactivity in the cell lysate was measured using a liquid scintillation counter. The cellular uptake of [^{14}C]DHA by ECs was expressed as cell/medium ratios calculated by dividing the radioactivity in 1 mg of protein through radioactivity in 1 μL of the incubation buffer.

Statistical analysis

Results are expressed as mean ± standard error of the mean. Statistical analyses were performed using GraphPad Prism 8.0 (GraphPad, San Diego, CA, USA). The unpaired *t*-test was used for between-group comparisons. Statistical differences between groups were analyzed using the one- or two-way analysis of variance (ANOVA) followed by Tukey's multiple-comparisons tests. Statistical analyses for evaluating two factors between groups were performed using the two-way ANOVA, followed by Šídák's multiple-comparisons tests. Differences were considered statistically significant at a *P*-value < 0.05.

Results

Pericytes regulate the MFSD2A expression on brain ECs through cell-to-cell interaction.

To evaluate the effect of pericytes on the MFSD2A expression in brain ECs, the MFSD2A protein expression levels in rat brain ECs were assessed using non-contact coculture models comprising rat brain ECs and pericytes. Fig. 1A shows the schematic diagrams of the experimental procedures using non-contact coculture models. First, ECs were cocultured with or without pericytes for 1 or 2 days in vitro. In the group of pericyte coculture for 3 days in vitro, the MFSD2A protein expression levels increased by 26% (P = 0.0323) compared to that of the EC monolayer for 3 days in vitro (Fig. 1B). The two-way ANOVA revealed significant effects of coculturing pericytes ($F(1, 32) = 7.496$, $P = 0.0100$) but not of time ($F(1, 32) = 0.7716$, $P = 0.3863$) or interaction between coculturing pericytes and time ($F(1, 32) = 0.7716$, $P = 0.3863$). Next, the pericytes were seeded at different densities into the 24-well transwell inserts and cultured with or without ECs for 3 days in vitro. The MFSD2A protein expression levels in the pericyte (10×10^4 cells) coculture group increased by 42.6% ($P = 0.0008$) compared to the EC monolayer group. The one-way ANOVA showed an effect for coculturing of pericytes on the MFSD2A protein expression levels (Fig. 1C; $F = 5.145$, $P = 0.0021$). Moreover, we examined whether or not the pericyte-derived soluble factors affected the MFSD2A protein expression in ECs. Fig. 1D shows the schematic diagrams of experimental procedures for evaluating the effect of soluble factors released by intact pericytes on ECs. The conditioned medium derived from pericyte or cell-free cultures was collected, and ECs were cultured for 3 days in vitro in each medium. Pericyte cultures did not affect the MFSD2A protein expression levels in ECs. These results indicate that the EC-to-pericyte interaction enhances the MFSD2A protein expression levels in ECs.

PDGFB/PDGFRβ signaling between brain ECs and pericytes regulates the MFSD2A expression on brain ECs.

PDGFRβ is exclusively expressed in perivascular pericytes and used as a characteristic marker for pericytes [16,17]. To determine whether or not PDGFB/PDGFRβ signaling between brain ECs and pericytes participates in the MFSD2A protein expression on brain ECs, we examined the effect of siPdgfrb transfection into rat brain pericytes on the MFSD2A protein expression in ECs. Fig. 2A shows the schematic diagrams of the experimental condition for siPdgfrb transfection into pericytes. First, we evaluated whether or not the transfection time period improves the siPdgfrb transfection efficiency. The siPdgfrb transfection significantly affects the PDGFRβ protein expression levels in pericytes, while the siPdgfrb transfection efficiency was independent of the transfection time period (Fig. 2B). The two-way ANOVA showed significant effects of siPdgfrb transfection ($F(1, 12) = 135.4$, $P = 0.0100$) but not of the transfection time period ($F(2, 12) = 0.5881$, $P = 0.3863$) or interaction between siPdgfrb transfection and the transfection time period ($F(2, 12) = 1.835$, $P = 0.2017$). Differences in the percentage of PDGFRβ protein expression levels between control and siPdgfrb groups were as follows: 82.26% (1 day in vitro, $P = 0.0006$), 124.1% (2 days in vitro, $P < 0.0001$), and 105.5% (3 days in vitro, $P < 0.0001$). Next, to validate the duration of the Pdgfrb knockdown in pericytes, pericytes were transfected with siPdgfrb for 1 day in vitro and then cultured by replacing with the EC medium for 3 days in vitro. The PDGFRβ protein expression levels in siPdgfrb groups decreased by 56% ($P = 0.0001$) compared to control groups (Fig. 2C). This result indicated that the effect of the Pdgfrb knockdown in pericytes continues for 3 days in vitro. Subsequently, we evaluated the effect of Pdgfrb-knockdown pericytes on the MFSD2A protein expression in ECs. Fig. 2D shows the schematic diagrams of the experimental procedures for evaluating the effect of Pdgfrb-knockdown pericytes on ECs. Pericytes seeded to the inside of 6-well transwell inserts were transfected with siPdgfrb or a negative control for 1 day in vitro and paced on a 6-well plate with ECs. ECs were cocultured with or without pericytes for 3 days in vitro in the EC medium. The MFSD2A protein expression levels were 26.6% higher in the pericyte coculture (control) groups than in the EC monolayer groups ($P = 0.0050$), and this increased expression of MFSD2A was inhibited ($P = 0.0004$) by Pdgfrb-knockdown pericytes (Fig. 2E). The one-way ANOVA showed an effect

of coculturing of pericytes on the MFSD2A protein expression levels ($F(2, 11) = 17.12$, $P = 0.0004$).

Pericytes increase plasma membrane localization of the MFSD2A protein in brain ECs.

We ascertained whether or not pericytes regulate the MFSD2A protein expression levels or plasma membrane localization of MFSD2A in brain ECs. Fig. 3A shows the schematic diagrams of the experimental procedures using non-contact coculture models comprising rat brain ECs and pericytes. ECs were cultured with or without pericytes for 1 or 3 days in vitro, and MFSD2A and occludin immunoreactivity in ECs were detected by immunofluorescence staining. The plasma membrane in ECs was identified by a localization of occludin, which is a Tj-associated protein and localized in the plasma membrane. MFSD2A proteins localized in the plasma membrane were determined by detecting areas with merged MFSD2A and occludin. In the group of pericyte coculture for 3 days in vitro, the area with merged MFSD2A and occludin increased 2.1 folds ($P = 0.0076$) compared to the EC monolayer for 3 days in vitro (Fig. 3B, C). The two-way ANOVA revealed significant effects of coculturing pericytes ($F(1, 11) = 9.978$, $P = 0.0091$) but not of the time ($F(1, 11) = 3.250$, $P = 0.0989$) or interaction between coculturing pericytes and time ($F(1, 11) = 3.250$, $P = 0.0989$).

PDGFB/PDGFRβ signaling between brain ECs and pericytes regulate the plasma membrane localization of the MFSD2A protein in brain ECs.

To determine whether or not PDGFB/PDGFRβ signaling between brain ECs and pericytes mediates the plasma membrane localization of the MFSD2A protein in brain ECs, we determined the presence/absence of an effect of AG1296, which is a tyrosine kinase inhibitor that binds to the intracellular domain of the PDGF receptor, on non-contact coculture models comprising rat brain ECs and pericytes. Fig. 4A shows the schematic diagrams of the experimental procedures using non-contact coculture models treated with

AG1296 or a vehicle. The area with merged MFSD2A and occludin was significantly larger in the pericyte coculture (vehicle) group than in the EC monolayer (vehicle) group, while AG1296 inhibited the increase in the area with merged MFSD2A and occludin by coculturing with pericytes (Fig. 4B, C). AG1296 did not affect the area with merged MFSD2A and occludin in the EC monolayer group. The one-way ANOVA showed an effect of coculturing with PCs on the area with merged MFSD2A and occludin ($F(3,39) = 6.254$, $P = 0.0014$). The percentage differences were as follows: 212.4% (EC monolayer [vehicle] vs. PC coculture [vehicle], $P = 0.0040$), 176.5% (EC monolayer [AG1296 10 μM] vs. pericyte coculture [vehicle], $P = 0.0210$), and 176.1% (PC coculture [vehicle] vs. pericyte coculture [AG1296 10 μM], $P = 0.0213$).

Pericytes upregulate the cellular uptake of DHA by brain ECs.

Finally, we examined whether or not pericytes facilitate the cellular uptake of DHA by brain ECs. MFSD2A mediates the cellular uptake of NE-DHA by brain ECs (Chapter 1). Fig. 5A shows the schematic diagrams of the experimental procedures for the cellular uptake of [^{14}C]DHA as NE-DHA using non-contact coculture models comprising rat brain ECs and pericytes. The cellular uptake of [^{14}C]DHA in the PC (4×10^4 cells) coculture group increased by 30% ($P = 0.0191$) compared to the EC monolayer group (Fig. 5B). The one-way ANOVA showed an effect of coculturing of PCs on the cellular uptake of [^{14}C]DHA by ECs ($F(X,X) = 3.946$, $P = 0.0191$).

Discussion

Pericytes play a critical role in the MFSD2A expression in BMECs [6], but how pericytes regulate the MFSD2A expression in BMECs remains unknown. MFSD2A regulates BBB integrity, and its reduction in relative to the pathological processes in nervous system diseases [10,11]. Therefore, elucidating the mechanism of regulating the MFSD2A expression is important. In this study, we investigated how pericytes regulate the expression and localization of MFSD2A in BMECs.

Using non-contact coculture models comprising rat brain ECs and pericytes, we demonstrated that ECs cocultured with pericytes show an elevated MFSD2A protein expression. The extent of increase in MFSD2A depends on coculture periods and cell numbers of pericytes (Fig. 1). Moreover, changes in the MFSD2A protein expression in BMECs are mediated by the cell-to-cell interaction rather than by the unidirectional secretion of soluble factors by intact pericytes (Fig. 1). These data suggested that soluble factors released by pericytes interacted with ECs to upregulate the MFSD2A protein expression in ECs.

Next, using Pdgfrb-knockdown pericytes, we ascertained whether or not PDGFB/PDGFRβ signaling between ECs and pericytes mediate the MFSD2A protein expression in ECs. Pdgfrb-knockdown pericytes failed to upregulate the MFSD2A protein expression to the extent of control (Fig. 2).

Furthermore, we evaluated the plasma membrane localization of the MFSD2A protein in ECs. Using non-contact coculture models, we showed that pericytes increase the plasma membrane localization of the MFSD2A protein in ECs accompanied with the increased MFSD2A protein expression levels (Fig. 3). Increased plasma localization of MFSD2A was inhibited by the tyrosine kinase inhibitor AG1296, which binds to the intracellular domain of the PDGF receptor (Fig. 4). These results suggested that PDGFB/PDGFRβ signaling between ECs and pericytes mediates the MFSD2A protein expression levels and the plasma membrane localization of the MFSD2A protein in ECs.

Finally, we confirmed that upregulation of the protein expression levels and plasma membrane localization of MFSD2A in ECs result in the functional improvement as cellular uptake of DHA. PCs induced the cellular uptake of DHA by ECs depending on the

number of pericytes (Fig. 5). Because proper localization of MFSD2A in BMECs is required for transport activity [6,7], the increased uptake of DHA by ECs would result from pericyte-induced plasma membrane localization of MFSD2A.

Pericytes and BMECs can communicate through direct contact, such as ion exchange via the gap junction and other paracrine molecules, to develop and maintain BBB [18–21]. However, in this study, we could not evaluate the interactions through their direct contact, owing to the use of non-contact cocultured models. Various ligand-receptor interactions exist between pericytes and BMECs in the CNS microvasculature, including PDGFB/PDGFRβ, VEGF/VEGFR2, TGF-β/TGFBR, and angiopoietin 1/Tie2 signaling pathways, which contribute to the angiogenesis, stabilization, and remodeling of the mature vasculature [18,22,23]. PDGFB derived from ECs is critical for a proper pericyte recruitment to blood vessels [24–26]. Furthermore, PDGFB/PDGFRβ signaling between pericytes and BMECs was involved in the MFSD2A protein expression levels and membrane localization in BMECs.

Previous studies on the mechanism regulating the MFSD2A expression and localization at BBB [27,28] showed that Wnt signaling transcriptionally regulates the MFSD2A expression [27] and that BBB permeability is controlled by the PTEN/AKT/NEDD4-2/MFSD2A axis [28]. The previous and present studies suggested that pericytes release soluble factors, which activate Wnt signaling and the PTEN/AKT/NEDD4-2/MFSD2A axis in BMECs, resulting from interaction with BMECs through PDGFB/PDGFRβ signaling. However, further studies are required to clarify the mechanism through which pericyte-derived soluble factors regulate the MFSD2A expression and membrane localization in ECs.

Conclusions

In conclusion, we demonstrated that pericytes induced the MFSD2A protein expression in ECs through PDGF-B/PDGFRβ signaling between pericytes and ECs. Furthermore, pericytes upregulated the MFSD2A protein expression levels and the plasma membrane localization of the MFSD2A protein in ECs. Increased plasma membrane localization of the MFSD2A protein can result in functionally activating MFSD2A. These

findings would be helpful to further understand the relationship between pericytes and MFSD2A under physiological and pathological conditions.

Figures

Fig. 1

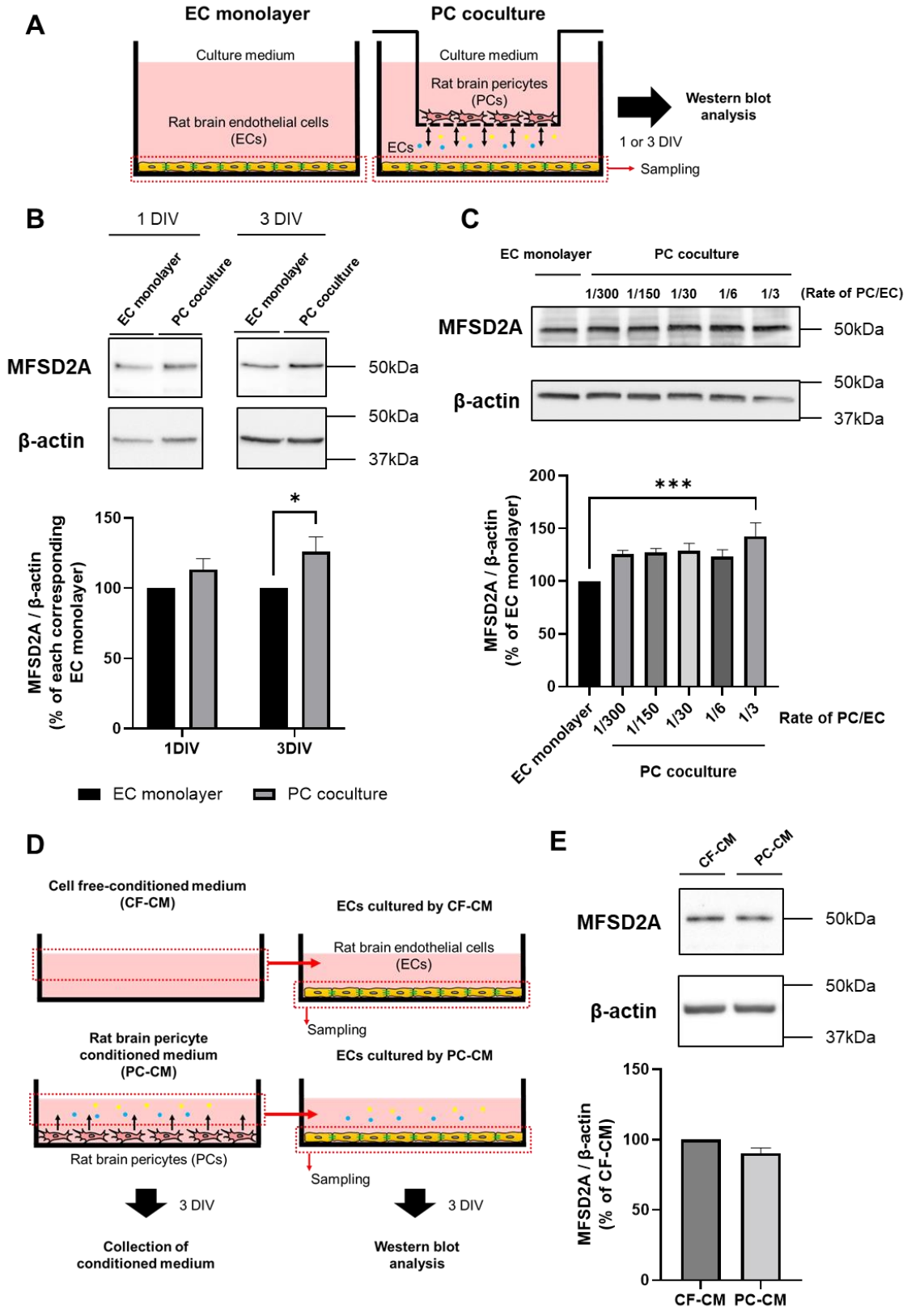

Fig. 1 Effect of pericytes on the MFSD2A expression in brain endothelial cells (ECs) through a cell-to-cell interaction

(A) A schematic diagram of experimental procedures using non-contact coculture models comprising rat brain endothelial cells (ECs) and pericytes. ECs with or without pericytes were cultured for 1 or 3 days in vitro. (B) The top panel shows representative western blotting images of MFSD2A and corresponding β-actin in ECs cultured with or without pericytes for 1 or 3 days in vitro. The bottom panel shows the quantified band intensities corrected by β-actin as the loading control (n = 7–11). (C) The top panel shows representative western blotting images of MFSD2A and corresponding β-actin in ECs cultured with or without pericytes with various cell numbers for 3 days in vitro. The bottom panel shows the quantified band intensities corrected by β-actin as the loading control (n = 3–12). (D) A schematic diagram of experimental procedures for collecting the conditioned medium with pericytes and treatment of ECs with them. (E) The top panel shows representative western blotting images of MFSD2A and corresponding β-actin in ECs cultured in the cell-free conditioned medium or pericyte-conditioned medium for 3 days in vitro. The bottom panel shows the quantified band intensities corrected by β-actin as the loading control (n = 4). Data are expressed as percentages of each corresponding EC monolayer or cell free-conditioned medium. The bars indicate mean ± standard error of mean. *$P < 0.05$ and ***$P < 0.001$, significantly different from each corresponding EC monolayer.

Fig. 2

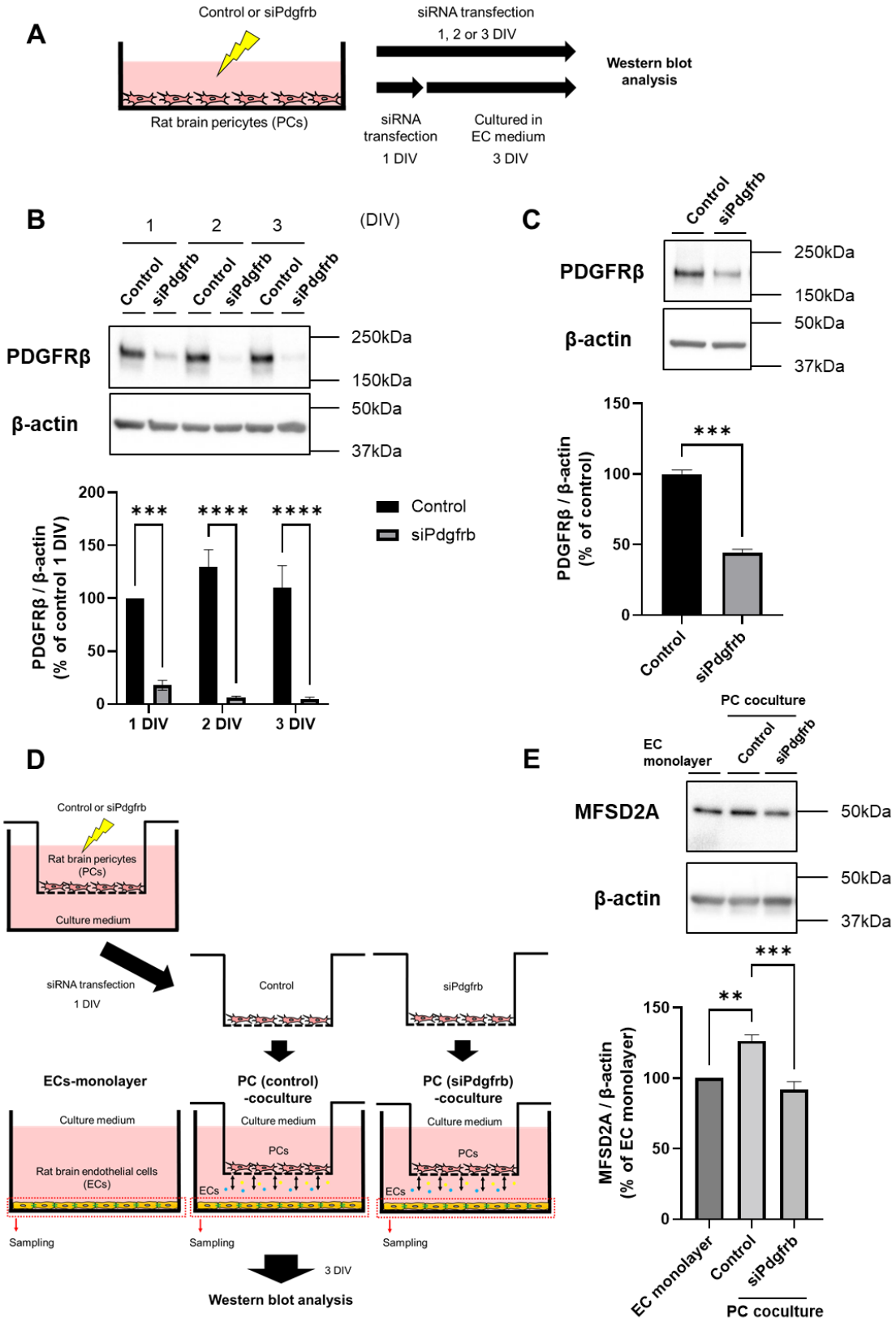
A
Control or siPdgfrb
Rat brain pericytes (PCs)
siRNA transfection
1, 2 or 3 DIV
Western blot analysis
siRNA transfection
1 DIV
Cultured in EC medium
3 DIV
B
1
2
3
(DIV)
Control
siPdgfrb
PDGFRβ
β-actin
250kDa
150kDa
50kDa
37kDa
PDGFRβ / β-actin (% of control 1 DIV)
***
****
****
Control
siPdgfrb
1 DIV
2 DIV
3 DIV
C
PDGFRβ / β-actin (% of control)
***
D
Control or siPdgfrb
Rat brain pericytes (PCs)
Culture medium
siRNA transfection
1 DIV
ECs-monolayer
PC (control) -coculture
PC (siPdgfrb) -coculture
Rat brain endothelial cells (ECs)
PCs
ECs
Sampling
3 DIV
Western blot analysis
E
PC coculture
EC monolayer
MFSD2A
50kDa
MFSD2A / β-actin (% of EC monolayer)
**
***

Fig. 2 Effect of PDGFRβ-knockdown pericytes on the MFSD2A expression in brain endothelial cells (ECs)

(A) A schematic diagram of experimental procedures for siRNA transfection to rat brain pericytes. (B) The top panel shows representative western blotting images of PDGFRβ and corresponding β-actin in pericytes transfected with siPdgfrb or negative-control siRNA (control) for 1–3 days in vitro. The bottom panel shows the quantified band intensities corrected by β-actin as the loading control (n = 3). (C) The top panel shows representative western blotting images of PDGFRβ and corresponding β-actin in pericytes transfected with siPdgfrb or a negative control (control). After a 24-h transfection, cells were cultured by replacing with the EC medium for 3 days in vitro. The bottom panel shows the quantified band intensities corrected by β-actin as the loading control (n = 3). (D) A schematic diagram of experimental procedures for evaluating the effect of Pdgfrb-knockdown pericytes on the MFSD2A protein expression in ECs. (E) The top panel shows representative western blotting images of MFSD2A and corresponding β-actin in ECs cultured with or without siPdgfrb- or negative control (control)-transfected pericytes. The bottom panel shows the quantified band intensities corrected by β-actin as the loading control (n = 4–5). Data are expressed as percentages of control in pericytes or the EC monolayer. The bars indicate mean ± standard error of mean. $^{**}P < 0.01$, $^{***}P < 0.001$, and $^{****}P < 0.0001$, significantly different from control pericytes or the EC monolayer.

Fig. 3

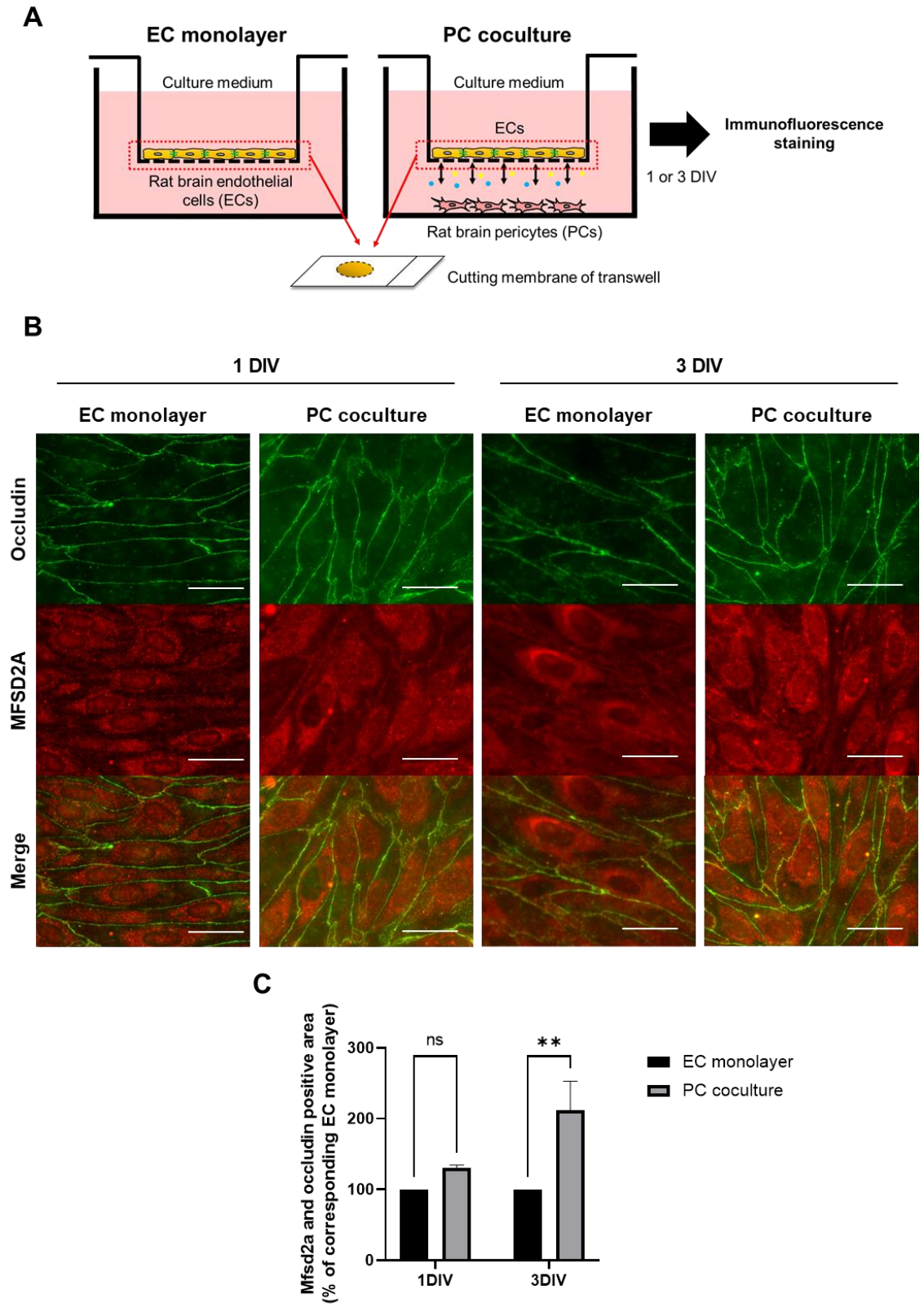
A
EC monolayer
PC coculture
Culture medium
Culture medium
ECs
Rat brain endothelial cells (ECs)
Rat brain pericytes (PCs)
Cutting membrane of transwell
1 or 3 DIV
Immunofluorescence staining
B
1 DIV
3 DIV
EC monolayer
PC coculture
EC monolayer
PC coculture
Occludin
MFSD2A
Merge
C
Mfsd2a and occludin positive area (% of corresponding EC monolayer)
300
200
100
0
ns
**
1DIV
3DIV
EC monolayer
PC coculture

Fig. 3 Effect of pericytes on the plasma membrane localization of the MFSD2A protein in brain endothelial cells (ECs)

(A) A schematic diagram of experimental procedures using non-contact coculture models comprising rat brain ECs and pericytes. ECs with or without pericytes were cultured for 1 or 3 days in vitro and then subjected to immunofluorescence staining. (B) Representative fluorescence images of occludin (green) and MFSD2A (red) and merged images of occludin and MFSD2A. MFSD2A and occludin double-positive areas are detected and quantified (C). Data are expressed as percentages of each corresponding EC monolayer (n = 3–4). The bars indicate mean ± standard error of mean. $^{**}P < 0.01$, significantly different from each corresponding EC monolayer.

Fig. 4

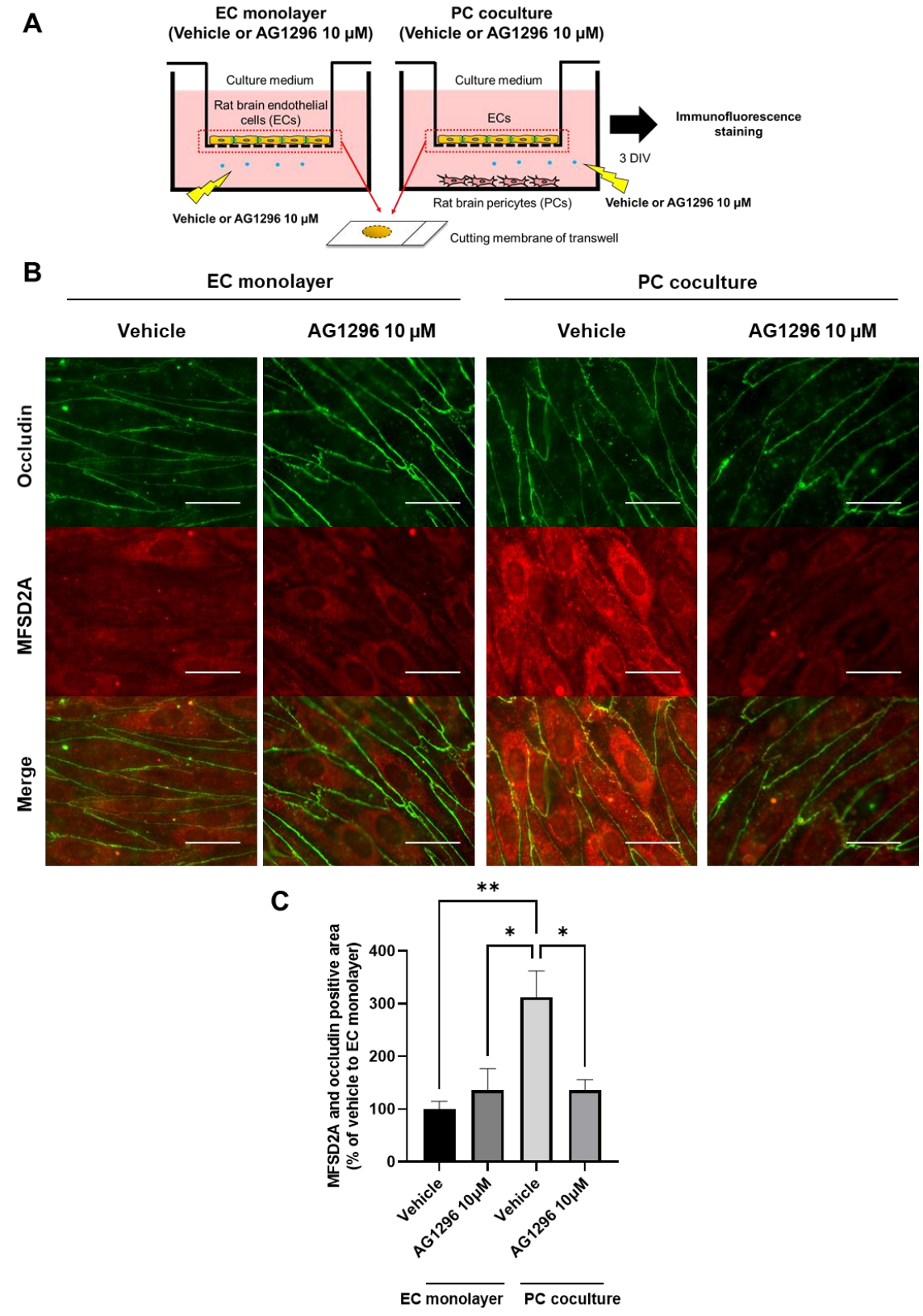
A
EC monolayer
(Vehicle or AG1296 10 μM)
PC coculture
(Vehicle or AG1296 10 μM)
Culture medium
Rat brain endothelial cells (ECs)
Culture medium
ECs
Immunofluorescence staining
3 DIV
Rat brain pericytes (PCs)
Vehicle or AG1296 10 μM
Vehicle or AG1296 10 μM
Cutting membrane of transwell
B
EC monolayer
PC coculture
Vehicle
AG1296 10 μM
Vehicle
AG1296 10 μM
Occludin
MFSD2A
Merge
C
MFSD2A and occludin positive area
(% of vehicle to EC monolayer)
400
300
200
100
0
**
*
*
Vehicle
AG1296 10μM
Vehicle
AG1296 10μM
EC monolayer
PC coculture

Fig. 4 Effect of pericytes treated with AG1296 on the plasma membrane localization of the MFSD2A protein in brain endothelial cells (ECs)

(A) A schematic diagram of experimental procedures using non-contact coculture models. Rat brain ECs were cocultured with or without pericytes, and cells were treated with a vehicle or AG1296 10 μM, which were added to the outsides of 24-well transwell inserts. After 3 days in vitro, ECs were subjected to immunofluorescence staining. (B) Representative fluorescence images of occludin (green) and MFSD2A (red) and merged images of occludin and MFSD2A. MFSD2A and occludin double-positive areas are detected and quantified (C). Data are expressed as percentages of the EC monolayer treated with a vehicle (n = 9–16). The bars indicate mean ± standard error of mean. **P* < 0.05 and ***P* < 0.01, significantly different from the EC monolayer treated with the vehicle.

Fig. 5

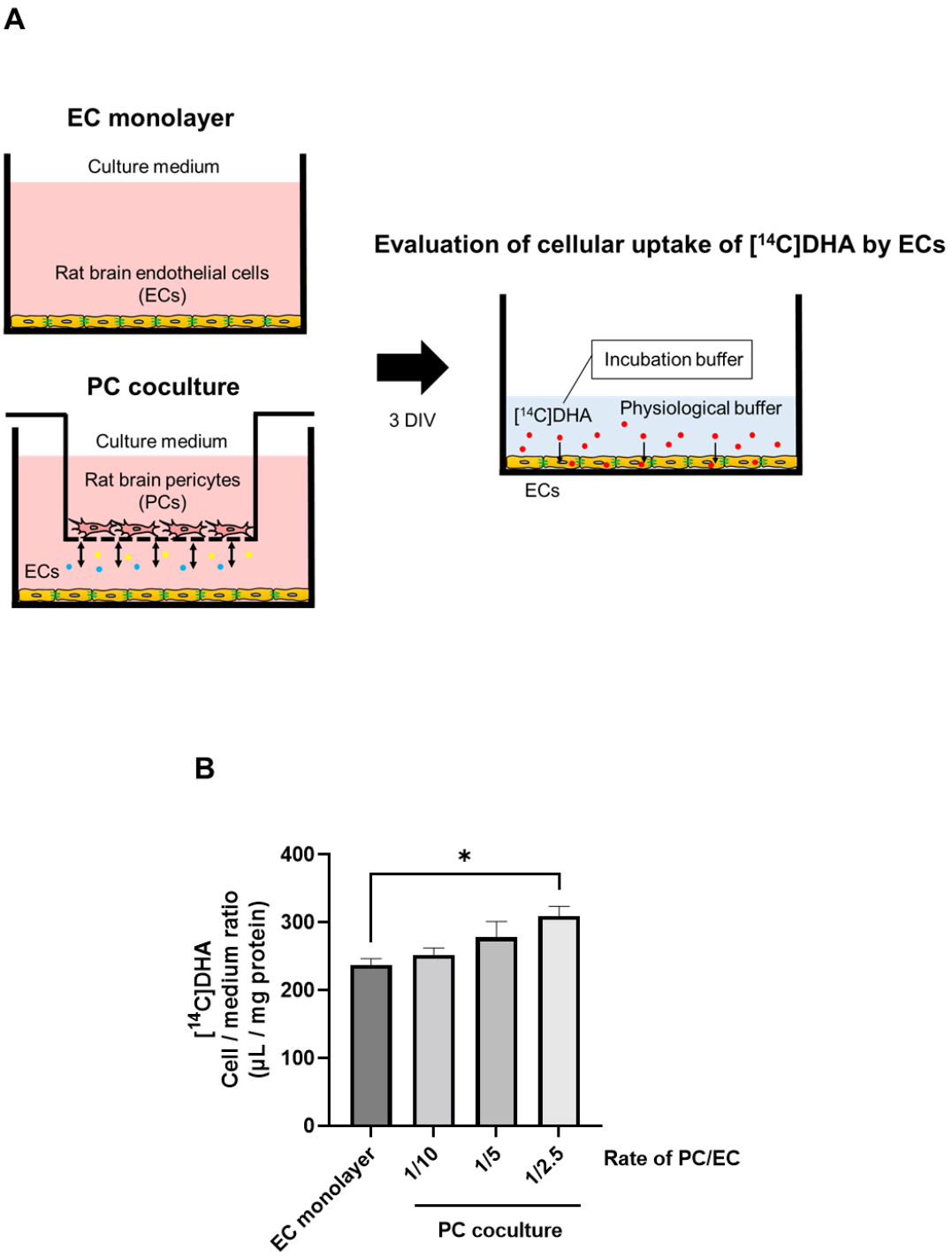
A
EC monolayer
Culture medium
Rat brain endothelial cells
(ECs)
PC coculture
Culture medium
Rat brain pericytes
(PCs)
ECs
3 DIV
Evaluation of cellular uptake of [14C]DHA by ECs
Incubation buffer
[14C]DHA
Physiological buffer
ECs
B
[14C]DHA
Cell / medium ratio
(μL / mg protein)
400
300
200
100
0
*
EC monolayer
1/10
1/5
1/2.5
Rate of PC/EC
PC coculture

Fig. 5 Effect of pericytes on the cellular uptake of [^{14}C]DHA by brain endothelial cells (ECs)

(A) A schematic diagram of experimental procedures of the cellular uptake of [^{14}C]DHA by rat brain ECs using non-contact coculture models comprising ECs and pericytes. ECs were cocultured with or without pericytes for 3 days in vitro and subjected to the cellular uptake assay. (B) Cellular uptake of [^{14}C]DHA by ECs for 2 min is expressed as cell/medium ratio (μL/mg protein). Data are expressed as mean ± standard error of mean (n = 7–8). *P < 0.05, significantly different from the EC monolayer.

References

1. Abbott NJ, Patabendige AA, Dolman DE, Yusof SR, Begley DJ. Structure and function of the blood-brain barrier. Neurobiol Dis. 2010;37(1):13-25.

2. Keaney J, Campbell M. The dynamic blood-brain barrier. Febs j. 2015;282(21):4067-79.

3. Sweeney MD, Sagare AP, Zlokovic BV. Blood-brain barrier breakdown in Alzheimer disease and other neurodegenerative disorders. Nat Rev Neurol. 2018;14(3):133-50.

4. Han L, Jiang C. Evolution of blood-brain barrier in brain diseases and related systemic nanoscale brain-targeting drug delivery strategies. Acta Pharm Sin B. 2021;11(8):2306-25.

5. Angers M, Uldry M, Kong D, Gimble JM, Jetten AM. Mfsd2a encodes a novel major facilitator superfamily domain-containing protein highly induced in brown adipose tissue during fasting and adaptive thermogenesis. Biochem J. 2008;416(3):347-55.

6. Ben-Zvi A, Lacoste B, Kur E, Andreone BJ, Mayshar Y, Yan H, et al. Mfsd2a is critical for the formation and function of the blood-brain barrier. Nature. 2014;509(7501):507-11.

7. Nguyen LN, Ma D, Shui G, Wong P, Cazenave-Gassiot A, Zhang X, et al. Mfsd2a is a transporter for the essential omega-3 fatty acid docosahexaenoic acid. Nature. 2014;509(7501):503-6.

8. Eser Ocak P, Ocak U, Sherchan P, Zhang JH, Tang J. Insights into major facilitator superfamily domain-containing protein-2a (Mfsd2a) in physiology and pathophysiology. What do we know so far? J Neurosci Res. 2020;98(1):29-41.

9. Andreone BJ, Chow BW, Tata A, Lacoste B, Ben-Zvi A, Bullock K, et al. Blood-Brain Barrier Permeability Is Regulated by Lipid Transport-Dependent Suppression of Caveolae-Mediated Transcytosis. Neuron. 2017;94(3):581-94.e5.

10. Yang YR, Xiong XY, Liu J, Wu LR, Zhong Q, Zhou K, et al. Mfsd2a (Major Facilitator Superfamily Domain Containing 2a) Attenuates Intracerebral Hemorrhage-

Induced Blood-Brain Barrier Disruption by Inhibiting Vesicular Transcytosis. J Am Heart Assoc. 2017;6(7).

11. Huang B, Li X. The Role of Mfsd2a in Nervous System Diseases. Front Neurosci. 2021;15:730534.

12. Zheng Z, Chopp M, Chen J. Multifaceted roles of pericytes in central nervous system homeostasis and disease. J Cereb Blood Flow Metab. 2020;40(7):1381-401.

13. Attwell D, Mishra A, Hall CN, O'Farrell FM, Dalkara T. What is a pericyte? J Cereb Blood Flow Metab. 2016;36(2):451-5.

14. Dohgu S, Takata F, Matsumoto J, Kimura I, Yamauchi A, Kataoka Y. Monomeric α-synuclein induces blood-brain barrier dysfunction through activated brain pericytes releasing inflammatory mediators in vitro. Microvasc Res. 2019;124:61-6.

15. Takata F, Dohgu S, Yamauchi A, Matsumoto J, Machida T, Fujishita K, et al. In vitro blood-brain barrier models using brain capillary endothelial cells isolated from neonatal and adult rats retain age-related barrier properties. PLoS One. 2013;8(1):e55166.

16. Lindahl P, Johansson BR, Levéen P, Betsholtz C. Pericyte loss and microaneurysm formation in PDGF-B-deficient mice. Science. 1997;277(5323):242-5.

17. Hellström M, Kalén M, Lindahl P, Abramsson A, Betsholtz C. Role of PDGF-B and PDGFR-beta in recruitment of vascular smooth muscle cells and pericytes during embryonic blood vessel formation in the mouse. Development. 1999;126(14):3047-55.

18. Huang H. Pericyte-Endothelial Interactions in the Retinal Microvasculature. Int J Mol Sci. 2020;21(19).

19. Muto T, Tien T, Kim D, Sarthy VP, Roy S. High glucose alters Cx43 expression and gap junction intercellular communication in retinal Müller cells: promotes Müller cell and pericyte apoptosis. Invest Ophthalmol Vis Sci. 2014;55(7):4327-37.

20. Monickaraj F, McGuire P, Das A. Cathepsin D plays a role in endothelial-pericyte interactions during alteration of the blood-retinal barrier in diabetic retinopathy. Faseb j. 2018;32(5):2539-48.

21. McGuire PG, Rangasamy S, Maestas J, Das A. Pericyte-derived sphingosine 1-phosphate induces the expression of adhesion proteins and modulates the retinal endothelial cell barrier. Arterioscler Thromb Vasc Biol. 2011;31(12):e107-15.

22. Mendelson K, Swendeman S, Saftig P, Blobel CP. Stimulation of platelet-derived growth factor receptor beta (PDGFRbeta) activates ADAM17 and promotes metalloproteinase-dependent cross-talk between the PDGFRbeta and epidermal growth factor receptor (EGFR) signaling pathways. J Biol Chem. 2010;285(32):25024-32.

23. Obermeier B, Daneman R, Ransohoff RM. Development, maintenance and disruption of the blood-brain barrier. Nat Med. 2013;19(12):1584-96.

24. Zhang Y, Cedervall J, Hamidi A, Herre M, Viitaniemi K, D'Amico G, et al. Platelet-Specific PDGFB Ablation Impairs Tumor Vessel Integrity and Promotes Metastasis. Cancer Res. 2020;80(16):3345-58.

25. Bjarnegård M, Enge M, Norlin J, Gustafsdottir S, Fredriksson S, Abramsson A, et al. Endothelium-specific ablation of PDGFB leads to pericyte loss and glomerular, cardiac and placental abnormalities. Development. 2004;131(8):1847-57.

26. Heldin CH, Ostman A, Rönnstrand L. Signal transduction via platelet-derived growth factor receptors. Biochim Biophys Acta. 1998;1378(1):F79-113.

27. Wang Z, Liu CH, Huang S, Fu Z, Tomita Y, Britton WR, et al. Wnt signaling activates MFSD2A to suppress vascular endothelial transcytosis and maintain blood-retinal barrier. Sci Adv. 2020;6(35):eaba7457.

28. Cui Y, Wang Y, Song X, Ning H, Zhang Y, Teng Y, et al. Brain endothelial PTEN/AKT/NEDD4-2/MFSD2A axis regulates blood-brain barrier permeability. Cell Rep. 2021;36(1):109327.

Chapter 5: Age-related blood–brain barrier disruption and microglia activation improved with dietary docosahexaenoic acid supplementation.

Introduction

The blood–brain barrier (BBB) is necessary for maintaining and regulating the neuroparenchymal microenvironment. This function of BBB regulates neurotoxic substances and brain nutrition through paracellular and transcellular routes. Brain microvascular endothelial cells (BMECs), which are the basic unit of BBB, mainly play a role in controlling penetration of various substances from blood to the brain. Tight junction (Tj)-associated proteins spanning intracellular BMECs regulate paracellular permeability, and Tj loss results in disruption of BBB integrity [1,2]. In addition, adherens junctions (Ajs), such as cadherin proteins, contribute to holding the cells together, providing the tissue structural support, and are essential for the formation of Tjs [3]. Major facilitator superfamily domain-containing protein-2a (MFSD2A), which is exclusively expressed in BMECs, is a DHA transporter and can restrict transcellular permeability by regulating endocytosis at a low level [4–7].

BBB integrity is impaired with aging [8–11], and BBB disruption is closely associated with various neurological diseases [11–13]. The leakage of plasma proteins as a consequence of BBB disruption contributes to neuronal damage and neuroinflammation through inflammatory activation of microglia [14–17].

Docosahexaenoic acid (DHA; 22:6n-3), an n-3 polyunsaturated fatty acid, has attracted attention because of its functional and structural importance in the brain. It is highly enriched in brain phospholipids and contributes to proper brain development and function [18,19]. Brain DHA levels decrease with age in association with age-related cognitive dysfunction [20]. Furthermore, DHA in microvessels of aged mice decrease corresponding to the age-associated downregulation of MFSD2A [21]. MFSD2A dysfunction results in impairment of lipid homeostasis in BMEC [22]. DHA exerts a protective effect on BBB impairment under pathological conditions [23,24]. Furthermore, dietary DHA intake affects the DHA concentration in brain microvessel membranes [25]. However, the effect of DHA on BBB integrity under physiological conditions or aging remains unknown. A decrease in DHA transport across BBB precedes age-related BBB disruption mediated by downregulations of Tjs and Ajs (chapter 1 and 2). Therefore, we considered that DHA regulates the expression of Tjs and Ajs in BMECs under physiological conditions and that a decrease in intracellular DHA in BMECs results in age-related BBB

disruption. The aim of the present study was to demonstrate that long-term dietary DHA supplementation inhibited age-related BBB disruption and activation of microglia in vivo and that DHA regulated the function of BBB under physiological conditions in vitro.

Material and Methods

Animals

All protocols involving experimental animals were approved by the Laboratory Animal Care and Use Committee of Fukuoka University (permit number: 2004001, 2204002). The 19-month-old male C57BL/6J mice and 3-week-old Wistar rats were purchased from Charles River Laboratory (Kanagawa, Japan) and Japan SLC, Inc. (Shizuoka, Japan). They were housed under a controlled temperature (22° ± 2°C) and light/dark cycle (lights on from 7:00 to 19:00), with access to water and chow diet *ad libitum*. The diet consisted of CLEA Rodent Diet CE-2 pellets from CLEA Japan, Inc. (Tokyo, Japan). After habituation for 1 week, the mice were divided into two groups. The mice in group 1 (CO-feed; control group) were fed a diet containing AIN-93G (American Institute of Nutrition 93-G; CLEA Japan, Inc.), in which soybean oil was replaced with 7% corn oil (CO). The mice in group 2 (DHA-feed; DHA group) were fed a diet containing AIN-93G, in which soybean oil was replaced with 4% fish oil DHA-46 and 3% CO. Fish oil DHA-46 was purchased from Tama Biochemical Co., Ltd. (Tokyo, Japan). Table 1 shows the fatty acid composition in CO and DHA feeds. After rearing for 13 weeks, the mice underwent experiments. We employed the experimental design in accordance with previous studies [26,27].

Table. 1 Fatty acid composition in CO and DHA feeds			
Fatty acid symbols	Fatty acid names	Ratio	
		CO feed	DHA feed
12 : 0	Lauric acid	0.1%	0.1%
14 : 0	Myristic acid	0.3%	1.2%
15 : 0	Pentadecanoic acid	-	0.2%
16 : 0	Palmitic acid	11.4%	10.1%
16 : 1	Palmitoleic acid	0.1%	1.3%
17 : 0	Heptadecanoic acid	-	0.3%
17 : 1	Heptadecenoic acid	-	0.2%
18 : 0	Stearic acid	1.5%	1.9%
18 : 1	Oleic acid	27.2%	17.0%
18 : 2n-6	Linoleic acid	56.9%	26.3%
18 : 3n-3	γ-linolenic acid	1.2%	0.8%
18 : 4n-3	Octadecatetraenoic acid	-	0.7%
20 : 0	Arachidic acid	0.3%	0.2%
20 : 1	Eicosenoic acid	0.2%	1.1%
20 : 2n-6	Eicosadienoic acid	-	0.1%
20 : 3n-3	11,14,17-Eicosatrienoic Acid	-	0.1%
20 : 4n-6	Arachidonic acid	-	1.6%
20 : 4n-3	Eicosatetraenoic acid	-	0.3%
20 : 5n-3	Eicosapentaenoic acid	-	3.8%
21 : 5n-3	Heneicosapentaenoic acid	-	0.2%
22 : 0	Behenic acid	-	0.1%
22 : 1	Brassidic acid	-	0.7%
22 : 4n-6	7,10,13,16-Docosatetraenoic acid	-	0.2%
22 : 5n-6	4, 7,10,13,16-Docosapentaenoic acid	-	1.5%
22 : 5n-3	Docosapentaenoic acid	-	1.4%
22 : 6n-3	Docosahexaenoic acid	-	27.0%
24 : 0	Lignoceric acid	0.1%	-
24 : 1	Tetracosenoic Acid	-	0.3%
Unidentified		0.6%	1.4%

Isolation of brain microvessels

Mice were anesthetized before Dulbecco's phosphate-buffered saline (-) (D-PBS) (Wako, Osaka, Japan; 045-29795;10 mL per mouse) was infused into the left ventricle of the heart. The brain tissue was triturated using a glass homogenizer coated with 1% bovine serum albumin (BSA)-Hanks' Balanced Salt Solution (HBSS; Thermo Fisher Scientific, Waltham, MA, USA; 14185-045) in 1 mL of Buffer A (HBSS containing 1% Phosphatase Inhibitor Cocktail [EDTA free; Nacalai Tesque, Kyoto, Japan; 07575-51], 1% Protease Inhibitor Cocktail for use with mammalian and tissue extracts [Nacalai Tesque; 25955-11], 1 mM of phenylmethylsulfonyl fluoride [PMSF; Sigma, St. Louis, MO, USA; P7626], and 15 µg/mL of deoxyribonuclease I [Sigma; D4513]) on ice. This suspension was transferred into a 1.5-mL tube and centrifuged at 1,000 × g for 10 min at 4°C. Next, the supernatant was aspirated, and the pellet was mixed with 1 mL of 17.5% dextran (Sigma; D8821)-HBSS. The suspension was then centrifuged at 4,400 × g for 15 min at 4°C. The supernatant with a lipid layer was removed, and the pellet was resuspended in Buffer B (Buffer A containing 1% BSA). Next, the suspension was filtered using a 10-µm nylon mesh membrane to trap the residue, including microvessels, on the surface of the membrane. HBSS was then passed through the membrane to remove debris from the residue. The microvessels on the membrane were then washed into a 1.5-mL tube with Buffer A and centrifuged at 20,000 × g for 5 min at 4°C. Finally, they were obtained at the bottom of the tube and stored at −80°C until use.

Extraction of total protein from brain microvessels

The microvessels were homogenized in a phosphoprotein lysis buffer containing 10 mM of Tris-HCl (pH 6.8; Nacalai Tesque; 35434-34), 100 mM of NaCl (Sigma; 28-2270-5), 1 mM of ethylenediamine tetraacetic acid (EDTA; pH 8.0; Wako; 311-90075), 1 mM of egtazic acid (EGTA; Wako; 346-01312), 10% glycerol, 1% Triton-X100 (Sigma; X100), 0.1% sodium dodecyl sulfate (Nacalai Tesque; 02873-75), 0.5% sodium deoxycholate (Sigma; D6750), 20 mM of sodium pyrophosphate (Sigma; S6422), 2 mM of sodium orthovanadate (Sigma; S6508), 1 mM of sodium fluoride (Wako; 196-01975), 1% protease

inhibitor cocktail (Sigma; P2714), 1% phosphatase inhibitor cocktail 2 (Sigma; P5726), 1% Phosphatase Inhibitor Cocktail 3 (Sigma; P0044), and 1 mM of PMSF (Sigma) using an electric mixer and sonicated on ice. Samples were centrifuged at 15,000 × g for 15 min at 4°C, and the supernatants were collected. The total protein concentration in the lysates obtained from microvessels or the whole brain was determined using the Pierce™ BCA Protein Assay Kit (Thermo Fisher Scientific; 23225).

Primary rat brain endothelial cell (EC) culture

The method of primary culture of ECs was as previously described [28,29]. Primary cultured ECs were plated on 100-mm dishes coated with collagen type IV (0.1 mg/mL, Sigma, St. Louis, MO, USA; C5533) and fibronectin (0.075 mg/mL, Sigma; F1141-5MG) for ECs. Primary cultured ECs were maintained in the EC medium (Dulbecco's Modified Eagle Medium [DMEM]/F12; Wako; 042-30555) supplemented with 10% fetal bovine serum (FBS; Biosera, Kansas, MO, USA; FB-1365/500), basic fibroblast growth factor (1.5 ng/mL, R&D, Minneapolis, MN, USA; 2099-FB-025), heparin (100 μg/mL, Sigma; H3149), insulin (5 μg/mL), transferrin (5 μg/mL), sodium selenite (5 ng/mL; insulin-transferrin-sodium selenite media supplement, Sigma; I1884), penicillin (100 units/mL), streptomycin (100 μg/mL; penicillin–streptomycin mixed solution, Nacalai Tesque, Kyoto, Japan; 09367-34), and gentamicin (50 μg/mL, Biowest, Riverside, MO, USA; L0012)] containing puromycin (4 μg/mL, Nacalai Tesque; 14861-84) at 37°C in a humidified atmosphere of 5% CO_2/95% air, for 3 days and typically reaching 70%–80% confluency.

Cell viability assay

Rat brain ECs were seeded to the bottoms of 96-well plates coated with collagen type IV (0.1 mg/mL, Nitta Gelatin Inc.; 638-05921) and fibronectin (0.025 mg/mL, Sigma; 2 × 10^4 cells/well) and maintained in the EC medium supplemented with 500 nM of hydrocortisone (Sigma; H0135). For evaluating cell viability, we used the Cell Counting Kit-8 (Dojindo, Kumamoto, Japan; 343-07623) following the manufacturer's protocol.

In vitro evaluation of the function of BBB

Rat brain ECs were seeded to the inside of 24-well transwell inserts coated with collagen type IV (0.1 mg/mL, Nitta Gelatin Inc.; 638-05921) and fibronectin (0.025 mg/mL, Sigma; 5×10^4 cells/well, 0.4-μm pore size; Corning, Midland, MI; 3470) and maintained in the EC medium supplemented with 500 nM of hydrocortisone (Sigma; H0135). ECs were cultured for 3 days with the EC medium supplemented with 500 nM of hydrocortisone. Subsequently, ECs were treated with DHA (Sigma; D2534-100MG) and eicosapentaenoic acid (EPA; Sigma, E2011-10MG) in the EC medium without FBS and supplemented with 500 nM of hydrocortisone. The permeability coefficients for sodium fluorescein (Na-F) and albumin-bound evans blue (ABE) and transendothelial electrical resistance (TEER) values were measured for evaluating barrier function in ECs treated with DHA, EPA (5 μM), or a vehicle control (0.1 % ethanol), as previously described [30,31].

xCELLigence experiments

The E-plate 16 (ACEA Biosciences, Inc., San Diego, CA, USA), which is coated with high-density gold arrays for measuring electrical impedance (ACEA Biosciences, USA), was coated with collagen type IV (0.1 mg/mL, Nitta Gelatin Inc.; 638-05921) and fibronectin (0.025 mg/mL, Sigma) before seeding rat brain ECs. For equilibration, the E-plate 16 was incubated with 100 μL of the EC medium for 30 min at 37°C. Subsequently, 100 μL (4×10^4 cells/100μL) of the suspension including ECs was added onto E-plate 16. EC-seeded E-plate 16 were cultured in the EC medium supplemented with 500 nM of hydrocortisone incubated at 37°C in a humidified atmosphere of 5% CO_2/95% air for 2 days. Electrical impedance was measured in real time using the xCELLigence RTCA system (ACEA Biosciences, Inc.). Culture media were replaced with the EC medium without FBS and supplemented with 500 nM of hydrocortisone including DHA, EPA (5 μM), or a vehicle control (0.1 % ethanol). Changes in impedance were monitored for another 24 h. The impedance was converted to the cell index and normalized to the time point before treatment using the xCELLigence RTCA software.

Western blotting

Equivalent amounts of protein from each sample were electrophoretically separated on 7.5% TGX Stain-Free gradient acrylamide gels (Bio-Rad, Hercules, CA; 161-0181) or 12% TGX Stain-Free acrylamide gels (Bio-Rad; 161-0185) and transferred to low-fluorescence polyvinylidene difluoride membranes (Bio-Rad; 1704274). Stain-free technology using the GelDoc go imaging system (Bio-Rad) was used for total protein normalization. Membranes were then blocked using Blocking One (Nacalai Tesque; 03953-95) and reacted with primary antibodies overnight. After washing, the membranes were incubated in horseradish peroxidase-conjugated goat anti-rabbit IgG (Bio-Rad; 170-6515) or goat anti-mouse IgG (Bio-Rad; 170-6516), as appropriate. Immunoreactive bands were detected using the Clarity Western ECL Substrate (Bio-Rad; 1705061). Images of the bands were digitally captured using the MultiImager II ChemiBOX (BioTools, Gunma, Japan), and band intensities were quantified using ImageJ software (National Institutes of Health Image, Bethesda, MD, USA). The relative intensity of each individual protein was expressed as the ratio of the corresponding protein to the total protein loading.

Immunofluorescence staining

Mice were anesthetized before D-PBS (5 mL per mouse) was infused into the left ventricle of the heart. After D-PBS infusion, the brain was fixed by infusing 4% Paraformaldehyde Phosphate Buffer Solution (PFA; Wako; 163-20145; 5mL per mouse) into the left ventricle of the heart. The brain tissues were stored in 4% PFA overnight at 4°C and replaced with 20% sucrose (Wako; 196-00015) until embedding in O.C.T. Compound (Sakura Finetek Japan, Tokyo, Japan; 4583) at −80°C. A 20-μm frozen section of brain tissue was prepared using a cryostat. The brain tissue section on a microscope slide was washed and activated at 95°C. The brain tissue section was then blocked using Blocking One Histo (Nacalai Tesque; 06349-64) and reacted with primary antibodies overnight. After washing, the brain tissue section was incubated overnight with Cy3-labeled Donkey Anti-goat IgG (1:100; Jackson ImmunoResearch, West Grove, PA, USA; 705-165-147), Alexa Fluor 488-labeled Donkey Anti-rabbit IgG (1:100; Thermo Fisher Scientific; A-21206), and

DyLight 488-labeled Lectin (1:200, Vector Laboratories, Newark, CA, USA; DL-1174), as appropriate. After washing, the brain tissue section was encapsulated by VECTASHIELD Mounting Medium with 4',6-diamidino-2-phenylindole (DAPI; Vector Laboratories, Newark, CA, USA; H-1200). All samples were imaged using a fluorescence microscope (BZ-X710, KEYENCE, Osaka, Japan).

Primary antibodies

Primary antibodies used for western blotting and immunofluorescence staining were as follows: ZO-1 (1:400; Invitrogen/Thermo Fisher Scientific; 61-7300), occludin (1:400; Invitrogen/Thermo Fisher Scientific; 33-1500), claudin-5 (1:1,000; Invitrogen/Thermo Fisher Scientific; 35-2500), cadherin (1:1,000; Cell Signaling Technology, Danvers, MA, USA; 4068S), and MFSD2A (1:1,000; Sigma; SAB3500576) for western blotting and fibrinogen (Dako Denmark/Agilent Technologies, Santa Clara, CA, USA; A0080) and Iba1 (1:100; Wako, 019-19741) for immunofluorescence staining.

Statistical analysis

Results are expressed as mean ± standard error of mean. Statistical analyses were performed using GraphPad Prism 8.0 (GraphPad, San Diego, CA, USA). The unpaired *t*-test was used to analyze between-group differences. Statistical differences between groups were analyzed using the one-way analysis of variance (ANOVA), followed by Tukey's multiple-comparisons tests. Statistical analyses for evaluating two factors between groups were performed using the two-way ANOVA, followed by Šídák's multiple-comparisons tests. Differences between means were considered statistically significant at a *P*-value < 0.05.

Results

The ZO-1 and MFSD2A protein expressions in microvessels of aged mice increased with DHA supplementation.

Microvessels of mice showed gradually decreased protein expressions of MFSD2A, ZO-1, and cadherin and an increased occludin expression with aging (Chapter 2). Therefore, we ascertained whether or not dietary DHA supplementation modulates age-related changes in protein expressions in microvessels. Dietary DHA supplementation upregulated the protein expression levels of ZO1 by 1.64 folds (P = 0.0213) and MFSD2A by 3.47 folds (P = 0.0071) compared to the control group (Fig. 1A, E). In occludin and pan-cadherin, these protein expression levels in the DHA group tended to increase in comparison with the control group (Fig. 1B, D).

DHA supplementation inhibited the leakage of fibrinogen through BBB in aged mice.

Fibrinogen leakage from blood to the brain increased with aging corresponding to decreased protein expression levels in ZO-1, cadherin, and MFSD2A (Chapters 1 and 2). Therefore, we examined whether or not the upregulation of ZO-1 or MFSD2A induced by DHA supplementation resulted in decreased fibrinogen leakage, showing functional improvement of BBB. In the whole hippocampus of the DHA group, the fibrinogen-positive area and intensity decreased in comparison with the control group. In particular, the fibrinogen-positive area and intensity were lower in the DHA group by 81.19% (P = 0.0181) and 83.10% (P = 0.0171) in CA2, respectively, and by 67.02% (P = 0.0638) and 68.90% (P = 0.0595) in CA3 than in the control group, respectively (Fig. 2). The two-way ANOVA revealed significant effects of dietary DHA supplementation in the fibrinogen-positive area ($F(1, 24) = 17.67$, P = 0.0003) and positive intensity ($F(1, 24) = 17.77$, P = 0.0003) but no significant effect of the area or interaction between dietary DHA supplementation and the area.

DHA supplementation inhibited the inflammatory activation of microglia in aged mice.

Microglia are activated in aging corresponding to the leakage of fibrinogen from peripheral blood (Chapter 2). Therefore, we ascertained whether or not the improvement of age-related BBB impairment with dietary DHA supplement resulted in inhibiting the inflammatory activation of microglia with aging. In the whole hippocampus, the Iba1-positive area and intensity decreased significantly with dietary DHA supplementation (Fig. 3). The two-way ANOVA revealed significant effects of dietary DHA supplementation in the Iba1-positive area ($F(1, 24) = 79.07$, $P < 0.0001$) and positive intensity ($F(1, 24) = 45.42$, $P < 0.0001$) but not of the area or interaction between the dietary DHA supplementation and the area. Fold changes in the Iba1-positive area and intensity relative to each corresponding control group were as follows: 0.3952 ($P = 0.0022$, CA1), 0.4156 ($P = 0.0013$, CA2), 0.5453 ($P < 0.0001$, CA3), and 0.4080 ($P = 0.0016$, DG) in the positive area and 0.3119 ($P = 0.0299$, CA1), 0.3447 ($P = 0.0144$, CA2), 0.4701 ($P = 0.0008$, CA3), and 0.3148 ($P = 0.0281$, DG) in the positive intensity.

Effects of DHA and EPA on cell viability of brain ECs in vitro

Using a primary culture of brain ECs, we evaluated the effect of DHA on the function of BBB. Because the DHA feed included low levels of EPA as n-3 polyunsaturated fatty acid, we validated the different effect on ECs between DHA and EPA. First, we evaluated the effects of DHA and EPA on the cell viability of ECs. DHA or EPA treatment at concentrations ranging from 0.1 to 5 μM significantly increased the cell viability up to 28.90% (DHA at 3 μM) and 31.13% (EPA at 0.1 μM), respectively, in comparison with the vehicle group, whereas concentrations above 30 μM of DHA and EPA showed significant decreases in cell viability by over 80% compared to the vehicle group (Fig. 4). The one-way ANOVA showed effects of DHA ($F(8, 173) = 31.15$, $P < 0.0001$) and EPA ($F(8, 127) = 59.75$, $P < 0.0001$) on cell viability.

DHA increased the protein expression levels of ZO-1, occludin, and MFSD2A of brain ECs in vitro.

We evaluated the protein expression levels of Tj-associated proteins and MFSD2A in brain ECs treated with DHA ranging from 0 to 10 μM, because of its cytotoxicity. The protein expressions of ZO-1, occludin, and MFSD2A in ECs treated with DHA were significantly increased compared to the vehicle-treated group (Fig. 5A, B, D), but the claudin-5 expression was not affected by the DHA treatment (Fig. 5B). The one-way ANOVA showed an effect of DHA on the protein expression levels of ZO-1 ($F(4, 16) = 5.569$, $P = 0.0053$), occludin ($F(4, 16) = 9.952$, $P = 0.0003$), and MFSD2A ($F(4, 25) = 3.504$, $P = 0.0210$). The percentage increases between groups in the protein expression levels of ZO-1, occludin, and MFSD2A were as follows: 22.75% (vehicle vs. DHA 5 μM, $P = 0.0172$) and 26.57% (vehicle vs. DHA 10 μM, $P = 0.0111$) in ZO-1, 22.93% (vehicle vs. DHA 5 μM, $P = 0.0073$) and 29.59% (vehicle vs. DHA 10 μM, $P = 0.0003$) and 22.18% (DHA 1 μM vs. DHA 10 μM, $P = 0.0115$) in occludin, and 23.49% (vehicle vs. DHA 10 μM, $P = 0.0277$) in MFSD2A.

EPA increased the protein expression levels of occludin and claudin-5 of brain ECs in vitro.

In addition, we ascertained whether or not EPA increased the protein expression levels of Tj-associated proteins and MFSD2A of brain ECs in a similar manner as DHA. In the EPA treatment group, the protein expressions of occludin and claudin-5 in ECs were significantly increased compared to the vehicle group (Fig. 6B, C), while that of ZO-1 or MFSD2A was not affected by the EPA treatment (Fig. 6A, D). The one-way ANOVA showed an effect of EPA on the protein expression levels in occludin ($F(4, 17) = 5.896$, $P = 0.0053$) and claudin-5 ($F(4, 17) = 5.309$, $P = 0.0058$). The percentage increases in the protein expression levels of occludin and claudin-5 were as follows: 51.98% (vehicle vs. DHA 10 μM, $P = 0.0172$) and 54.43% (DHA 1 μM vs. DHA 10 μM, $P = 0.0059$) in occludin and 55.01% (vehicle vs. DHA 5 μM, $P = 0.0164$) and 60.01% (vehicle vs. DHA 10 μM, $P = 0.0084$) in claudin-5.

Both DHA and EPA upregulated the function of BBB in vitro.

We measured the permeability coefficients to Na-F and ABE and TEER values in brain ECs treated with DHA, EPA, or a vehicle control for evaluating barrier function. TEER values of ECs treated with DHA (5 μM) and EPA (5 μM) increased by 56.85% (P = 0.0004) and 31.21% (P = 0.0473) compared to that of ECs treated with a vehicle, respectively (Fig. 7A). The permeability coefficients of Na-F for ECs treated with DHA and EPA decreased by 43.35% (P < 0.0001) and 41.53% (P < 0.0001) compared to that for ECs treated with a vehicle, respectively (Fig. 7B). Corresponding to the permeability coefficients of Na-F, that of ABE for ECs in the DHA and EPA groups decreased by 30.46% (P = 0.0004) and 28.77% (P = 0.0006) compared to the vehicle group, respectively (Fig. 7C). The one-way ANOVA showed effects of DHA and EPA on TEER values ($F(2, 28) = 9.962$, P = 0.0005) and permeability coefficients of Na-F ($F(2, 28) = 21.84$, P < 0.0001) and ABE ($F(2, 28) = 12.87$, P = 0.0001).

Response profile of brain ECs treated with DHA and EPA using xCELLigence biosensor technology

Electrical impedance measured by xCELLigence biosensor technology is associated with TEER values and reflects subtle changes [32,33]. Using this system, we evaluated the effects of DHA and EPA on dynamic changes in the barrier function of brain ECs. Statistical differences were analyzed using the normalized cell index relative to the vehicle per 4 h. The normalized cell index in the DHA group increased from 20 to 24 h compared to the vehicle group (Fig. 8A). In the EPA group, the normalized cell index increased from 12 to 24 h compared to the vehicle group and reached the upper limit at 20 h (Fig. 8B). Electrical impedance revealed that ECs were more sensitive to EPA than to DHA. The two-way ANOVA revealed significant effects of DHA ($F(1, 56) = 38.21$, P < 0.0001) and EPA ($F(1, 56) = 51.37$, P < 0.0001), time in DHA ($F(6, 56) = 4.976$, P = 0.0004) and EPA ($F(6, 56) = 3.089$, P = 0.0110), and interactions between treatment and time in DHA ($F(6, 56) = 4.973$, P = 0.0004) and EPA ($F(6, 56) = 3.092$, P = 0.0110). Fold changes in the normalized cell index compared to the corresponding time point of the

vehicle group were as follows: 0.05489 (20 h, vehicle vs. DHA, $P = 0.0009$) and 0.08111 (20 h, vehicle vs. DHA, $P < 0.0001$) in the DHA group and 0.06556 (12 h, vehicle vs. EPA, $P = 0.0145$), 0.08636 (16 h, vehicle vs. EPA, $P = 0.0006$), 0.08970 (20 h, vehicle vs. EPA, $P = 0.0003$), and 0.08556 (24 h, vehicle vs. EPA, $P = 0.0006$) in the EPA group.

Discussion

In this study, we focused on the effect of long-term intake of DHA on BBB integrity in aging of mice. Furthermore, we investigated the potential of DHA and EPA for regulating homeostasis of BBB integrity in vitro.

First, we demonstrated that the protein expression levels of ZO-1 and MFSD2A increased in microvessels of DHA-fed aged mice, while the expressions of occludin, claudin-5, and pan-cadherin showed no significant changes (Fig. 1). Furthermore, leakage of fibrinogen decreased in DHA-fed aged mice. The protein expression levels of ZO-1, MFSD2A, and pan-cadherin in microvessels decreased with aging (Chapter 2), and endogenous DHA levels in BMECs decreased in aged mice [21]. These results and previous reports suggested that endogenous DHA levels in BMECs were associated with the regulation of protein expression levels of ZO-1 and MFSD2A, while pan-cadherin was not markedly affected by endogenous DHA levels. Cadherin is essential for the formation of Tjs [3]. Because the protein expression levels of Tjs and Ajs were not markedly affected by long-term intake of DHA, except for ZO-1, cadherin may not be associated with age-related decrease in the ZO-1 protein expression. Furthermore, the protein expression of MFSD2A increased 3.47 folds. However, this increase may not have resulted in upregulating the functional activity of MFSD2A in DHA transport at BBB, because previous studies showed that dietary DHA supplementation contributed to increase in brain DHA levels but not to functional upregulation [34,35]. Perhaps the protein expression of MFSD2A increased for handling plasma DHA in peripheral blood. Further studies are required to investigate the effect of dietary DHA supplementation on DHA transport at BBB. Another possible explanation for the increase in the MFSD2A protein expression is that MFSD2A inhibited BBB permeability as a consequence of regulating transcytosis. The upregulation of MFSD2A was associated with decreased BBB permeability [7,36]. Therefore, we suggested that decreased ZO-1 and MFSD2A in aging are associated with age-related BBB disruption, which is attributed to the decline in brain DHA levels with aging.

Microglial activation, which is evoked by fibrinogen, a plasma protein [16,17], is related to BBB impairment caused by aging (Chapter 2). Furthermore, we demonstrated that dietary DHA supplementation suppressed age-related microglial activation accompanied with improvement of BBB disruption (Fig. 3). These results suggested that

age-related microglial activation is induced by BBB disruption resulting from reduced brain DHA levels during aging. Therefore, these results raise two possible explanations for the anti-inflammatory effect of DHA on microglial activation: (1) indirect effect mediated by the protection of BBB integrity to reduce fibrinogen leakage or (2) the direct anti-inflammatory effect on microglia to suppress microglial activation [37,38]. Therefore, further investigations are required to reveal the effect of DHA on inflammatory activation of microglia with aging.

Using in vitro BBB models comprising rat BMECs, we investigated the direct effect of DHA on the function of BBB. In addition, we ascertained whether or not the effect of DHA on BBB function differed from the effect of EPA, because the DHA feed used in this study included some EPA as n-3 unsaturated fatty acid. DHA increased the protein expressions of ZO-1 and occludin (Fig. 5). Unlike DHA, EPA induced the protein expressions of occludin and cludin-5 (Fig. 6). Consequently, both DHA and EPA upregulated the function of BBB under physiological conditions (Fig. 7). However, using xCELLigence biosensor technology, we found that the reaction time differed between DHA and EPA (Fig. 8). In intestinal ECs of a inflammatory bowel disease mice model, the expressions of ZO-1 and occludin were upregulated by DHA, and EPA increased the protein levels of claudin-1 and occludin [39,40]. Therefore, DHA and EPA may exert divergent effects on the protein expression of Tjs in BMECs. Brain levels of EPA are low or undetectable [41], because EPA undergoes β-oxidation more readily than DHA [42]. Thus, the rapid response of ECs to EPA may have been caused by EPA-derived metabolites. In contrast, DHA is highly integrated in the phospholipid membrane. DHA released from phospholipid through the activity of phospholipase A2 is metabolized into various bioactive docosanoids [19]. These results suggest that DHA exerts a long-term effect of maintaining the BBB integrity rather than EPA. However, further investigation is required to clarify the mechanisms of action of DHA and EPA in maintaining BBB integrity.

Figures

Fig. 1

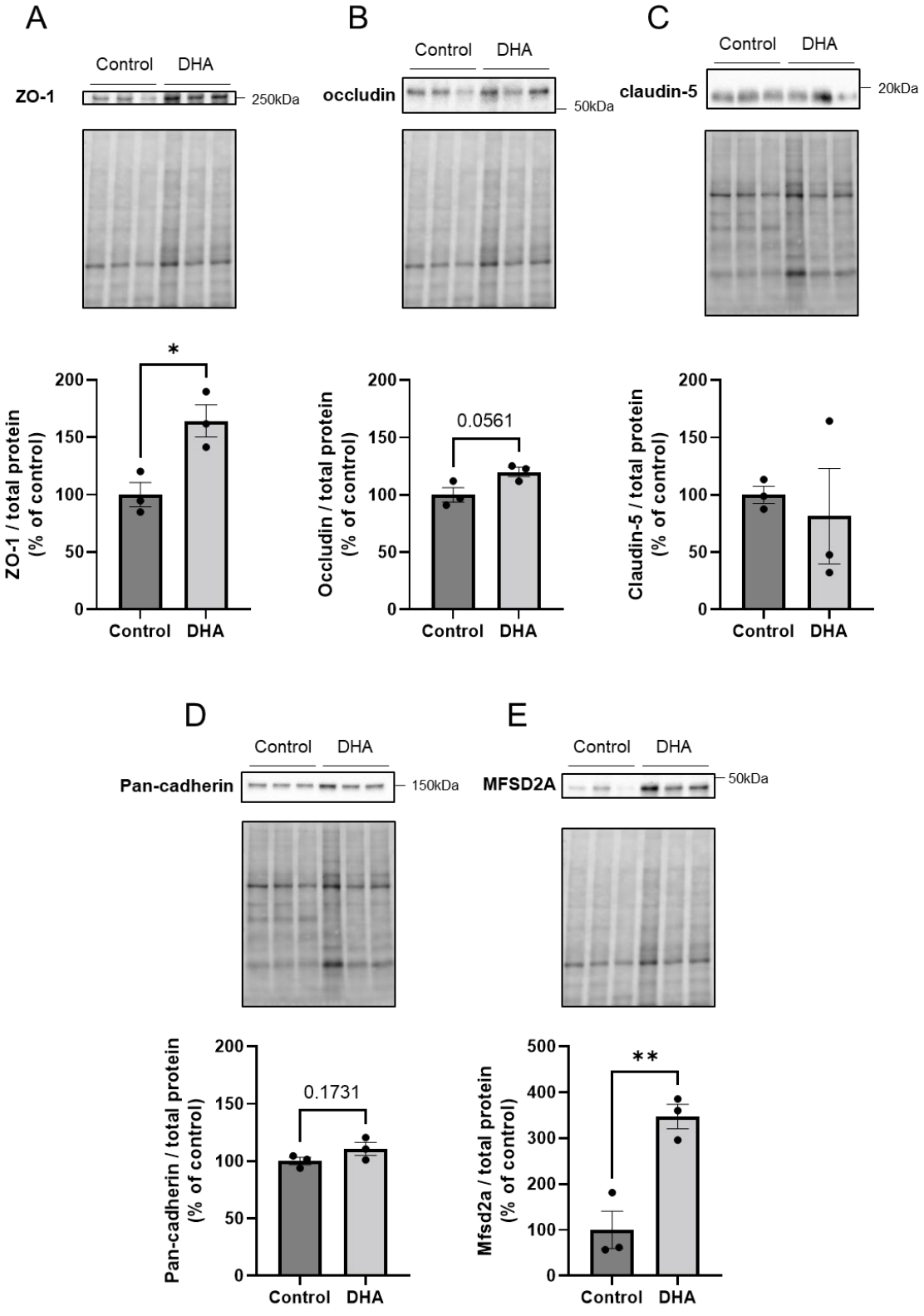

Fig 1. ZO-1, occludin, claudin-5, pan-cadherin, and MFSD2A expression levels in brain microvessels isolated from CO-fed and DHA-fed aged mice

Representative western blotting images of ZO-1 (A), occludin (B), claudin-5 (C), pan-cadherin (D), and MFSD2A (E) in CO-fed (control group) and DHA-fed (DHA group) aged mice. Band intensities quantified by densitometry. Total protein levels measured by Stain-free technology used as the loading controls for total protein normalization. Data are expressed as percentages of the control group's protein level. The bars indicate mean ± standard error of mean (n = 3). Each closed symbol represents an individual value. *P < 0.05 and **P < 0.01, significantly different compared to the control group.

Abbreviations: ZO-1, zonula occludens-1; MFSD2A, major facilitator superfamily domain-containing protein-2a; CO, corn oil; DHA, docosahexaenoic acid

Fig. 2

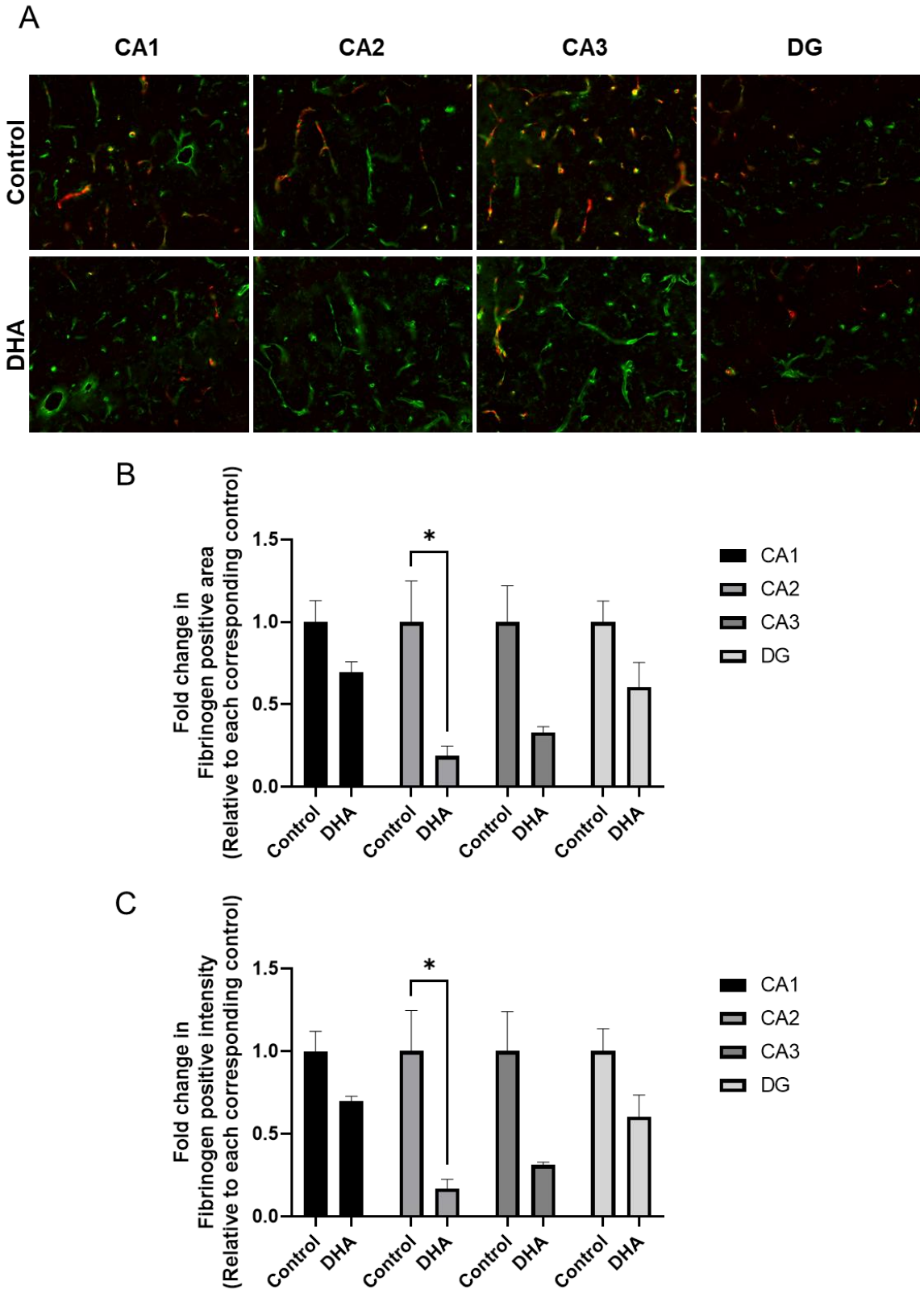
A
CA1
CA2
CA3
DG
Control
DHA
B
Fold change in Fibrinogen positive area (Relative to each corresponding control)
1.5
1.0
0.5
0.0
*
Control
DHA
CA1
CA2
CA3
DG
C
Fold change in Fibrinogen positive intensity (Relative to each corresponding control)
1.5
1.0
0.5
0.0
*
Control
DHA
CA1
CA2
CA3
DG

Fig. 2 Fibrinogen expression levels in the hippocampus of CO- and DHA-fed aged mice

Representative fluorescence images of fibrinogen (red) and lectin (green) in CA1, CA2, CA3, and DG of the hippocampus of CO- (control group) and DHA-fed (DHA group) aged mice (A). Fibrinogen-positive areas (B) and intensity (C) detected and quantified by fluorescence microscopy. Data are expressed as fold changes in each corresponding control (n = 3). The bars indicate mean ± standard error of mean.

Abbreviations: CA, Cornu Ammonis; DG, dentate gyrus; CO, corn oil; DHA, docosahexaenoic acid

Fig. 3

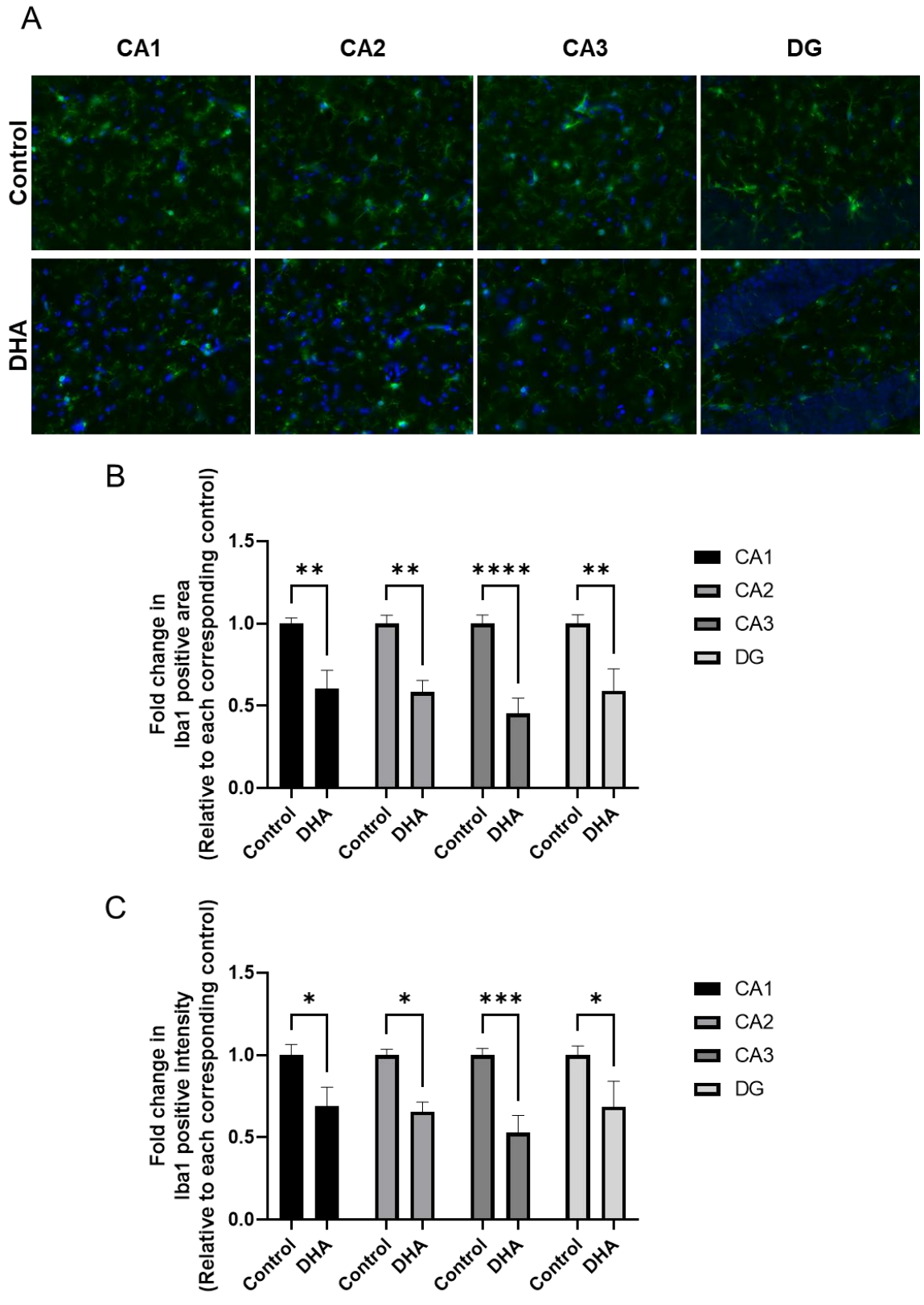
A
CA1
CA2
CA3
DG
Control
DHA
B
Fold change in Iba1 positive area (Relative to each corresponding control)
1.5
1.0
0.5
0.0
**
**
****
**
Control
DHA
Control
DHA
Control
DHA
Control
DHA
CA1
CA2
CA3
DG
C
Fold change in Iba1 positive intensity (Relative to each corresponding control)
1.5
1.0
0.5
0.0
*
*
***
*
Control
DHA
Control
DHA
Control
DHA
Control
DHA
CA1
CA2
CA3
DG

Fig. 3 Iba1 expression levels in the hippocampus of CO- and DHA-fed aged mice.

Representative fluorescence images of Iba1 (green) and DAPI (blue) in CA1, CA2, CA3, and DG of the hippocampus of CO-fed (control group) and DHA-fed (DHA group) aged mice (A). Iba1-positive areas (B) and intensity (C) detected and quantified by fluorescence microscopy. Data are expressed as fold changes in each corresponding control (n = 3–6). The bars indicate mean ± standard error of mean.

Abbreviations: CA, Cornu Ammonis; DG, dentate gyrus; Iba1, Ionized calcium-binding adapter molecule 1; DAPI, 4',6-diamidino-2-phenylindole; CO, corn oil; DHA, docosahexaenoic acid

Fig. 4

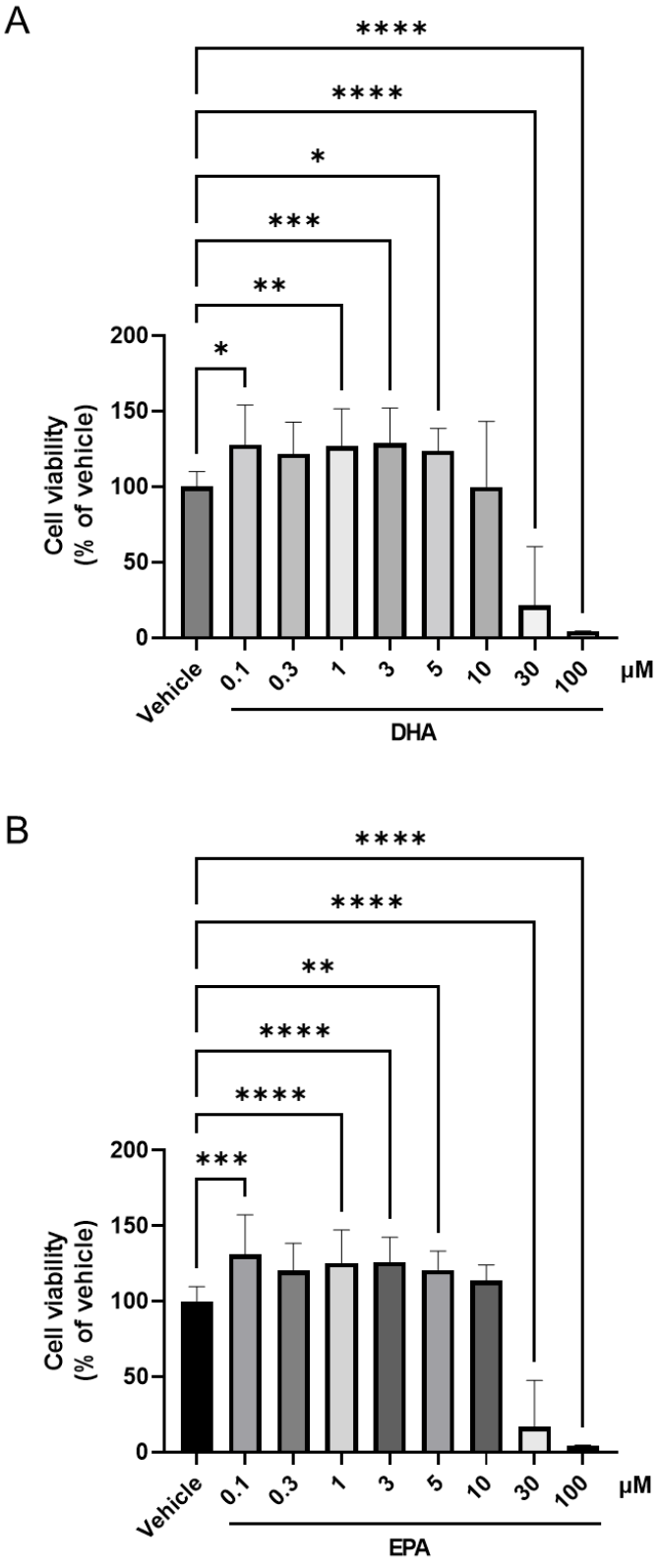
A
****
****
*
***
**
*
200
150
100
50
0
Cell viability
(% of vehicle)
Vehicle
0.1
0.3
1
3
5
10
30
100
μM
DHA
B
****
****
**
****
****
***
200
150
100
50
0
Cell viability
(% of vehicle)
Vehicle
0.1
0.3
1
3
5
10
30
100
μM
EPA

Fig. 4 Cell viability in brain ECs treated with DHA or EPA in vitro

Rat brain ECs seeded on 96-well plates were treated with DHA (0.1 to 100 μM) (A), EPA (0.1 to 100 μM) (B), or a vehicle including 0.1% ethanol for 24 h. The cell viability was evaluated using the Cell Counting Kit-8. Data are expressed as percentage of vehicle (n = 4–40). The bars indicate mean ± standard error of mean. **P* < 0.05, ***P* < 0.01, ****P* < 0.001, and *****P* < 0.0001, significantly different compared to the vehicle group.

Abbreviations: DHA, docosahexaenoic acid; EPA, eicosapentaenoic acid

Fig. 5

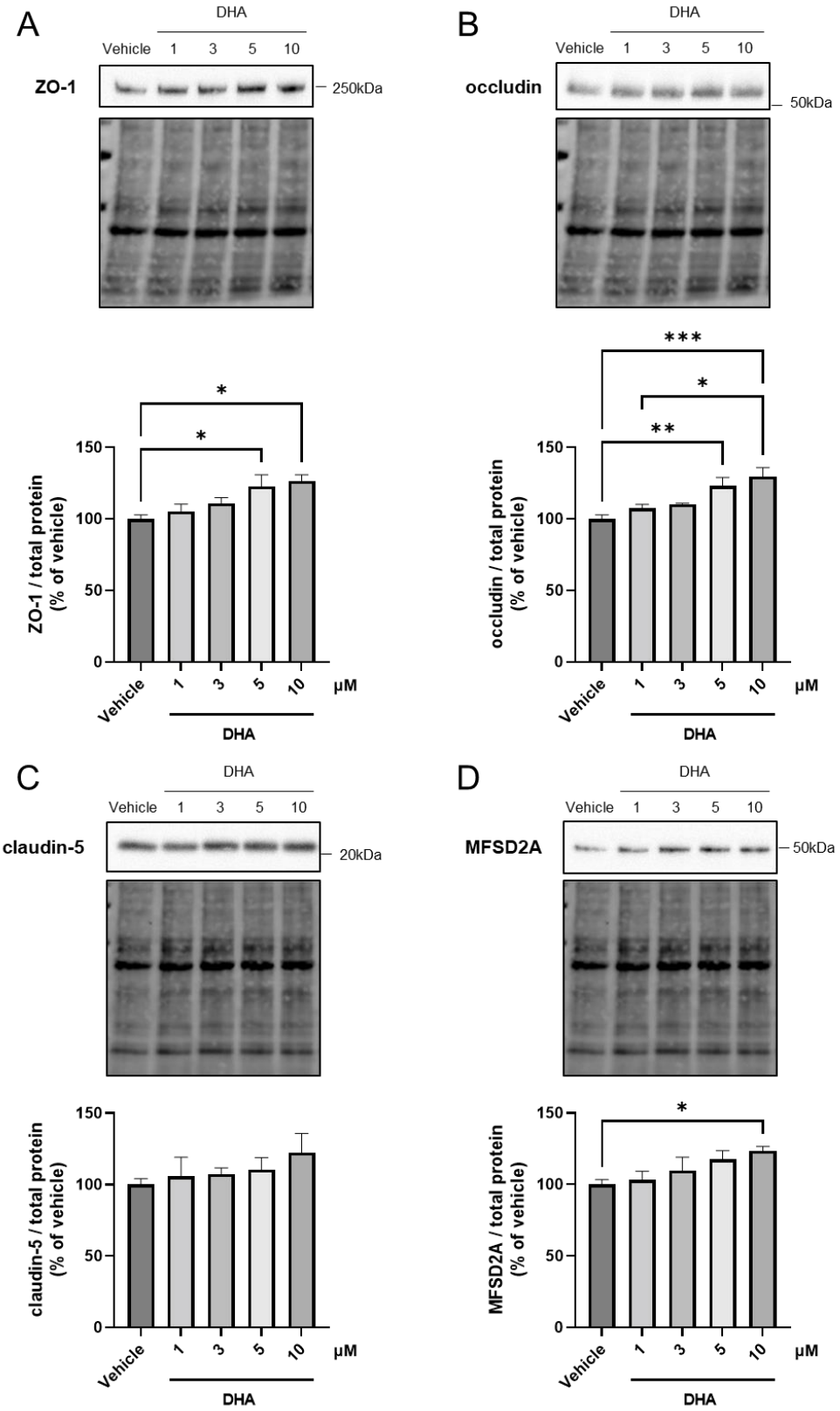
A
DHA
Vehicle 1 3 5 10
ZO-1
250kDa
ZO-1 / total protein (% of vehicle)
150
100
50
0
*
*
Vehicle 1 3 5 10 μM
DHA
B
DHA
Vehicle 1 3 5 10
occludin
50kDa
occludin / total protein (% of vehicle)
***
*
**
C
DHA
Vehicle 1 3 5 10
claudin-5
20kDa
claudin-5 / total protein (% of vehicle)
D
DHA
Vehicle 1 3 5 10
MFSD2A
50kDa
MFSD2A / total protein (% of vehicle)
*

Fig 5. ZO-1, occludin, claudin-5, and MFSD2A expression levels in brain ECs treated with DHA in vitro.

Rat brain EC-seeded 35-mm dishes were treated with DHA (1 to 10 μM) or a vehicle including 0.1% ethanol for 24 h. Representative western blotting images of ZO-1 (A), occludin (B), claudin-5 (C), and MFSD2A (D) in ECs treated with DHA and band intensities quantified by densitometry. Total protein levels measured by Stain-free technology used as the loading controls for total protein normalization. Data are expressed as percentages of the vehicle group's protein level. The bars indicate mean ± standard error of mean (n = 3 - 9). *P < 0.05, **P < 0.01, and ***P < 0.001, significantly different compared to the vehicle group.

Abbreviations: ZO-1, zonula occludens-1; MFSD2A, major facilitator superfamily domain-containing protein-2a; DHA, docosahexaenoic acid

Fig. 6

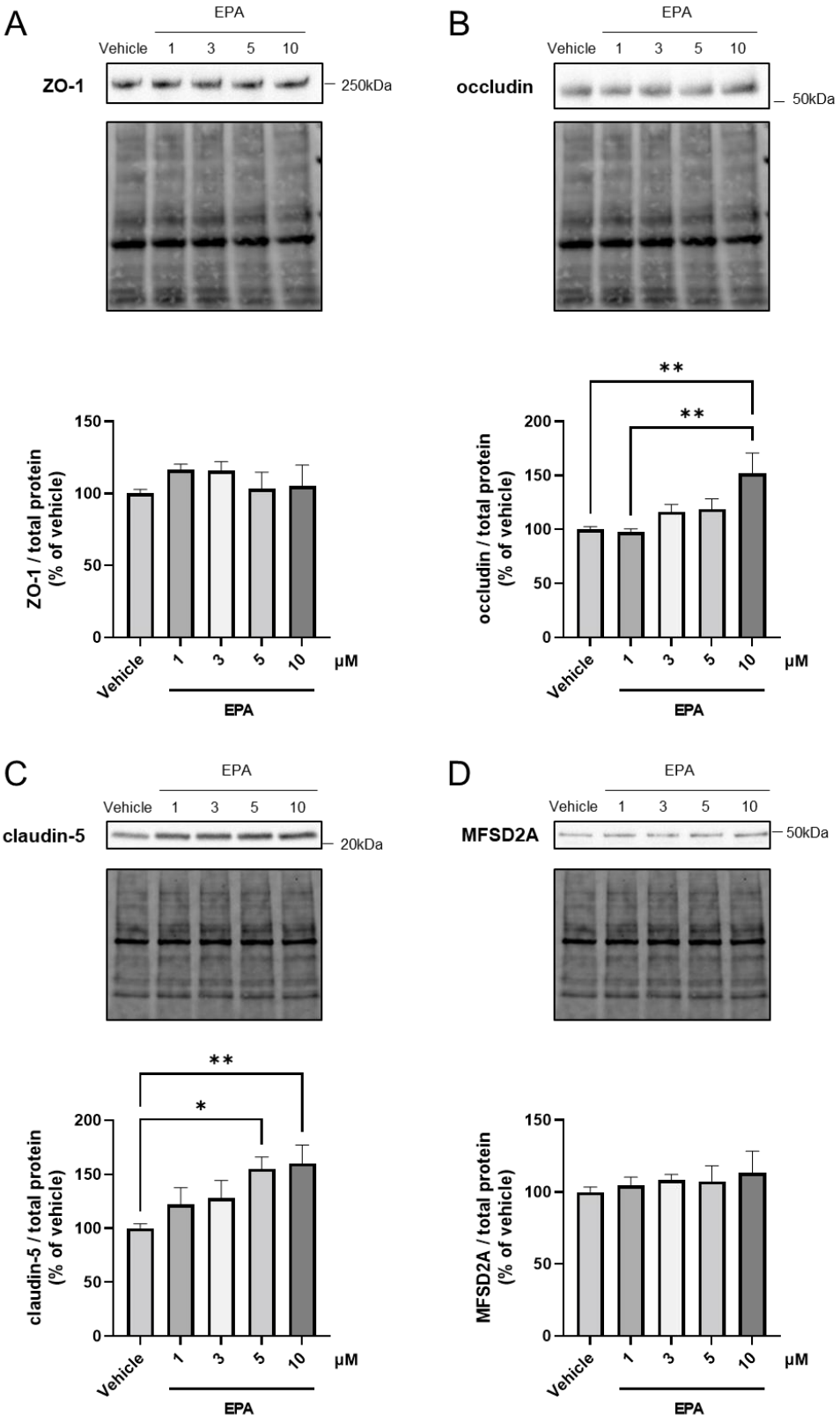
A
EPA
Vehicle 1 3 5 10
ZO-1
250kDa
ZO-1 / total protein (% of vehicle)
150
100
50
0
Vehicle 1 3 5 10 μM
EPA
B
EPA
Vehicle 1 3 5 10
occludin
50kDa
occludin / total protein (% of vehicle)
**
**
200
150
100
50
0
Vehicle 1 3 5 10 μM
EPA
C
EPA
Vehicle 1 3 5 10
claudin-5
20kDa
claudin-5 / total protein (% of vehicle)
**
*
200
150
100
50
0
Vehicle 1 3 5 10 μM
EPA
D
EPA
Vehicle 1 3 5 10
MFSD2A
50kDa
MFSD2A / total protein (% of vehicle)
150
100
50
0
Vehicle 1 3 5 10 μM
EPA

Fig 6. ZO-1, occludin, claudin-5, and MFSD2A expression levels in brain ECs treated with EPA in vitro

Rat brain EC-seeded 35-mm dishes were treated with EPA (1 to 10 μM) or a vehicle including 0.1% ethanol for 24 h. Representative western blotting images of ZO-1 (A), occludin (B), claudin-5 (C), and MFSD2A (D) in ECs treated with EPA and band intensities quantified by densitometry. Total protein levels measured by Stain-free technology used as the loading controls for total protein normalization. Data are expressed as percentages of the vehicle group's protein level. The bars indicate mean ± standard error of mean (n = 3 - 9). *P < 0.05 and **P < 0.01, significantly different compared to the vehicle group.

Abbreviations: ZO-1, zonula occludens-1; MFSD2A, major facilitator superfamily domain-containing protein-2a; EPA, eicosapentaenoic acid

Fig. 7

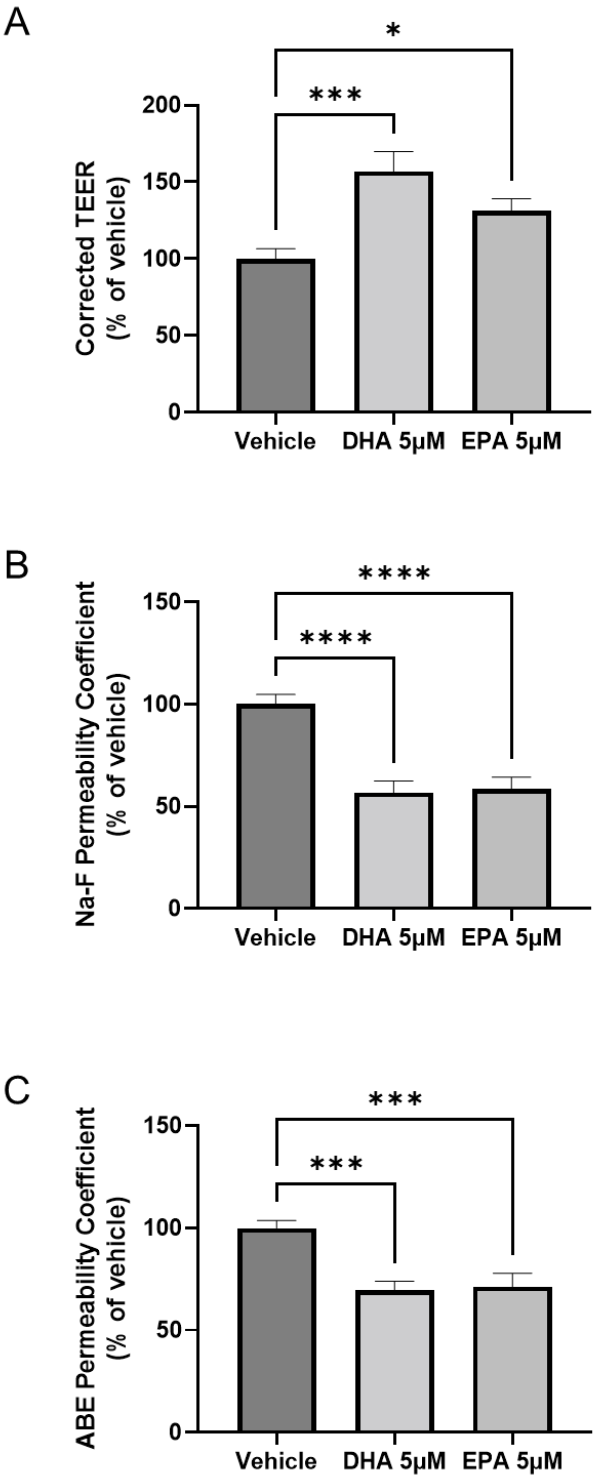
A
*
***
200
150
100
50
0
Corrected TEER
(% of vehicle)
Vehicle
DHA 5μM
EPA 5μM
B
****
****
150
100
50
0
Na-F Permeability Coefficient
(% of vehicle)
Vehicle
DHA 5μM
EPA 5μM
C
***
***
150
100
50
0
ABE Permeability Coefficient
(% of vehicle)
Vehicle
DHA 5μM
EPA 5μM

Fig. 7 Barrier function of brain ECs treated with DHA or EPA in vitro

Rat brain ECs seeded to the inside of 24-well transwell inserts were cultured in the EC medium supplemented with 500 nM of hydrocortisone for 3 days after passage. Culture media existed in 24-well transwell inserts, and the 24-well plate inside was replaced with the fresh serum-free EC medium supplemented with 500 nM of hydrocortisone. The EC medium including DHA 5 μM, EPA 5 μM, or ethanol 0.1% as a vehicle was added to the inside of 24-well transwell inserts. ECs treated with DHA or EPA were cultured for another 24 h, and TEER values (A) and permeability coefficients of Na-F (B) and ABE (C) to ECs were measured. Results are expressed as the percentage of the vehicle group. TEER values and permeability coefficients to Na-F and ABE of the vehicle group are $156.5\ \Omega \times cm^2$, 8.111×10^{-5} cm/min, and 1.406×10^{-5} cm/min, respectively. Data are expressed as percentages of the vehicle group. The bars indicate mean ± standard error of mean (n = 9–12). *$P < 0.05$, ***$P < 0.001$, and ****$P < 0.0001$, significantly different from the vehicle group.

Abbreviations: DHA, docosahexaenoic acid; EPA, eicosapentaenoic acid; TEER, transendothelial electrical resistance

Fig. 8

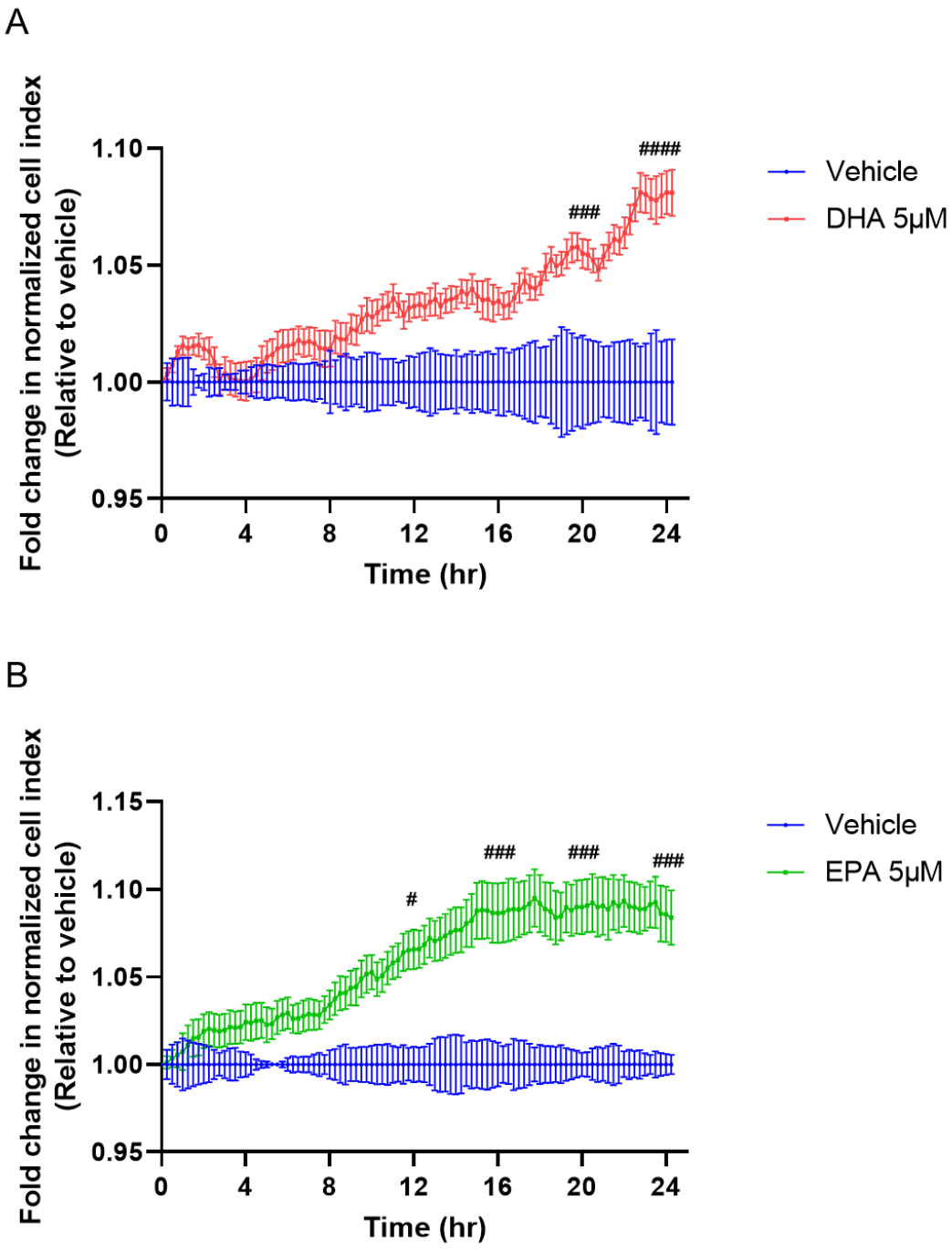
A
Fold change in normalized cell index
(Relative to vehicle)
1.10
1.05
1.00
0.95
0
4
8
12
16
20
24
Time (hr)
####
###
Vehicle
DHA 5μM
B
Fold change in normalized cell index
(Relative to vehicle)
1.15
1.10
1.05
1.00
0.95
0
4
8
12
16
20
24
Time (hr)
#
###
###
###
Vehicle
EPA 5μM

Fig. 8 Electrical impedance in brain ECs treated with DHA or EPA

Rat brain ECs seeded on E-plate 16 were cultured for 2 days in the EC medium supplemented with 500 nM of hydrocortisone while measuring electrical impedance in real time. Before ECs were treated with DHA 5 μM, EPA 5 μM, or a vehicle (0.1% ethanol), culture media were replaced with the fresh serum-free EC medium supplemented with 500 nM of hydrocortisone. Changes in impedance were monitored for another 24 h. Results are expressed as fold changes in the normalized cell index relative to the vehicle group for 24 h after the DHA (A) or EPA (B) treatment. Time courses of the normalized cell index in ECs treated with DHA (red line), EPA (green line), or a vehicle (blue line) in panels A and B. The bars indicate mean ± standard error of mean (n = 3–7). $^{\#}P < 0.05$, $^{\#\#\#}P < 0.001$, and $^{\#\#\#\#}P < 0.0001$, significantly different from the vehicle group at the corresponding time point.

Abbreviations: DHA, docosahexaenoic acid; EPA, eicosapentaenoic acid

References

1. Abbott NJ, Patabendige AA, Dolman DE, Yusof SR, Begley DJ. Structure and function of the blood-brain barrier. Neurobiol Dis. 2010;37(1):13-25.

2. Correale J, Villa A. The blood-brain-barrier in multiple sclerosis: functional roles and therapeutic targeting. Autoimmunity. 2007;40(2):148-60.

3. Wolburg H, Lippoldt A. Tight junctions of the blood-brain barrier: development, composition and regulation. Vascul Pharmacol. 2002;38(6):323-37.

4. Angers M, Uldry M, Kong D, Gimble JM, Jetten AM. Mfsd2a encodes a novel major facilitator superfamily domain-containing protein highly induced in brown adipose tissue during fasting and adaptive thermogenesis. Biochem J. 2008;416(3):347-55.

5. Ben-Zvi A, Lacoste B, Kur E, Andreone BJ, Mayshar Y, Yan H, et al. Mfsd2a is critical for the formation and function of the blood-brain barrier. Nature. 2014;509(7501):507-11.

6. Nguyen LN, Ma D, Shui G, Wong P, Cazenave-Gassiot A, Zhang X, et al. Mfsd2a is a transporter for the essential omega-3 fatty acid docosahexaenoic acid. Nature. 2014;509(7501):503-6.

7. Eser Ocak P, Ocak U, Sherchan P, Zhang JH, Tang J. Insights into major facilitator superfamily domain-containing protein-2a (Mfsd2a) in physiology and pathophysiology. What do we know so far? J Neurosci Res. 2020;98(1):29-41.

8. Verheggen ICM, de Jong JJA, van Boxtel MPJ, Gronenschild E, Palm WM, Postma AA, et al. Increase in blood-brain barrier leakage in healthy, older adults. Geroscience. 2020;42(4):1183-93.

9. Montagne A, Barnes SR, Sweeney MD, Halliday MR, Sagare AP, Zhao Z, et al. Blood-brain barrier breakdown in the aging human hippocampus. Neuron. 2015;85(2):296-302.

10. Mooradian AD, Haas MJ, Chehade JM. Age-related changes in rat cerebral occludin and zonula occludens-1 (ZO-1). Mech Ageing Dev. 2003;124(2):143-6.

11. Erdő F, Denes L, de Lange E. Age-associated physiological and pathological changes at the blood-brain barrier: A review. J Cereb Blood Flow Metab. 2017;37(1):4-24.

12. Desai BS, Monahan AJ, Carvey PM, Hendey B. Blood-brain barrier pathology in Alzheimer's and Parkinson's disease: implications for drug therapy. Cell Transplant. 2007;16(3):285-99.

13. Li M, Li Y, Zuo L, Hu W, Jiang T. Increase of blood-brain barrier leakage is related to cognitive decline in vascular mild cognitive impairment. BMC Neurol. 2021;21(1):159.

14. Abbott NJ, Rönnbäck L, Hansson E. Astrocyte-endothelial interactions at the blood-brain barrier. Nat Rev Neurosci. 2006;7(1):41-53.

15. Ahn SJ, Anrather J, Nishimura N, Schaffer CB. Diverse Inflammatory Response After Cerebral Microbleeds Includes Coordinated Microglial Migration and Proliferation. Stroke. 2018;49(7):1719-26.

16. Piers TM, East E, Villegas-Llerena C, Sevastou IG, Matarin M, Hardy J, et al. Soluble Fibrinogen Triggers Non-cell Autonomous ER Stress-Mediated Microglial-Induced Neurotoxicity. Front Cell Neurosci. 2018;12:404.

17. Ryu JK, Davalos D, Akassoglou K. Fibrinogen signal transduction in the nervous system. J Thromb Haemost. 2009;7 Suppl 1(Suppl 1):151-4.

18. Petermann AB, Reyna-Jeldes M, Ortega L, Coddou C, Yévenes GE. Roles of the Unsaturated Fatty Acid Docosahexaenoic Acid in the Central Nervous System: Molecular and Cellular Insights. Int J Mol Sci. 2022;23(10).

19. Lacombe RJS, Chouinard-Watkins R, Bazinet RP. Brain docosahexaenoic acid uptake and metabolism. Mol Aspects Med. 2018;64:109-34.

20. Mohajeri MH, Troesch B, Weber P. Inadequate supply of vitamins and DHA in the elderly: implications for brain aging and Alzheimer-type dementia. Nutrition. 2015;31(2):261-75.

21. Yang AC, Stevens MY, Chen MB, Lee DP, Stähli D, Gate D, et al. Physiological blood-brain transport is impaired with age by a shift in transcytosis. Nature. 2020;583(7816):425-30.

22. Zhou J, Chi X, Cheng M, Huang X, Liu X, Fan J, et al. Zika virus degrades the ω-3 fatty acid transporter Mfsd2a in brain microvascular endothelial cells and impairs lipid homeostasis. Sci Adv. 2019;5(10):eaax7142.

23. Chen X, Wang Q, Zhan L, Shu A. Effects and mechanisms of docosahexaenoic acid on the generation of angiopoietin-2 by rat brain microvascular endothelial cells under an oxygen- and glucose-deprivation environment. Springerplus. 2016;5(1):1518.

24. Liu ZH, Chen NY, Tu PH, Wu CT, Chiu SC, Huang YC, et al. DHA Attenuates Cerebral Edema Following Traumatic Brain Injury via the Reduction in Blood-Brain Barrier Permeability. Int J Mol Sci. 2020;21(17).

25. Pifferi F, Jouin M, Alessandri JM, Haedke U, Roux F, Perrière N, et al. n-3 Fatty acids modulate brain glucose transport in endothelial cells of the blood-brain barrier. Prostaglandins Leukot Essent Fatty Acids. 2007;77(5-6):279-86.

26. Takeyama E, Islam A, Watanabe N, Tsubaki H, Fukushima M, Mamun MA, et al. Dietary Intake of Green Nut Oil or DHA Ameliorates DHA Distribution in the Brain of a Mouse Model of Dementia Accompanied by Memory Recovery. Nutrients. 2019;11(10).

27. Islam A, Takeyama E, Mamun MA, Sato T, Horikawa M, Takahashi Y, et al. Green Nut Oil or DHA Supplementation Restored Decreased Distribution Levels of DHA Containing Phosphatidylcholines in the Brain of a Mouse Model of Dementia. Metabolites. 2020;10(4).

28. Dohgu S, Takata F, Matsumoto J, Kimura I, Yamauchi A, Kataoka Y. Monomeric α-synuclein induces blood-brain barrier dysfunction through activated brain pericytes releasing inflammatory mediators in vitro. Microvasc Res. 2019;124:61-6.

29. Takata F, Dohgu S, Yamauchi A, Matsumoto J, Machida T, Fujishita K, et al. In vitro blood-brain barrier models using brain capillary endothelial cells isolated from neonatal and adult rats retain age-related barrier properties. PLoS One. 2013;8(1):e55166.

30. Takata F, Dohgu S, Matsumoto J, Machida T, Sakaguchi S, Kimura I, et al. Oncostatin M-induced blood-brain barrier impairment is due to prolonged activation of STAT3 signaling in vitro. J Cell Biochem. 2018;119(11):9055-63.

31. Dohgu S, Sumi N, Nishioku T, Takata F, Watanabe T, Naito M, et al. Cyclosporin A induces hyperpermeability of the blood-brain barrier by inhibiting autocrine

adrenomedullin-mediated up-regulation of endothelial barrier function. Eur J Pharmacol. 2010;644(1-3):5-9.

32. Sun M, Fu H, Cheng H, Cao Q, Zhao Y, Mou X, et al. A dynamic real-time method for monitoring epithelial barrier function in vitro. Anal Biochem. 2012;425(2):96-103.

33. Hucklesby JJW, Anchan A, O'Carroll SJ, Unsworth CP, Graham ES, Angel CE. Comparison of Leading Biosensor Technologies to Detect Changes in Human Endothelial Barrier Properties in Response to Pro-Inflammatory TNFα and IL1β in Real-Time. Biosensors (Basel). 2021;11(5).

34. Pan Y, Morris ER, Scanlon MJ, Marriott PJ, Porter CJH, Nicolazzo JA. Dietary docosahexaenoic acid supplementation enhances expression of fatty acid-binding protein 5 at the blood-brain barrier and brain docosahexaenoic acid levels. J Neurochem. 2018;146(2):186-97.

35. Ouellet M, Emond V, Chen CT, Julien C, Bourasset F, Oddo S, et al. Diffusion of docosahexaenoic and eicosapentaenoic acids through the blood-brain barrier: An in situ cerebral perfusion study. Neurochem Int. 2009;55(7):476-82.

36. Eser Ocak P, Ocak U, Sherchan P, Gamdzyk M, Tang J, Zhang JH. Overexpression of Mfsd2a attenuates blood brain barrier dysfunction via Cav-1/Keap-1/Nrf-2/HO-1 pathway in a rat model of surgical brain injury. Exp Neurol. 2020;326:113203.

37. Charrière K, Ghzaiel I, Lizard G, Vejux A. Involvement of Microglia in Neurodegenerative Diseases: Beneficial Effects of Docosahexahenoic Acid (DHA) Supplied by Food or Combined with Nanoparticles. Int J Mol Sci. 2021;22(19).

38. Martinat M, Rossitto M, Di Miceli M, Layé S. Perinatal Dietary Polyunsaturated Fatty Acids in Brain Development, Role in Neurodevelopmental Disorders. Nutrients. 2021;13(4).

39. Zhang Z, Xue Z, Yang H, Zhao F, Liu C, Chen J, et al. Differential effects of EPA and DHA on DSS-induced colitis in mice and possible mechanisms involved. Food Funct. 2021;12(4):1803-17.

40. Zhao J, Shi P, Sun Y, Sun J, Dong JN, Wang HG, et al. DHA protects against experimental colitis in IL-10-deficient mice associated with the modulation of intestinal epithelial barrier function. Br J Nutr. 2015;114(2):181-8.

41. Chen CT, Ma DW, Kim JH, Mount HT, Bazinet RP. The low density lipoprotein receptor is not necessary for maintaining mouse brain polyunsaturated fatty acid concentrations. J Lipid Res. 2008;49(1):147-52.

42. Chen CT, Liu Z, Ouellet M, Calon F, Bazinet RP. Rapid beta-oxidation of eicosapentaenoic acid in mouse brain: an in situ study. Prostaglandins Leukot Essent Fatty Acids. 2009;80(2-3):157-63.

General discussion

In this series of studies, we investigated that involvement of brain pericytes in age-related blood–brain barrier (BBB) dysfunction. Furthermore, we examined whether or not decreased docosahexaenoic acid (DHA) levels in brain endothelial cells contributed to age-related BBB disruption and subsequent brain inflammation. In vitro study, we used primary cultures of brain endothelial cells and pericytes isolated from rats not mice, because of low yields of these cells isolated from mice. To summarize the present findings, we propose mechanisms by which brain pericytes contribute to the age-related BBB dysfunction, as shown in schematic diagrams.

In the young adult brain, pericytes upregulate the function of BBB, and brain DHA uptake is a consequence of the induction of the protein expression and proper localization of the major facilitator superfamily domain-containing protein-2a (MFSD2A) in the plasma membrane. This increase in MFSD2A would be associated with a low level of endocytosis in brain microvascular endothelial cells (BMECs). Furthermore, DHA levels in BMECs can maintain the protein expression levels of tight junction-associated proteins and MFSD2A.

The loss of pericytes in the middle-aged brain contributes to a decrease in protein expression levels of MFSD2A. Brain DHA transport is decreased because of the downregulation of MFSD2A. However, the protein expression levels of occludin and claudin-5 in BMECs increased, suggesting a probably compensatory action in BMECs to the downregulation of cadherin and MFSD2A induced by a loss of pericytes. BBB integrity is maintained in the middle-aged brain, while brain DHA uptake is decreased. These changes do not markedly contribute to age-related BBB disruption. Connexin43 and N-cadherin play an important role in intercellular connections between pericytes and BMECs. Therefore, decrease in these proteins may result in pericyte loss.

In the aged brain, pericytes exhibit features of cellular senescence, which damage BBB, leading to decreased protein expression levels of ZO-1 and cadherin in BMECs. Senescence-associated secretory phenotype factors secreted by senescent pericytes may have induced the loss of BBB integrity and neuroinflammation. Subsequently, BBB disruption permits plasma proteins, such as fibrinogen, to enter the brain across BBB. In consequence, the extravasated fibrinogen activates microglia, which probably induces neuronal damages. Furthermore, decreases in ZO-1 and inflammatory activation of microglia are attributable to low DHA levels in brain as a result of the downregulation of MFSD2A. The region variability of fibrinogen leakages suggested that BBB in hippocampal

CA1 is likely affected by aging. Therefore, DHA transport across the BBB through paracellular routes is likely to be increased in a specific region of hippocampus.

Age-related BBB dysfunction probably induces the accumulation of neuronal damages, which underlies the pathological process of age-related neurodegenerative disorders. To establish a preventive strategy for neurological diseases, further studies on age-related BBB dysfunction are required. However, the present findings suggest that brain pericytes are a target for preventing age-related BBB dysfunction.

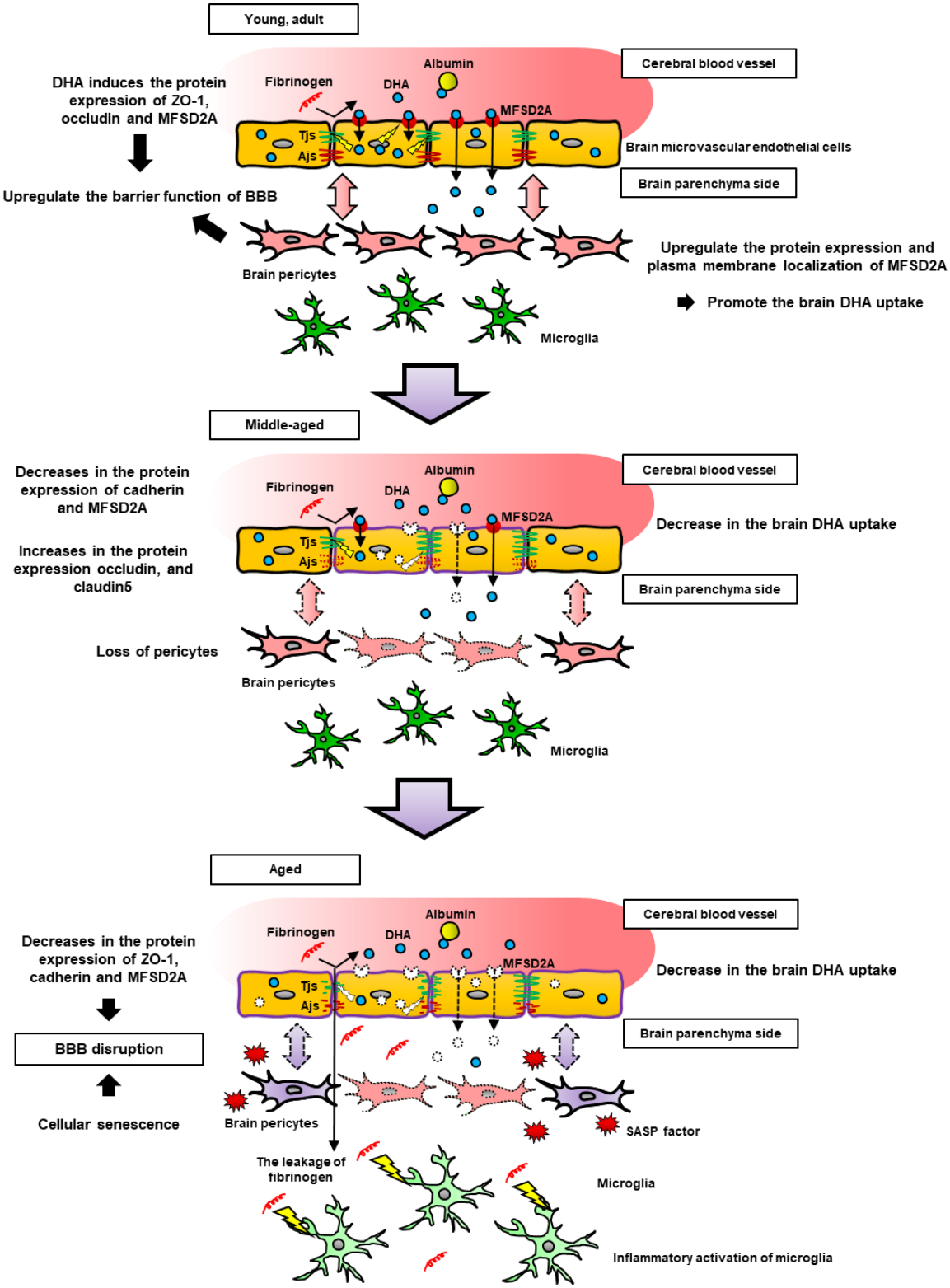
Young, adult
DHA induces the protein expression of ZO-1, occludin and MFSD2A
Upregulate the barrier function of BBB
Albumin
Fibrinogen
DHA
MFSD2A
Tjs
Ajs
Cerebral blood vessel
Brain microvascular endothelial cells
Brain parenchyma side
Brain pericytes
Microglia
Upregulate the protein expression and plasma membrane localization of MFSD2A
Promote the brain DHA uptake
Middle-aged
Decreases in the protein expression of cadherin and MFSD2A
Increases in the protein expression occludin, and claudin5
Loss of pericytes
Decrease in the brain DHA uptake
Aged
Decreases in the protein expression of ZO-1, cadherin and MFSD2A
BBB disruption
Cellular senescence
SASP factor
The leakage of fibrinogen
Inflammatory activation of microglia

Acknowledgments

謝辞

本研究の機会を与えられ、終始懇切な御指導ならびに御鞭撻を賜りました福岡大学薬学部応用薬剤学教室 道具 伸也 教授、ならびに 片岡 泰文 前教授に心より深甚なる謝意を表します。

本論文を査読して頂き、貴重な御意見と御校閲を賜りました福岡大学薬学部臨床疾患薬理学教室 岩崎 克典 教授ならびに福岡大学薬学部生物薬剤学教室 山内 淳史 教授に謹んで感謝致します。

本研究の遂行にあたり、終始有益な御助言と御指導、御協力、御校閲を賜りました福岡大学薬学部応用薬剤学教室 髙田 芙友子 准教授に感謝し、心より御礼申し上げます。

本研究に対して、多大なる御協力と御助言を賜りました福岡大学薬学部生物薬剤学教室 中川 慎介 准教授、松本 純一 助教、福岡大学薬学部 薬物送達学教室 古賀 充久 准教授、福岡大学薬学部応用薬剤学教室 稲田 紘舜 助教、福岡大学薬学部実務薬剤学教室 冨永 宏治 准教授、福岡大学薬学部臨床疾患薬理学教室 渡辺 拓也 助教、第一薬科大学薬学部薬学科地域医療薬学センター 首藤 英樹 教授、岡山大学薬剤部 木村 郁哉 博士、九州大学五感応用デバイス研究開発センター 坂井 研太 助教に謹んで感謝の意を表します。

本研究の遂行に多大なる御協力を賜りました有留 尚孝 学士、横谷 みき 学士、安永 美保 学士、森 徹 学士、安森 光 学士、後藤 佑希 学士、髙尾 真央 学士、下村 舞桜 学士、髙尾 暁 学士、栗山 侑子 学士、今村 心実 学士、中島 正稀 学士、新垣 翔 学士、土井 優奈 学士、井上 湧太郎 学士、丸山 愛加 学士、森 桜子 学士、堤 郁香 学士に心から感謝致します。また、本研究にご協力を賜りました福岡大学薬学部応用薬剤学教室の皆さんをはじめ、これまで私を支えてくれた多くの方々に厚くお礼申し上げます。

最後に、本研究生活を通して惜しみない支援を賜りました父 憲夫、母 由起子、義父 中村 秀徳、義母 中村 菜穂子、妻 優里と、頑張る元気と前へ進む勇気を与えてくれた長女 妃与里、次女 菜々乃の二人の子供に心から感謝致します。